THE
PHYSICAL REVIEW
A Journal of Experimental and Theoretical Physics
VOL. 46, NO. 11 DECEMBER 1, 1934 SECOND SERIES

Diffuse Scattering of X-Rays from Sylvine—More Exact Measurements

G. E. M. JAUNCEY* AND W. D. CLAUS, *Washington University, St. Louis*
(Received October 1, 1934)

Harvey's S values for sylvine at 295°K agree qualitatively with the theoretical S values calculated from James and Brindley's quantum-mechanical f and E_{ff} values. Quantitatively, the difference between experiment and theory is too great for comfort. Accordingly, we have made a more exact and careful determination of the experimental S values and have found a remarkable agreement between experiment and theory. This shows the excellence of the present theory of diffuse scattering and the accuracy of the f and E_{ff} values which James and Brindley have calculated by approximate methods. Our results are not in accord with the idea that the probability distribution is the same for all electrons. Also experiment has shown that turning the crystal plate in its own plane has no effect on the diffuse scattering in a given direction. This indicates that the atoms of sylvine possess spherical symmetry as far as the scattering of x-rays is concerned. Spherical symmetry is assumed in the theory.

1. INTRODUCTION

ACCORDING to the most recent development of the theory, the diffuse scattering of x-rays by crystals consisting of two kinds of atoms (such as KCl) is given by

$$S=S_1+S_2/(1+\alpha \text{ vers } \phi)^2, \tag{1}$$

where

$$S_1=(f_1^2+f_2^2-F_1^2-F_2^2)/(Z_1+Z_2) \tag{2}$$

and

$$S_2=1-\frac{\sum(E_{jj}^2)_1+\sum(E_{jj}^2)_2-\sum|E_{jk}|_1^2-\sum|E_{jk}|_2^2}{Z_1+Z_2}. \tag{3}$$

The various symbols are defined in the paper by Harvey, Williams and Jauncey,[1] the numerical subscripts referring to the two kinds of atoms. It has become the custom to use another symbol, S_{class}, which is defined by

$$S_{class}=S_1+S_2. \tag{4}$$

On the basis of wave mechanics, James and Brindley[2] have calculated values of E_{jj} (their f_0) and of f for the K^+ and Cl^- ions in sylvine. Values of F are obtained by multiplying the values of f by the Debye-Waller[3] temperature factors, using 230°K for the characteristic temperature of KCl and assuming the existence of zero point energy. The theoretical values of S and S_{class} can therefore be calculated.

Harvey has obtained experimental S_{class} values for sylvine at room temperature, first for an average wave-length of a band of x-rays[4] and second for monochromatic x-rays.[5] In both cases he obtained a maximum value of S_{class} of 2.95 at about $(\sin\phi/2)/\lambda=0.365$. Although the wave-

* The senior author was aided in part by a grant from the Rockefeller Foundation to Washington University for research in science.

[1] G. G. Harvey, P. S. Williams and G. E. M. Jauncey, Phys. Rev. **46**, 365 (1934).

[2] R. W. James and G. W. Brindley, Phil. Mag. **12**, 81 (1931).

[3] P. Debye, Ann. d. Physik **43**, 49 (1914); I. Waller, Zeits. f. Physik **17**, 248 (1923).

[4] G. G. Harvey, Phys. Rev. **38**, 593 (1931).

[5] G. G. Harvey, Phys. Rev. **43**, 591 (1933).

mechanical S_{class} curve has the same general shape as the experimental S_{class} curve, there is a distinct difference between the absolute values of the ordinates of the two curves as shown by the fact that the maximum theoretical S_{class} value is 2.46 at $(\sin\phi/2)/\lambda=0.59$. The difference between the experimental and theoretical values of $x(=(\sin\phi/2)/\lambda)$ for the maximum S_{class} values might be explained as due to error in drawing the experimental curves since the points are somewhat scattered, but a difference of about 0.5 in the two maximum values of S_{class} is too great for comfort. We have therefore made a careful investigation of the diffuse scattering from sylvine in order to find out whether the above discrepancy between theory and experiment can be reduced or removed.

A second object of this research was to find out whether the diffuse scattering in a given direction depends on the orientation of the crystal with respect to the plane of scattering.

2. Experimental Method

Because we desired greater accuracy in our readings we used a band of wave-lengths from the continuous spectrum of x-rays from a tungsten target tube operated at 51.5 kv peak rather than monochromatic rays as in the experiments of Harvey[5] and Williams.[6] The experimental method has been described in previous papers.[7, 8, 9] Referring to the paper by Jauncey and May,[9] let us introduce

$$v=\frac{[e^{-\mu t/\cos\theta}-e^{-\mu t/\cos(\phi-\theta)}]\cos(\phi-\theta)\cos\frac{1}{2}\phi}{\mu t[\cos\theta-\cos(\phi-\theta)]e^{-\mu t/\cos\frac{1}{2}\phi}}, \quad (5)$$

where ϕ is the angle of scattering, θ is the angle between the normal to the crystal slab and the primary beam, and μ and t are respectively the absorption coefficient and thickness of the crystal. Then, if D is the electrometer deflection corresponding to a setting θ and ϕ is kept constant, the graph of D/v against θ is a horizontal straight line excepting where Laue spots occur as shown in Fig. 1. As pointed out by

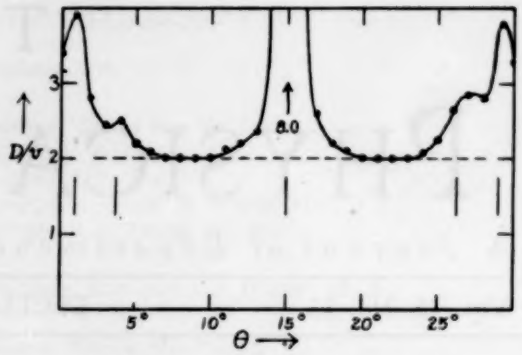

Fig. 1. Graph of D/v against θ for $\phi=30°$. The horizontal portion of the curve is important in diffuse scattering. Each experimental point of this portion is the average of numerous readings. The Laue spots occur at $\pm(\phi/2-\theta)=0°$, 11.3° and 14°.

Jauncey and Williams[7] it is essential to separate the Laue spots from the diffuse scattering. Previously we have plotted D against θ and this gives rise to an approximate straight line with a small slope. Fig. 1 shows how well the experimental points fall on a horizontal line. For the case where a principal axis of the crystal is perpendicular to the plane of scattering, the values of θ at which Laue spots occur are given by

$$\theta=\phi/2\pm\tan^{-1}h/k, \quad (6)$$

where h and k are integers and either but not both may be zero. Eq. (6) holds so long as the wave-length

$$\lambda=(2d\sin\theta)/(h^2+k^2)^{\frac{1}{2}} \quad (7)$$

is contained in the continuous spectrum. The positions of the Laue spots according to Eqs. (6) and (7) are indicated by the vertical lines in Fig. 1.

Because $v=1$ when $\theta=\phi/2$, the average value of D/v for points not at or near Laue spots is the value assumed for D_ϕ in the right side of Eq. (17) of the paper by Jauncey and Pennell.[8] The same ionization chamber and thickness of paraffin were used as are described in this paper and so the numerical value 0.314 included in the formula for S_{exp} is the same as that used by Jauncey and Pennell. For clarity it might be well to point out that 0.314 stands for

$$\frac{Z'\rho't'}{W'}\times\frac{1}{\cos 45°}\times\frac{K_{90°}T'_{90°}}{K_0(1+\alpha)^2}. \quad (8)$$

[5] P. S. Williams, Phys. Rev. **46**, 83 (1934).
[7] G. E. M. Jauncey and P. S. Williams, Phys. Rev. **44**, 794 (1933).
[8] G. E. M. Jauncey and Ford Pennell, Phys. Rev. **43**, 505 (1933).
[9] G. E. M. Jauncey and H. L. May, Phys. Rev. **23**, 128 (1924).

The value of ρt for the crystal is 0.325 g/cm².

Jauncey and Pennell determined the intensity distribution in the spectrum by means of their Eq. (7a). This, however, assumes that the Lorentz factor[10] is proportional to $\lambda^3/\sin 2\theta$. This is the factor for monochromatic rays when the method of integrated reflection is used. However, the "white" Lorentz factor is proportional to $\lambda^2/\sin^2\theta$ and would seem to apply to our determination of the spectral distribution. In addition to the Lorentz factor there is some uncertainty concerning the proper value of μ to be used since μ should be increased by the extinction coefficient. This coefficient probably becomes a greater proportion of the ordinary absorption coefficient at shorter wave-lengths. We therefore determined three curves—the first curve was the graph of the actual electrometer reading against λ, while the second and third curves were the graphs of the readings corrected for the "monochromatic" and "white" Lorentz factors, respectively, both the second and third curves being also corrected for the ordinary absorption coefficient. By experiment we determined that 0.75 g/cm² of aluminum was necessary to reduce the primary rays to half value when the rays had already passed through the paraffin ($\rho' t' = 0.493$ g/cm²), the sylvine crystal and 0.170 g/cm² of aluminum which was permanently placed in the primary beam during the scattering experiments. From each of the above three curves a modified curve for the spectral distribution of the rays getting through the added 0.75 g/cm² of aluminum was calculated, using the values of μ for various wave-lengths in aluminum as given by Compton's tables.[11] Now comparing the area under each modified curve with that under the corresponding original curve we find that the fractions to which the primary rays are reduced are: First curve, 0.463; second curve, 0.433; third curve, 0.332. Obviously the first curve agrees best with the experimental value 0.5 and this is the curve, Fig. 2, we have used for the spectral distribution curve.

At first we compared the scattering from KCl with that from paraffin and used Jauncey and Pennell's formula for calculating S_{exp}. However, in this formula it is assumed that the scattering

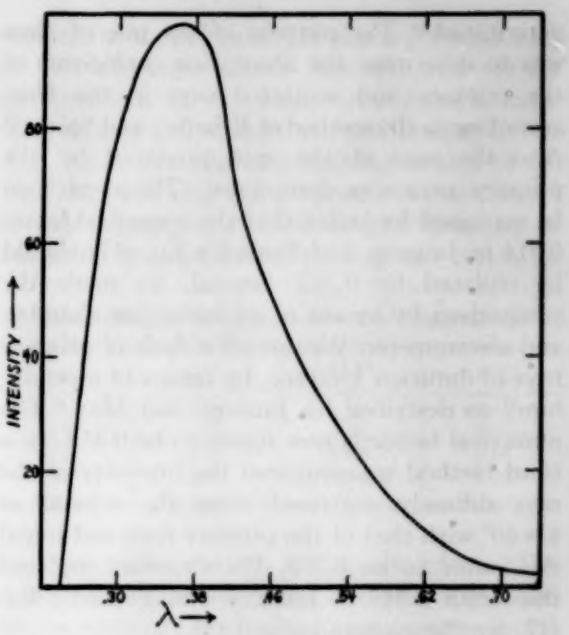

FIG. 2. Distribution-in-wave-length of the intensity in the continuous spectrum. Half-value absorption in aluminum of this spectrum corresponds to an average wave-length of about 0.38A.

from paraffin at 90° is entirely incoherent so that the Breit-Dirac[12] formula holds. However, from Fig. 2 it is seen that there is some intensity of $\lambda = 0.7$A present and at this wave-length some coherent radiation occurs at $\phi = 90°$. Since this part of the spectral distribution curve is somewhat uncertain,[13] we measured the absolute value of the spatial scattering coefficient per unit solid angle at $\phi = 90°$ from paraffin. This necessitates the comparison of two intensities whose ratio is in the order of 1 to 10,000. First, we made the comparison by a photographic method. A photographic film was cut into 24 rectangular pieces and these pieces were arranged in two piles of 12 pieces each. One pile was exposed to the primary x-rays for several seconds and the other to the scattered rays for several hours. Each piece was run through the microphotometer[14] and the photographic density

[10] See F. C. Blake, Rev. Mod. Phys. **5**, 169 (1933).
[11] A. H. Compton, *X-Rays and Electrons*, p. 184.
[12] G. Breit, Phys. Rev. **27**, 362 (1926); P. A. M. Dirac, Proc. Roy. Soc. **A111**, 405 (1926).
[13] The minimum wave-length as given by the Duane-Hunt relation is 0.24A so that second order reflection from the rocksalt occurs at θ greater than that corresponding to first-order reflection of $\lambda = 0.48$A and so a correction in the curve had to be made.
[14] See W. D. Claus, Phys. Rev. **38**, 604 (1931).

determined.[15] The purpose of the pile of films was to determine the absorption coefficients of the primary and scattered rays in the films according to the method of Brindley and Spiers.[16] Also the area of the spot produced by the primary rays was determined. The result can be expressed by saying that the numerical factor 0.314 in Jauncey and Pennell's Eq. (17) should be replaced by 0.352. Second, we made the comparison by means of an ionization chamber and electrometer. We cut off a flash of primary rays of duration 1/60 sec. by means of a pendulum[17] as described by Jauncey and May.[9] The numerical factor is now found to be 0.358. In a third method we compared the intensity of the rays diffusely scattered from the crystal at $\phi=40°$ with that of the primary rays and found the factor to be 0.355. We therefore replaced the factor 0.314 in Jauncey and Pennell's Eq. (17) by the average value 0.355.

3. Comparison with Wave-Mechanical Values

Values of the theoretical quantity defined by the left side of Jauncey and Pennell's Eq. (17) can be calculated from James and Brindley's[2] wave-mechanical values of f and E_{jj} together with the values of $\Sigma|E_{jk}|^2$ given by Waller and Hartree[18] and Harvey, Williams and Jauncey.[1] The values of S_{exp} and S_{th} are given in Table I. The results are also shown by the solid curve of Fig. 3. It is seen how well the experimental values agree with the theoretical. The maximum S_{exp} of 2.31 corresponds very well with the maximum S_{th} of 2.36 at $\phi=25°$. Assuming an average wave-length of 0.38A (obtained from half-value absorption) this corresponds to $x=0.57$. The reason for the slight difference between the values given here and in the introduction to this paper is that S_{class} was used there and monochromatic rays were assumed instead of the band of wave-lengths actually used.

Table I. *Diffuse scattering from sylvine.*

ϕ	S_{exp}	S_{th}	ϕ	S_{exp}	S_{th}
10°	1.50	1.65	37°	1.99	2.06
15°	1.95	2.05	40°	1.90	1.95
20°	2.23	2.28	45°	1.70	1.79
25°	2.31	2.36	50°	1.56	1.62
30°	2.27	2.28	60°	1.32	1.37
33°	2.14	2.21	75°	1.14	1.12
35°	2.01	2.13	90°	1.01	0.97

The excellence of the agreement shown in Table I indicates the correctness of the present theory of diffuse scattering and also the high accuracy of James and Brindley's[2] f and E_{jj} values which were calculated by approximate methods. The broken curve of Fig. 3 is based upon the assumption that the probability distribution is the same for all electrons so that $\Sigma E_{jj}^2=f^2/Z$, i.e., $f''=f$ in the notation used by Jauncey.[19] Our results show that this assumption is incorrect. The omission of the negative term $-\Sigma|E_{jk}|^2/Z$ from S_2 makes a maximum increase of 0.08 in S_{th} at $\phi=29°$. The inclusion of the negative term thus gives slightly better agreement with S_{exp} at this value of ϕ.

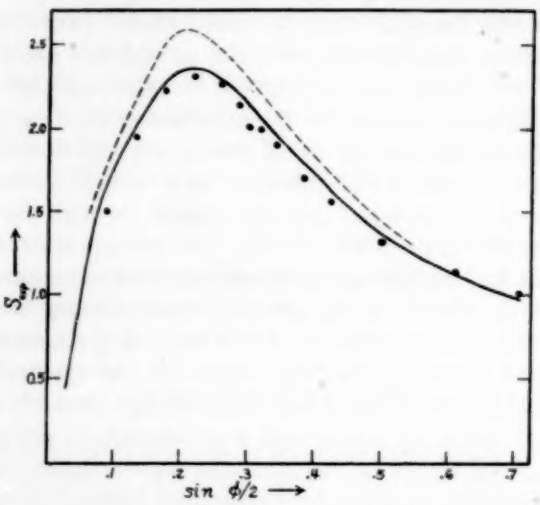

Fig. 3. Diffuse scattering of x-rays from sylvine. Black circles, experimental points; solid curve, electrons having different probability distributions; broken curve, electrons having equal probability distributions.

[15] See G. E. M. Jauncey and H. W. Richardson, J. O. S. A. **24**, 125 (1934).

[16] G. W. Brindley and F. W. Spiers, Phil. Mag. **16**, 686 (1933).

[17] The approximate distance by which the pendulum should be pulled out before being released can be calculated but the exact distance can be found experimentally by plotting the electrometer deflection against the distance. There is a point of inflection at the correct distance. Also at the correct distance the readings repeat very well but as the distance departs from the correct value the readings scatter more and more.

[18] I. Waller and D. R. Hartree, Proc. Roy. Soc. **A124**, 119 (1929).

[19] G. E. M. Jauncey, Phys. Rev. **42**, 453 (1932).

We wish to notice that the difference between S_{exp} and S_{th} at $\phi=35°$ is somewhat larger than our experimental error which we place at about 0.05 in S_{exp} in this region. We made repeated trials in this region and always found S_{exp} somewhat less than S_{th}. A rather large difference also occurs at $\phi=10°$ and 15°; but at these small angles the experimental difficulties increase and the difference is probably not greater than the experimental error. Considering all the values of ϕ, there is a tendency for all the experimental points to fall below the theoretical curve. This is probably due to error in the determination of the numerical factor mentioned at the end of the last section.

4. Effect of Crystal Orientation

In all the work done hitherto in this laboratory x-rays have for convenience been scattered from a crystal with one axis perpendicular to the scattering plane. We have now tried the effect of turning the crystal plate in its own plane upon the S_{exp} values. When the crystal is oriented so that no principal axis is perpendicular to the scattering plane, Eqs. (6) and (7) for the positions of the Laue spots become more complicated and contain a third integer l. The S_{exp} values for the axis making angles of 0°, 22.5° and 45° with the perpendicular are shown in the second, third and fourth columns of Table II. It is seen that turning the crystal in its own plane has no noticeable effect. The theory of diffuse scattering has been developed on the assumption of spherical symmetry in the atoms.[20] Our results are in accord with this assumption in the case of sylvine.

Table II. *Effect of crystal orientation*—S_{exp} values.

ϕ	0°	22.5°	45°
15°	1.95	1.99	1.93
25°	2.31	2.31	2.29
35°	2.01	2.00	2.01
50°	1.56	1.54	1.54

[20] G. E. M. Jauncey, Phys. Rev. **37**, 1193 (1931).

DECEMBER 1, 1934 PHYSICAL REVIEW VOLUME 46

The Verdet Constant of Heavy Water

Francis G. Slack, *Department of Physics, Vanderbilt University*

(Received October 1, 1934)

The Verdet constants of samples of water containing 0, 31.1, and 99.7 percents of heavy hydrogen atoms have been measured for the wave-lengths λ5893 and λ5460.7A at 20°C. The results are given in tabular form. From these data the Verdet constant of pure heavy water (H^2_2O) is found to be 3.93 percent less than that of ordinary water for both wave-lengths. Non-linearity of the Verdet constant-concentration relation leads to the calculation of an apparent Verdet constant for H^1H^2O which is 0.85 percent less than the Verdet constant of ordinary water. Values of the relative molecular rotatory power and of the magnetic rotatory dispersions are also given.

THE Verdet constants of ordinary and of heavy water have been measured for two wave-lengths of light.

The measurements were made by use of the Schmidt and Haensch Faraday effect apparatus. The optical system of the instrument consists of a triple field polarizer with the Lippich half-shade adjustment and an analyzing Nicol whose position may be read to 0.01°. The magnetic field was produced by the attached electromagnet with an iron core, drilled parallel to the magnetic field. The mean axial field strength was determined by calibration against a standard solenoid by the ballistic galvanometer deflection method. The test coil used between the magnet pole pieces in calibration was of approximately the same dimensions as the cell used to contain the liquids whose Verdet constants were determined. The current for the electromagnet was supplied from storage batteries, and was determined by

the measurement of the potential drop across a standard resistance by means of a Wolff potentiometer. Current measurements were made before and after each observation and the average of these values used to determine, from the magnet calibration curve, the actual field strength at the time of observation. Two different field strengths were used in each determination. The light sources used were the sodium and mercury arcs with appropriate filters to transmit only the lines λ5893 and λ5460.7A.

The liquids under observation were sealed in water-jacketed Pyrex cells approximately 5 cm long with thin cover glass ends cemented on with picein. The rotations due to these glass ends were measured and corrected for, the corrections being of the order of one percent of the total rotations. The temperature of each specimen was held constant to within 1.0°C by a constant flow of water through the jacket. The temperature of the liquid is taken as the average of thermometer readings at the inlet and at the outlet from the jacket. These readings differed at most by a few tenths of a degree. The two cells, made by Eck and Krebs of New York, were the same length to within one part in 4000. Measurements of the Verdet constant of ordinary water made in the two different cells agreed within the estimated precision.

Samples of heavy water of two different concentrations and one sample of ordinary water were kindly loaned by Dr. H. C. Urey and his assistants. These samples were freshly distilled and were sealed in the cells before delivery. The concentrations of these samples were also determined by Dr. Urey's staff.

The results of the measurements are given in Table I. Column 1 gives the concentration of the solutions in mol fractions of H^2_2O. Column 2 gives the specific gravity as computed from the known concentrations by the equation of Luten,[1] and using the value $D^{25}_{25} = 1.1079$ given by Taylor and Selwood[2] for 100 percent H^2_2O. The indices of refraction in column 3 are taken from the data of Luten[1] by interpolation from his tables. Columns 4, 5 and 6, respectively, give the wavelength, temperature and field strength at which the measurements were taken. Each value in columns 5, 6 and 7 is the average of at least two independent sets of observations. Columns 7 and 8 give the Verdet constants as measured. The values in column 8 are to be taken as the final values and are the weighted means of the values shown in column 7, corrected[3] to 20°C. By extrapolation the values 0.012554 ± 0.000030

[1] D. B. Luten, Jr., Phys. Rev. **45**, 161 (1934).
[2] H. S. Taylor, and P. W. Selwood, J. Am. Chem. Soc. **56**, 998 (1934); H. S. Taylor, J. Frank. Inst. **218**, 1 (1934).
[3] Int. Crit. Tab. **6**, 425 (1929).

TABLE I. *The Verdet constants of solutions of H^2_2O in H^1_2O.*

Concentration mol fraction (H^2_2O)	Specific gravity (D^{25}_{25})	Refractive index (20°C)	Wavelength (A)	Temp. of liquid (°C)	Field strength (gauss)	Verdet constant (min./g-cm)	Verdet constant (20°C)
0.000	1.0000	1.33449	5460.7	20.89	2205	0.015426	0.015397
.000	1.0000	1.33449	5460.7	20.40	1953	.015333	±.000030
.000	1.0000	1.33300	5893	19.80	2207	.013069	.013067
.000	1.0000	1.33300	5893	19.80	1954	.013065	±.000030
.311	1.0333	1.33302	5460.7	20.00	2202	.015293	.015274
.311	1.0333	1.33302	5460.7	20.00	1945	.015256	±.000030
.311	1.0333	1.33158	5893	20.00	2206	.012979	.012963
.311	1.0333	1.33158	5893	20.00	1952	.012948	±.000030
.997	1.1076	1.32977	5460.7	20.23	2196	.014798	.014793
.997	1.1076	1.32977	5460.7	19.90	1960	.014782	±.000030
.997	1.1076	1.32845	5893	19.90	2191	.012583	.012556
.997	1.1076	1.32845	5893	19.90	1960	.012530	±.000030
1.000	1.1079	1.32976	5460.7	20.00			.014791*
1.000	1.1079	1.32844	5893	20.00			.012554*

* These values obtained by extrapolation.

and 0.014791 ± 0.000030 min./gauss-cm are obtained for the Verdet constants of 100 percent H^2_2O at 20°C for the wave-lengths λ5893 and λ5460.7 respectively.

Discussion of Results

These measurements show the Verdet constant of heavy water (H^2_2O) to be 3.93 percent less than that for ordinary water (H^1_2O) at each of the two wave-lengths investigated. Thus the rotatory power relative to H^1_2O is independent of wave-length in this region. The indices of refraction for the two waters at λ5893 differ by approximately 0.34 percent and the dispersions ($dn/d\lambda$) between the wave-lengths λ5893 and λ5461 differ by more than 11 percent.[1] The failure of the linear relations between Verdet constant and concentration and between magnetic rotatory dispersion and concentration is striking. This does not necessarily indicate a violation of the Schönrock rule of mixtures, however, for we must recall the possibility of H^1H^2O molecules in the solution. Assuming the equilibrium constant $K=(H^1H^2O)^2/(H^2_2O)(H^1_2O)=3.27$ as found by Topley and Eyring[4] we may compute from the known ratio of the number of heavy to light hydrogen atoms the percent of each type of molecule in a solution. This calculation results in the following concentrations for the 0.311 solution: 10.61 percent H^2_2O; 48.38 percent H^1_2O; 40.98 percent H^1H^2O. Assuming the linear relation between Verdet constant and concentration we may then calculate the apparent Verdet constant of a liquid consisting only of the H^1H^2O molecules. The values so obtained are 0.012955 and 0.015266 min./gauss-cm for the wave-lengths λ5893 and λ5460.7, respectively. These values are both 0.85 percent less than the corresponding values for ordinary water, indicating approximate independence of wave-length for the relative rotatory power as was seen above in the case of H^2_2O. The assumption of any other equilibrium constant ($K=4$, for example) does not lead to this result. This thus indicates a means of checking the equilibrium constant of such solutions by measurement of the Verdet constant at different wave-lengths. Further checks by measurements on several different concentrations are suggested.

The relative molecular rotatory power (Ω) of H^2_2O with respect to H^1_2O at 20°C for λ5893 and for λ5460.7 is 0.9640 assuming molecular weights of 20.027 and 18.014 for the respective molecules. Lack of data on the density of H^1H^2O prevents calculation of its molecular rotatory power.

The magnetic rotatory dispersion in the wave-length region used may also be obtained from the data. Expressed in min./g-cm per A the values for H^1_2O, H^2_2O, and H^1H^2O are, respectively, 5.39×10^{-6}; 5.18×10^{-6}; 5.35×10^{-6}.

Although the value measured for the Verdet constant of ordinary water (λ5893) agrees within the precision of measurements stated in the table with the value given in the *International Critical Tables*, this precision is stated for comparative purposes only and not for the absolute values.

The experimental work was done in the Ernest Kempton Adams laboratory of the Columbia University Department of Physics. We wish to express our great appreciation to Professors G. B. Pegram and H. W. Webb for the use of this laboratory and equipment. We are of course also greatly indebted to Dr. H. C. Urey and his assistants for the loan of the specimens of heavy water.

[4] B. Topley, and H. Eyring, J. Chem. Phys. **2**, 217 (1934); A. Farkas, and L. Farkas, J. Chem. Phys. **2**, 468 (1934).

Atomic Energy Relations. I*

R. F. BACHER† AND S. GOUDSMIT, *University of Michigan*

(Received August 10, 1934)

A simple method for the calculation of approximate energies of atomic levels is presented in this paper. It is based on the derivation of linear relations which express the unknown energy in terms of *observed* energy values of the atom and its ions. It is shown that the degree of approximation increases with the amount of experimental data available for use in the calculation and also how the best formulas can be obtained for each case. Several tables are given containing formulas for configurations involving s and p electrons. They are applied to the spectra of carbon, nitrogen and oxygen and the energy values so determined are compared with those known from observations. In an appendix the method of approximation is compared with the quantum mechanical perturbation method.

I. INTRODUCTION

THE energy states of a system consisting of several electrons in a central field can be found approximately by the use of the perturbation method in the solution of the wave equation. The problem of determining the energy states with an accuracy approaching that with which they are known experimentally is sufficiently complicated of solution, that at present it has been carried out for the two electron case only. For many electrons the problem has been solved in the first order by Slater[1] and calculations have been made for several elements with wave functions determined by the method of Hartree. These calculations, while remarkably good when the complexity of the problem is considered are still not accurate enough in general to be of much use in the prediction and the correlation of atomic energy states. For this purpose it is desirable to have an easier and more accurate way of obtaining the energy states.

In this article we shall develop approximate relations between the energy states of an atom and its ions. An unknown energy level can then be calculated by expressing it in terms of observed energy values. This is much less difficult than the direct quantum mechanical calculation because the relations derived here are simple linear expressions. Furthermore, the relations possess the favorable property that the degree of accuracy increases rapidly with the amount of experimental information used. In almost all important cases the results are sufficiently accurate to be of value for spectroscopic purposes whereas such accuracy can hardly ever be reached with other methods used at present for the calculation of energies.

The method by which observed energies are used for the prediction of unknown levels is based on principles which are also very simple. In a one-electron atom or ion (that is one electron outside of a core of closed shells), the observed energy levels give direct information about the binding energy of that outer electron. If we add an electron the observed energies of the two-electron ion compared with those of the one-electron ion give information about the change in energy due to the interaction between the two electrons. From the observed energies in three- and more-electron spectra further details about the interaction can be obtained and it is this information which is used for the calculation of unknown energies.

II. THE MANY PARTICLE PROBLEM

(a) Let us consider the one-particle problem, for example one electron outside a core of closed shells. We shall denote its quantum states by A, B, C, etc., and the energies to remove the particle by $W(A)$, $W(B)$, $W(C)$, etc. We add a particle and consider next the configuration AB of the two particle system.[2] If there were no

* This is the first of a series of articles on this subject. Later papers will contain relations in isoelectronic spectra, formulas for configurations involving other than s and p electrons, a special treatment of the cases in which electrons are "lacking" from a complete shell and other extensions of the method presented here.

† At present at Columbia University.

[1] J. C. Slater, Phys. Rev. **34**, 1293 (1929).

[2] For the present it is assumed that all degeneracies have been removed. It should further be noted that we assume that it is possible to ascribe each energy level to a definite configuration. This condition is fulfilled in all cases in which this method of approximation can be successfully applied.

interaction between the two particles the total energy to remove both would be

$$W_0(AB)=W(A)+W(B). \quad (1)$$

The energy actually observed, $W(AB)$, differs from this by an amount $w(AB)$ which we shall call "pair energy" and which is defined by the relation

$$W(AB)=W(A)+W(B)+w(AB). \quad (2)$$

The "pair energy" represents the influence of the interaction of the two particles on the total energy.

Let us consider three particles in the configuration ABC. If there were no interaction the total energy would be

$$W_0(ABC)=W(A)+W(B)+W(C). \quad (3)$$

This will of course be a very rough approximation to the energy actually observed, $W(ABC)$. By using the values of the "pair energies" one is led to a next approximation

$$W_1(ABC)=W(A)+W(B)+W(C)+w(AB)+w(AC)+w(BC)$$

or

$$W_1(ABC)=W(AB)+W(AC)+W(BC)-W(A)-W(B)-W(C). \quad (4)$$

The notation will be simplified by writing $\sum W(\alpha\beta)$ to indicate the sum of two-particle energies and $\sum W(\alpha)$ for the sum of one-particle energies, the sums to be extended over the states of the configuration such as in Eq. (4). In this notation Eq. (4) can be written

$$W_1(ABC)=\sum W(\alpha\beta)-\sum W(\alpha). \quad (5)$$

The right sides of Eqs. (4) of (5) contain only observed energies. This expression is often a good approximation to the actual energy $W(ABC)$. The difference between the actual energy and this approximation we shall call the "triple energy," $w(ABC)$. It is defined by the equation

$$W(ABC)=W(A)+W(B)+W(C)+w(AB)+w(AC)+w(BC)+w(ABC)$$

or

$$W(ABC)=\sum W(\alpha\beta)-\sum W(\alpha)+w(ABC). \quad (6)$$

The "triple energy" represents the change in the total energy due to the influence of the third particle on the interaction of the other two.

In the system of four particles we can set up three successive approximations $W_0(ABCD)$, $W_1(ABCD)$, and $W_2(ABCD)$ which we shall call "zeroth," "first," and "second approximation," respectively. W_0 uses only the one-electron energies, W_1 includes the "pair energies" and W_2 the "pair" and "triple energies." The expressions are

$$W_0(ABCD)=\sum W(\alpha), \quad (7)$$

$$W_1(ABCD)=\sum W(\alpha)+\sum w(\alpha\beta)=\sum W(\alpha\beta)-2\sum W(\alpha), \quad (8)$$

$$W_2(ABCD)=\sum W(\alpha)+\sum w(\alpha\beta)+\sum w(\alpha\beta\gamma)=\sum W(\alpha\beta\gamma)-\sum W(\alpha\beta)+\sum W(\alpha). \quad (9)$$

The difference between the last approximation and the energy actually observed gives the "quadruple energy," defined by

$$W(ABCD)=\sum W(\alpha)+\sum w(\alpha\beta)+\sum w(\alpha\beta\gamma)+w(ABCD). \quad (10)$$

The energy of a system containing five particles can be built up in much the same way as those of systems containing fewer particles. $W_3(ABCDE)$ appearing in this case for the first time contains in addition to the energy of the pairs and the triples also the energy of the quadruples.

$$W_0(ABCDE)=\sum W(\alpha), \quad (11)$$

$$W_1(ABCDE)=\sum W(\alpha\beta)-3\sum W(\alpha), \quad (12)$$

$$W_2(ABCDE)=\sum W(\alpha\beta\gamma)-2\sum W(\alpha\beta)+3\sum W(\alpha), \quad (13)$$

$$W_3(ABCDE)=\sum W(\alpha\beta\gamma\delta)-\sum W(\alpha\beta\gamma)+\sum W(\alpha\beta)-\sum W(\alpha). \quad (14)$$

It is clear that the procedure which has been followed above can be continued and thus extended to any desired number of particles. Indeed the approximate energy including the interaction in groups one less than the total number of particles may easily be written for the case of n particles.

$$W_{n-2}(A_1A_2\cdots A_n)=\sum W(\alpha_1\alpha_2\cdots\alpha_{n-1})$$
$$-\sum W(\alpha_1\alpha_2\cdots\alpha_{n-2})+\cdots$$
$$+(-1)^{n-1}\sum W(\alpha_1\alpha_2)+(-1)^n\sum W(\alpha_1). \quad (15)$$

The fact that in all important cases the "pair," "triple," "quadruple energies," etc., form a rapidly decreasing series is the reason for the usefulness of this method of approximation.

It has been tacitly assumed in the relations which have been developed above that it is possible to determine on which states of the $(f-1)$, $(f-2)$, etc., particle systems, a particular state of the f particle system is built. It is necessary to know for each state into what state of the single particle problem it will be transformed if the interaction between the particles is removed. Although this is always uniquely determined theoretically, there are cases where it is not known with certainty. For atoms, this happens when levels of different configurations lie so near together that the large perturbations make it difficult to assign configurations to the individual levels. For the important low energy states of atoms, this difficulty occurs infrequently.

A further difficulty which appears in the atomic problem when only the electrostatic interaction is considered, is the high degree of degeneracy. Due to this degeneracy, it seems at first impossible to determine for a multiplet of a configuration of equivalent electrons, on which multiplet of the ion it is built. This is purely a formal difficulty which can be overcome and it will be discussed later (section III) when the atomic problem is presented in greater detail.

(b) It has been shown in the preceding section how the energy states of the many particle problem can be related to those of the cases of successively less particles down to and including the one particle problem. It is frequently the case, however, that some of the energies which are needed for the determination are not known. In such a case it will be shown that the energy of the given many-particle problem can still be found (somewhat less accurately, to be sure) in terms of those which are known. Suppose that one wishes to express the energy of a state of the five particle problem in terms of those of four, three and two particles, without using the energies of the one particle problem. For this purpose we consider Eq. (9). In the five particle case there are four other equations similar to (9) which may be written for $W_2(ABCE)$, $W_2(ABDE)$, $W_2(ACDE)$ and $W_2(BCDE)$. With these five relations it is possible to eliminate the quantities $W(A)$, $W(B)$, $W(C)$, $W(D)$, and $W(E)$ from relation (14). In the result it is necessary to replace the approximate energy $W_2(ABCD)$ by the exact energy $W(ABCD)$, and similarly for the others, because the approximate energies involve a knowledge of the single particle energies. The result is given in (16), the energy of the five particle problem now being written $W_2'(ABCDE)$ due to the approximations that have been made.

$$W_2'(ABCDE)=3/4\sum W(\alpha\beta\gamma\delta)$$
$$-1/2\sum W(\alpha\beta\gamma)+1/4\sum W(\alpha\beta). \quad (16)$$

It is not necessary to go through this lengthy algebraic elimination to obtain (16). Since there are three coefficients which may be adjusted, we can fix them such that the 0th, 1st and 2nd approximations of both sides are identical. The number of approximations which can be balanced in this way depends entirely upon the number of coefficients on the right side of the equation and that may change according to the specific case considered. This observation leads to the following practical method of determining the coefficients. Let us first rewrite (16) with unknown coefficients as in (17).

$$W_2'(ABCDE)=x\sum W(\alpha\beta\gamma\delta)$$
$$-y\sum W(\alpha\beta\gamma)+z\sum W(\alpha\beta). \quad (17)$$

If the 0th order approximations are to be the same on both sides of (17) then the coefficients must be so adjusted that a particular state, say A, occurs the same number of times on each side. In the first sum there are four terms containing A, in the second sum six and in the last four, and A occurs once on the left side. This gives the numbers needed for (18).

$$(A) \quad 1=4x-6y+4z. \quad (18)$$

Proceeding similarly with a pair of states, for example (AB) and next with a group of three, (ABC), we get two more equations.

$$(AB) \quad 1=3x-3y+z, \tag{19}$$

$$(ABC) \quad 1=2x-y. \tag{20}$$

The solution of Eqs. (18), (19) and (20) gives the coefficients of (16).

The same method used above to determine the coefficients can be used to get an idea of the relative approximation of the formulas. Let us compare (13) and (16) which give $W_2(ABCDE)$ and $W_2'(ABCDE)$.

$$W_2(ABCDE)=\sum W(\alpha\beta\gamma)-2\sum W(\alpha\beta)+3\sum W(\alpha), \tag{13}$$

$$W_2'(ABCDE)=3/4\sum W(\alpha\beta\gamma\delta)-1/2\sum W(\alpha\beta\gamma)+1/4\sum W(\alpha\beta). \tag{16}$$

Each of these relations is a second approximation, that is, the interaction in groups of three as well as the interaction in pairs has been taken into account. $W_2'(ABCDE)$, however, is a somewhat better approximation. If we consider the interaction in groups of four, for example in a particular group of four $(ABCD)$, it is seen that the interaction of this group of four occurs once in $W(ABCDE)$. This interaction does not appear at all in the expression given above for $W_2(ABCDE)$ while it occurs with a factor 3/4 in the expression for $W_2'(ABCDE)$, so the latter is a better approximation to the exact energy $W(ABCDE)$ than $W_2(ABCDE)$.

In the practical application of these relations to atoms, one seldom knows the energies of all ions down to the single electron case. We shall now show that this method can be used when the energies are only those of the electrons outside the core. Let us take a group of three electrons in states A, B and C outside a core of two electrons in states D and E. The symbol * will be used to indicate an energy relative to the core, thus $W^*(ABC)$ is defined by (21).

$$W^*(ABC)=W(ABCDE)-W(DE). \tag{21}$$

From (4) we can write a relation for $W_1^*(ABC)$.

$$W_1^*(ABC)=W^*(AB)+W^*(AC)+W^*(BC)-W^*(A)-W^*(B)-W^*(C). \tag{22}$$

In terms of total energies including the core (22) may be written as (23).

$$W_1''(ABCDE)=W(ABDE)+W(ACDE)+W(BCDE)-W(ADE)-W(BDE)-W(CDE)+W(DE). \tag{23}$$

Since the energies of the singles and pairs cancel in this equation, it is a first approximation. In addition, all those groups of three which involve the core states D and E also cancel and the only one which is not considered is the triple $w(ABC)$. This triple energy is just the difference between the exact energy and the first approximation in the three electron problem, so it appears that, including terms of the second approximation, Eq. (22) which expresses the energies of the three electrons relative to the core, neglects the same interaction which is neglected in the problem of three electrons without a core. There are, however, in the problem including the core, several quadruple energies (those not containing both D and E) and of course the quintuple energy which are also neglected. Since these are in general considerably smaller than the triple energy which was neglected it is apparent that the energies may well be considered relative to the core, and the resulting equation may be expected to hold nearly as well as the similar equation for the same particles without core.

(c) In order to get an idea of the accuracy to be expected from the relations presented above, the method of approximations will be compared with the usual perturbation theory. Table I

TABLE I. *Relation of the energy corrections in the recurrence method to those in the perturbation method.*

Perturbation energies \ Energy corrections	Pairs	Triples	Quadruples	Quintuples	Etc.
1st order	x				
2nd order	x	x			
3rd order	x	x	x		
4th order	x	x	x	x	
etc.					

shows the relation between the two methods. The columns in this table give the energy corrections as they have been applied in this paper, first the pair energy, next the triples, etc. The rows list successively the energy corrections given by the ordinary perturbation theory. The energy correction which arises from the source

indicated at the head of a row or column is split up into all the individual parts, designated by crosses in that row or column. Thus, there is a contribution to the total pair energy from each order of the perturbation starting with the first. It is, indeed, immediately apparent that if the relation considered is a first approximation or better and if the *exact* energies of the two particle problem are used in that relation, then all the higher orders of the pair interaction have been included. It appears from Table I that the triple energy enters for the first time in the second order of the perturbation theory. It also appears that if the pair energy is considered then the *complete* first order of the perturbation theory is included. Similarly if the triple energy is considered then the complete second order of the perturbation theory is included, etc. The proof of these statements will be found in Appendix I. It will appear that the first approximation is expected to hold better than a first order calculation by the perturbation theory since the part of the second order which is included in the former is considerable.

IIIa. Absolute Atomic Energies

The recurrence method described in the preceding section will next be applied to the problem of atomic energy states. The present treatment is limited to those states involving s and p electrons; the states involving d electrons will be treated separately, later. It is essential for the application of the recurrence method to be able to correlate states of successive stages of ionization. The great degeneracy of the problem offers a serious complication. To overcome this complication it is necessary to introduce quantum numbers which describe the system with all degeneracy removed, and second to correlate these non-degenerate states with the degenerate states which are found from experiment. This involves no fundamental difficulties and can be carried out by a procedure which has already been used several times for atomic energy problems and which originated with the well-known sum relations of Pauli.

Let us consider the problem of an atom with electrostatic and spin-orbit interaction of the electrons neglected. If a magnetic field is introduced the degeneracy is completely removed and each electron is in a particular quantum state which is characterized by the quantum numbers n, l, s, m_s, and m_l representing for each electron, respectively, the total quantum number, the orbital quantum number, the spin quantum number and the projections of the spin and orbital momenta on the magnetic field. If we now introduce the electrostatic interaction between the electrons but still neglect the spin-orbit interaction (Russell-Saunders coupling), each state is characterized by a particular value of the resultant spin S, a particular value of the resultant orbital moment L and their magnetic projection M_S and M_L. It is necessary to find how the states characterized by the quantum numbers n, l, s, m_s and m_l of the individual electrons are related with those denoted by S, L, M_S and M_L.

Since M_S and M_L are the total projections of the spin and orbital momenta, we have the relations

$$M_S=\sum m_s, \quad M_L=\sum m_l. \tag{24}$$

The sums are taken over all the electrons. In a few cases where there is only one level with a given M_S and M_L, the sum relations (24) are sufficient to correlate these with the individual electron quantum states. In general, however, this correlation is somewhat more involved.

Two electrons

Let us first consider two equivalent p electrons. In Table II are gathered all the states of p^2 for which $M_S+M_L\geqq 0$. It is known that this configuration gives rise to multiplets ^3P ($S=1$, $L=1$), ^1D ($S=0$, $L=2$) and ^1S ($S=0$, $L=0$). The first two columns give the various states of the individual electrons omitting the quantum numbers n, l and s. If one of these states has energy $W(A)$ and $W(B)$ for the individual electrons then the particular combination of multiplets found in the last column has the energy $W(AB)$ as is indicated at the bottom of the table. The third column gives the total projections M_S and M_L. The last column gives the multiplet or combination of multiplets which can be assigned to each individual non-degenerate state. It is clear that each of the first four rows are states belonging to ^3P since only for ^3P is

TABLE II. *Configuration* p^2.

p m_s	p m_l	m_s	m_l	M_S	M_L	p^2 Multiplets
1/2	1	1/2	0	1	1	^3P
1/2	1	1/2	−1	1	0	^3P
1/2	0	1/2	−1	1	−1	^3P
−1/2	1	−1/2	0	−1	1	^3P
1/2	1	−1/2	1	0	2	^1D
1/2	1	−1/2	0	0	1	$1/2\,{}^3P+1/2\,{}^1D$
1/2	0	−1/2	1			$1/2\,{}^3P+1/2\,{}^1D$
1/2	1	−1/2	−1	0	0	$1/2\,{}^3P+1/6\,{}^1D+1/3\,{}^1S$
1/2	0	−1/2	0			$2/3\,{}^1D+1/3\,{}^1S$
1/2	−1	−1/2	1			$1/2\,{}^3P+1/6\,{}^1D+1/3\,{}^1S$
$W(A)$		$W(B)$		M_S	M_L	$W(AB)$

TABLE III. *Configuration* sp.

s m_s	p m_s	m_l	M_S	M_L	sp Multiplets
1/2	1/2	1	1	1	^3P
1/2	1/2	0	1	0	^3P
1/2	1/2	−1	1	−1	^3P
−1/2	−1/2	1	−1	1	^3P
1/2	−1/2	1	0	1	$1/2\,{}^3P+1/2\,{}^1P$
−1/2	1/2	1			$1/2\,{}^3P+1/2\,{}^1P$
1/2	−1/2	0	0	0	$1/2\,{}^3P+1/2\,{}^1P$
−1/2	1/2	0			$1/2\,{}^3P+1/2\,{}^1P$
$W(A)$	$W(B)$		M_S	M_L	$W(AB)$

there a projection $M_S=\pm 1$. Similarly the fifth state belongs to ^1D since only for ^1D is there a projection $M_L=2$. The assignment of the combination of multiplets to the states with $M_S=0$, $M_L=1$ and those with $M_S=0$, $M_L=0$ cannot be made in this way. To the first set belong ^3P and ^1D and to the second ^3P, ^1D and ^1S. The coefficients in the linear combinations which are correlated with each state can be found by standard quantum mechanical methods, for example by the famous ξ, η method. They can also be found directly from the recurrence method, as is demonstrated in Appendix 2. Since we neglect the spin-orbit interaction, it is not necessary to distinguish between the various J-levels of each multiplet. In order to find the energies it is not necessary to know the coefficients for the $M_S=0$, $M_L=1$ group since ^3P and ^1D are determined elsewhere, but for the determination of the coefficients in more complicated configurations directly from the recurrence method, it is necessary to know the proper linear combination for each individual state. It should be noted that the sum of the coefficients for each state, as well as the sum of the coefficients of a particular multiplet in a group with given M_S and M_L, is 1.

Table III gives the configuration sp, showing the linear combination of ^3P and ^1P for each non-degenerate state with $M_S+M_L\geqq 0$. All those states with $M_S=\pm 1$ are ^3P alone, while the two sets with $M_S=0$ are ^3P and ^1P together. The coefficients in the linear combinations can be found in a way similar to that used above for p^2 or they can be written directly as 1/2, since one state with $M_S=0$ and $M_L=1$ can be obtained from the other by changing the signs of the spins. The same is true for the two states with $M_S=0$ and $M_L=0$. It is not necessary to give a table for s^2 since this gives but one multiplet, ^1S. With the help of these tables for the two electron systems, we can now build configurations of more than two electrons, restricting ourselves at present to s electrons and to equivalent p electrons.

Three electrons

The first three electron system to be considered is the configuration p^3 which gives the multiplets ^4S, ^2D and ^2P. The first three columns of Table IV give the individual electron states A, B and C. The fifth column gives the linear combination of multiplets assigned to each state. The first state is uniquely ^4S and the second ^2D. The assignment of linear combinations to the other states is discussed in detail in Appendix 2. The last column of Table IV gives the sum of the two electron states $(AB)+(AC)+(BC)$ on which the three electron states are built. For example, if we consider the first state we find that each of the three possible two electron states belong to $p^2\,{}^3P$ in Table II.

The configuration sp^2 gives the multiplets ^4P, ^2P, ^2D and ^2S. The first three columns of Table V give the states of the individual electrons. The fifth column gives the linear combination of multiplets corresponding to each state. Each of the first three states is uniquely ^4P and each of the next two is uniquely ^2D. The proper linear combination to be assigned to the other states is discussed in Appendix 2. The last two columns give the multiplets of p^2 and sp, respectively, on which the three electron states of sp^2 are built.

Table VI gives the non-degenerate states of

TABLE IV. *Configuration p^3.*

p m_s	p m_l	p m_s	p m_l	p m_s	p m_l	M_S	M_L	p^3 Multiplets	Multiplets from pairs
1/2	1	1/2	0	1/2	−1	3/2	0	^4S	$3\,^3P$
1/2	1	1/2	0	−1/2	1	1/2	2	^2D	$3/2\,^3P+3/2\,^1D$
1/2	1	1/2	0	−1/2	0	1/2	1	$1/2\,^2D+1/2\,^2P$	$3/2\,^3P+7/6\,^1D+1/3\,^1S$
1/2	1	1/2	−1	−1/2	1			$1/2\,^2D+1/2\,^2P$	$3/2\,^3P+7/6\,^1D+1/3\,^1S$
1/2	1	−1/2	1	−1/2	0	−1/2	2	^2D	$3/2\,^3P+3/2\,^1D$
1/2	1	−1/2	1	−1/2	−1	−1/2	1	$1/2\,^2D+1/2\,^2P$	$3/2\,^3P+7/6\,^1D+1/3\,^1S$
1/2	0	−1/2	1	−1/2	0			$1/2\,^2D+1/2\,^2P$	$3/2\,^3P+7/6\,^1D+1/3\,^1S$
1/2	1	1/2	0	−1/2	−1	1/2	0	$1/3\,^4S+1/6\,^2D+1/2\,^2P$	$2\,^3P+2/3\,^1D+1/3\,^1S$
1/2	1	1/2	−1	−1/2	0			$1/3\,^4S+2/3\,^2D$	$2\,^3P+\,^1D$
1/2	0	1/2	−1	−1/2	1			$1/3\,^4S+1/6\,^2D+1/2\,^2P$	$2\,^3P+2/3\,^1D+1/3\,^1S$
$W(A)$		$W(B)$		$W(C)$		M_S	M_L	$W(ABC)$	$W(AB)+W(AC)+W(BC)$

TABLE V. *Configuration sp^2.*

s m_s	p m_s	p m_l	p m_s	p m_l	M_S	M_L	sp^2 Multiplets	Multiplets from pairs p^2	Multiplets from pairs sp
1/2	1/2	1	1/2	0	3/2	1	^4P	^3P	$2\,^3P$
1/2	1/2	1	1/2	−1	3/2	0	^4P	^3P	$2\,^3P$
1/2	1/2	0	1/2	−1	3/2	−1	^4P	^3P	$2\,^3P$
1/2	1/2	1	−1/2	1	1/2	2	^2D	^1D	$3/2\,^3P+1/2\,^1P$
−1/2	1/2	1	−1/2	1	−1/2	2	^2D	^1D	$3/2\,^3P+1/2\,^1P$
1/2	1/2	1	−1/2	0	1/2	1	$1/3\,^4P+1/2\,^2D+1/6\,^2P$	$1/2\,^3P+1/2\,^1D$	$3/2\,^3P+1/2\,^1P$
1/2	1/2	0	−1/2	1			$1/3\,^4P+1/2\,^2D+1/6\,^2P$	$1/2\,^3P+1/2\,^1D$	$3/2\,^3P+1/2\,^1P$
−1/2	1/2	1	1/2	0			$1/3\,^4P\quad\quad+2/3\,^2P$	^3P	$^3P+\ ^1P$
1/2	1/2	1	−1/2	−1	1/2	0	$1/3\,^4P+1/6\,^2D+1/6\,^2P+1/3\,^2S$	$1/2\,^3P+1/6\,^1D+1/3\,^1S$	$3/2\,^3P+1/2\,^1P$
1/2	1/2	0	−1/2	0			$2/3\,^2D\quad\quad+1/3\,^2S$	$2/3\,^1D+1/3\,^1S$	$3/2\,^3P+1/2\,^1P$
1/2	1/2	−1	−1/2	1			$1/3\,^4P+1/6\,^2D+1/6\,^2P+1/3\,^2S$	$1/2\,^3P+1/6\,^1D+1/3\,^1S$	$3/2\,^3P+1/2\,^1P$
−1/2	1/2	1	1/2	−1			$1/3\,^4P\quad\quad+2/3\,^2P$	^3P	$^3P+\ ^1P$
$W(A)$	$W(B)$		$W(C)$		M_S	M_L	$W(ABC)$	$W(BC)$	$W(AB)+W(AC)$

s^2p and is very simple since the two s electrons form a closed shell.

With the information available in Tables IV, V and VI it is now possible to write the energies of the three electron problem directly from Eq. (4). From the first state of Table IV, for example, we may write

$$W_1(p^3\,^4S)=3W(p^2\,^3P)-3W(p\,^2P). \quad (25)$$

It is important to note that these energies must be measured either with respect to the naked nucleus or to the core, if there is one inside the p electrons. From the second state of Table IV we have

TABLE VI. *Configuration s^2p.*

s m_s	s m_s	p m_s	p m_l	M_S	M_L	s^2p multiplets	Multiplets from pairs s^2	Multiplets from pairs sp
1/2	−1/2	1/2	1	1/2	1	^2P	^1S	$3/2\,^3P+1/2\,^1P$
1/2	−1/2	1/2	0	1/2	0	^2P	^1S	$3/2\,^3P+1/2\,^1P$
1/2	−1/2	−1/2	1	−1/2	1	^2P	^1S	$3/2\,^3P+1/2\,^1P$

$$W_1(p^3\,^2D)=3/2\ W(p^2\,^3P)+3/2\ W(p^2\,^1D)-3W(p\,^2P). \quad (26)$$

$W_1(p^3\,^2P)$ can easily be found by elimination from the other states which are known in Table IV. The energies of the various multiplets of p^3, sp^2, s^2p and s^2s' found in this way are presented in Table VII. The W's are omitted in Table VII for convenience.

TABLE VII. *Results for three electrons.*

	p^3		sp^2	s^2p	s^2s'
$p^3\,^4S=$	$3\,^3P$			$-3\,^3P$	
$^2D=$	$3/2\,^3P+3/2\,^1D$			$-3\,^3P$	
$^2P=$	$3/2\,^3P+5/6\,^1D+2/3\,^1S$			$-3\,^3P$	
$sp^2\,^4P=$	^3P		$2\,^3P$	$-2\,^3P$	$-^3S$
$^2P=$	^3P		$1/2\,^3P+3/2\,^1P$	$-2\,^3P$	$-^1S$
$^2D=$		^1D	$3/2\,^3P+1/2\,^1P$	$-2\,^3P$	$-^3S$
$^2S=$		^1S	$3/2\,^3P+1/2\,^1P$	$-2\,^3P$	$-^3S$
	s^3	ss'	sp	p	s and s'
$s^2p\,^3P=$	^3S				
$s^2s'\,^3S=$	^3S	$3/2\,^3S+1/2\,^1S$	$3/2\,^3P+1/2\,^1P$	$-^3P$	$-2\,^3S$
					$-2\,^1S\ -^3S'$

TABLE VIII. *Configuration* p^4.

p m_s	m_l	p m_s	m_l	p m_s	m_l	p m_s	m_l	M_S	M_L	Multiplets
1/2	1	1/2	0	1/2	−1	−1/2	1	1	1	^3P
1/2	1	1/2	0	1/2	−1	−1/2	0	1	0	^3P
1/2	1	1/2	0	1/2	−1	−1/2	−1	1	−1	^3P
−1/2	1	−1/2	0	−1/2	−1	1/2	−1	−1	1	^3P
1/2	1	1 2	0	−1/2	1	−1/2	0	0	2	^1D
1/2	1	1/2	−1	−1/2	1	−1/2	0	0	1	$1/2\ ^3P+1/2\ ^1D$
1/2	1	1/2	0	−1/2	1	−1/2	−1			$1/2\ ^3P+1/2\ ^1D$
1/2	1	1/2	−1	−1/2	1	−1/2	−1	0	0	$2/3\ ^1D+1/3\ ^1S$
1/2	1	1/2	0	−1/2	0	−1/2	−1			$1/2\ ^3P+1/6\ ^1D$ $+1/3\ ^1S$
1/2	0	1/2	−1	−1/2	1	−1/2	0			same
(A)		(B)		(C)		(D)				(ABCD)

Four electrons

The configuration p^4 gives rise to the multiplets ^3P, ^1D and ^1S. Table VIII shows the various states of the individual electrons and the linear combination of the multiplets which represents each state with $M_S+M_L \geqq 0$. Table IX is a similar table for the configuration sp^3. The energies of the various multiplets of p^4, sp^3 and also s^2p^2 in terms of the three, two and one electron energies are gathered in Table X. These relations include the single, pair and triple energies and should therefore be rather good approximations to the actual energies of the states. In the notation of the preceding section these relations are second approximations and should be written, for example, $W_2(p^4\ ^3P)$.

The relations given in Table X are suitable for finding the energy of a state of either the four, three, two or one electron system in terms of the others. It may happen that there is not sufficient information and it is desired to get a relation, say, between the four, three and two electron states. Relations which give the relative energies for this case can be obtained directly from Table X, by subtraction. If we wish the absolute energies we can get them in the following way for example for $p^4\ ^3P$. From Table X we have

$$W_2(p^4\ ^3P)=4/3\ (p^3\ ^4S)+5/3\ (p^3\ ^2D)+(p^3\ ^2P)-4(p^2\ ^3P)-5/3\ (p^2\ ^1D)-1/3\ (p^2\ ^1S)+4(p\ ^2P). \quad (27)$$

The energies given here are all relative to the closed shell beneath. If we rewrite Eq. (27) giving the energies relative to the ion $p\ ^2P$ we find that the terms $(p\ ^2P)$ cancel with the exception of a single one.

$$W_2^*(p^4\ ^3P)=4/3\ (p^3\ ^4S^*)+5/3\ (p^3\ ^2D^*)+(p^3\ ^2P^*)-4(p^2\ ^3P^*)-5/3\ (p^2\ ^1D^*)-1/3\ (p^2\ ^1S^*)+(p\ ^2P). \quad (28)$$

TABLE IX. *Configuration* sp^3.

s m_s	p m_s	m_l	p m_s	m_l	p m_s	m_l	M_S	M_L	sp^3 Multiplets
1/2	1/2	1	1/2	0	1/2	−1	2	0	^5S
1/2	1/2	1	1/2	0	−1/2	1	1	2	^3D
−1/2	1/2	1	1/2	0	−1/2	1	0	2	$1/2\ ^3D+1/2\ ^1D$
1/2	1/2	1	−1/2	0	−1/2	1			$1/2\ ^3D+1/2\ ^1D$
1/2	1/2	1	1/2	0	−1/2	0	1	1	$1/2\ ^3D$ $+1/2\ ^3P$
1/2	1/2	1	1/2	−1	−1/2	1			$1/2\ ^3D$ $+1/2\ ^3P$
1/2	1/2	1	1/2	0	−1/2	−1	1	0	$1/4\ ^5S+1/12\ ^3S+1/6\ ^3D$ $+1/2\ ^3P$
1/2	1/2	0	1/2	−1	−1/2	1			same
1/2	1/2	1	1/2	−1	−1/2	0			$1/4\ ^5S+1/12\ ^3S+2/3\ ^3D$
−1/2	1/2	1	1/2	0	1/2	−1			$1/4\ ^5S+3/4\ ^3S$
−1/2	1/2	1	1/2	0	−1/2	0	0	1	$1/4\ ^3D+1/4\ ^1D+1/4\ ^3P+1/4\ ^1P$
−1/2	1/2	1	1/2	−1	−1/2	1			same
1/2	1/2	1	−1/2	1	−1/2	−1			"
1/2	1/2	0	−1/2	1	−1/2	0			"
−1/2	1/2	1	1/2	0	−1/2	−1	0	0	$1/6\ ^5S+1/6\ ^3S+1/12\ ^3D+1/12\ ^1D+1/4\ ^3P+1/4\ ^1P$
−1/2	1/2	0	1/2	−1	−1/2	1			same
1/2	−1/2	1	−1/2	0	1/2	−1			"
1/2	−1/2	0	−1/2	−1	1/2	1			"
−1/2	1/2	1	1/2	−1	−1/2	0			$1/6\ ^5S+1/6\ ^3S+1/3\ ^3D+1/3\ ^1D$
1/2	−1/2	1	−1/2	−1	1/2	0			same
1/2	1/2	0	1/2	−1	−1/2	0	1	−1	$1/2\ ^3D$ $+1/2\ ^3P$
1/2	1/2	1	1/2	−1	−1/2	−1			$1/2\ ^3D$ $+1/2\ ^3P$
(A)	(B)		(C)		(D)				(ABCD)

TABLE X. *Results for four electrons.*

	p^2	sp^2	p^3	sp	p	s
$p^4\ {}^3P =$	$4/3\ {}^4S+5/3\ {}^3D+\ {}^1P$		$-4\ {}^3P-5/3\ {}^1D-1/3\ {}^1S$		$+4\ {}^3P$	
$\ {}^1D =$	$3\ {}^3D+\ {}^1P$		$-3\ {}^3P-8/3\ {}^1D-1/3\ {}^1S$		$+4\ {}^3P$	
$\ {}^1S =$	$4\ {}^3P$		$-3\ {}^3P-5/3\ {}^1D-4/3\ {}^1S$		$+4\ {}^3P$	
$sp^3\ {}^5S =$	${}^4S$	$+3\ {}^4P$	$-3\ {}^3P$	$-3\ {}^3P$	$+3\ {}^3P$	$+{}^5S$
$\ {}^3S =$	${}^4S$	$+1/3\ {}^4P+8/3\ {}^3P$	$-3\ {}^3P$	$-{}^3P-2\ {}^1P$	$+3\ {}^3P$	$+{}^3S$
$\ {}^3D =$	${}^2D$	$+4/3\ {}^4P+1/6\ {}^3P+3/2\ {}^2D$	$-3/2\ {}^3P-3/2\ {}^1D$	$-5/2\ {}^3P-1/2\ {}^1P$	$+3\ {}^3P$	$+{}^3S$
$\ {}^1D =$	${}^2D$	$+3/2\ {}^3P+3/2\ {}^1D$	$-3/2\ {}^3P-3/2\ {}^1D$	$-3/2\ {}^3P-3/2\ {}^1P$	$+3\ {}^3P$	$+{}^3S$
$\ {}^3P =$	${}^3P$	$+4/3\ {}^4P+1/6\ {}^3P+5/6\ {}^3D+2/3\ {}^5S$	$-3/2\ {}^3P-5/6\ {}^1D-2/3\ {}^1S$	$-5/2\ {}^3P-1/2\ {}^1P$	$+3\ {}^3P$	$+{}^3S$
$\ {}^1P =$	${}^3P$	$+3/2\ {}^3P+5/6\ {}^1D+2/3\ {}^3S$	$-3/2\ {}^3P-5/6\ {}^1D-2/3\ {}^1S$	$-3/2\ {}^3P-3/2\ {}^1P$	$+3\ {}^3P$	$+{}^3S$

	s^2p	sp^2	p^3	sp	s^2	p	s
$s^2p^3\ {}^3P =$	$2\ {}^3P$	$+4/3\ {}^4P+2/3\ {}^3P$	${}^3P$	$-3\ {}^3P-{}^1P$	${}^1S$	$+2\ {}^3P$	$+2\ {}^3S$
$\ {}^1D =$	$2\ {}^3P$	$+2\ {}^3D$	$-{}^1D$	$-3\ {}^3P-{}^1P$	${}^1S$	$+2\ {}^3P$	$+2\ {}^3S$
$\ {}^1S =$	$2\ {}^3P$	$+2\ {}^3S$	$-{}^1S$	$-3\ {}^3P-{}^1P$	${}^1S$	$+2\ {}^3P$	$+2\ {}^3S$

TABLE XI. *Configuration* sp^4.

s m_s	p m_s	m_l	p m_s	m_l	p m_s	m_l	p m_s	m_l	M_S	M_L	Multiplets
1/2	1/2	1	1/2	0	1/2	−1	−1/2	1	3/2	1	${}^4P$
1/2	1/2	1	1/2	0	−1/2	1	−1/2	0	1/2	2	${}^2D$
−1/2	1/2	1	1/2	0	1/2	−1	−1/2	1	1/2	1	$1/3\ {}^4P+2/3\ {}^2P$
1/2	1/2	1	1/2	0	−1/2	1	−1/2	−1			$1/3\ {}^4P+1/6\ {}^2P+1/2\ {}^2D$
1/2	1/2	1	1/2	−1	−1/2	1	−1/2	0			same
−1/2	1/2	1	1/2	0	1/2	−1	−1/2	0	1/2	0	$1/3\ {}^4P+2/3\ {}^2P$
1/2	1/2	1	1/2	0	−1/2	0	−1/2	−1			$1/3\ {}^4P+1/6\ {}^2P+1/6\ {}^2D+1/3\ {}^2S$
1/2	1/2	0	1/2	−1	−1/2	1	−1/2	0			same
1/2	1/2	1	1/2	−1	−1/2	1	−1/2	−1			$2/3\ {}^2D+1/3\ {}^2S$
(*A*)	(*B*)		(*C*)		(*D*)		(*E*)		M_S	M_L	(*ABCDE*)

Now it is possible to eliminate this state by using the relations for p^3 from Table VII. This can be done in a variety of ways since p^3 gives three multiplets[3] but if we use the relation for ${}^4S$ we find

$$W_2^*(p^4\ {}^3P)=1/3\ (p^3\ {}^4S^*)+5/3\ (p^3\ {}^2D^*)+(p^3\ {}^2P^*)-(p^2\ {}^3P^*)-5/3\ (p^2\ {}^1D^*)-1/3\ (p^2\ {}^1S^*). \quad (29)$$

This expression cannot be expected to be as accurate as (27) since (27) is a second approximation and we have obtained (29) by elimination with a first approximation. The accuracy of (29) will be about that of a first approximation relation such as those in Table VII. No table of the relations of this lower approximation is given, since they can be obtained directly from Tables VII and X by elimination. Furthermore, several relations can be obtained for each state and the most desirable one will depend upon the information available in the particular example at hand.

Five, six and seven electrons

In the set of five electron systems we consider the configurations sp^4, p^5 and s^2p^3. Table XI gives the individual electron states for sp^4 and the linear combination of the multiplets ${}^4P$, ${}^2P$, ${}^2D$ and ${}^2S$ which characterizes each state. Several states which give no additional information about the energies are omitted. The energy relations for the various states of sp^4, p^5 and s^2p^3 are given in the following equations.

sp^4 $$W_3(sp^4\ {}^4P)=(p^4\ {}^3P)+(sp^3)[5/4\ {}^5S+5/3\ {}^3D+{}^3P+1/12\ {}^3S]-(p^3)[4/3\ {}^4S+5/3\ {}^2D+{}^2P]-(sp^2)[11/3\ {}^4P+1/3\ {}^2P+5/3\ {}^2D+1/3\ {}^2S]+(p^2)[4\ {}^3P+5/3\ {}^1D+1/3\ {}^1S]+(sp)[7/2\ {}^3P+1/2\ {}^1P]-4(p\ {}^2P)-(s\ {}^2S),$$

[3] If we use any of the other relations the resulting equations, though different, are quite as good as (23). The relative accuracy of these different expressions depends on the relative accuracy of the relations used from Table VII.

$$W_3(sp^4\ {}^2P) = (p^4\ {}^3P) + (sp^3)[4/3\ {}^3S + 5/12\ {}^3D + 5/4\ {}^1D + 1/4\ {}^3P + 3/4\ {}^1P]$$
$$- (p^3)[4/3\ {}^4S + 5/3\ {}^2D + {}^2P] - (sp^2)[2/3\ {}^4P + 10/3\ {}^3P + 5/3\ {}^2D + 1/3\ {}^2S]$$
$$+ (p^2)[4\ {}^3P + 5/3\ {}^1D + 1/3\ {}^1S] + (sp)[2\ {}^3P + 2\ {}^1P] - 4(p\ {}^2P) - (s\ {}^2S),$$

$$W_3(sp^4\ {}^2D) = (p^4\ {}^1D) + (sp^3)[9/4\ {}^3D + 3/4\ {}^1D + 3/4\ {}^3P + 1/4\ {}^1P] - (p^3)[3\ {}^2D + {}^2P]$$
$$- (sp^2)[2\ {}^4P + {}^2P + 8/3\ {}^2D + 1/3\ {}^2S] + (p^2)[3\ {}^3P + 8/3\ {}^1D + 1/3\ {}^1S]$$
$$+ (sp)[3\ {}^3P + {}^1P] - 4(p\ {}^2P) - (s\ {}^2S),$$

$$W_3(sp^4\ {}^2S) = (p^4\ {}^1S) + (sp^3)[3\ {}^3P + {}^1P] - 4(p^3\ {}^2P) - (sp^2)[2\ {}^4P + {}^2P + 5/3\ {}^2D + 4/3\ {}^2S]$$
$$+ (p^2)[3\ {}^3P + 5/3\ {}^1D + 4/3\ {}^1S] + (sp)[3\ {}^3P + {}^1P] - 4(p\ {}^2P) - (s\ {}^2S),$$

p^5 $$W_3(p^5\ {}^2P) = (p^4)[3\ {}^3P + 5/3\ {}^1D + 1/3\ {}^1S] - (p^3)[2\ {}^4S + 5\ {}^2D + 3\ {}^2P]$$
$$+ (p^2)[6\ {}^3P + 10/3\ {}^1D + 2/3\ {}^1S] - 5(p\ {}^2P),$$

s^2p^3 $$W_3(s^2p^3\ {}^4S) = 3(s^2p^2\ {}^3P) + (sp^3)[5/4\ {}^5S + 3/4\ {}^3S] - 3(s^2p\ {}^2P) - (sp^2)[4\ {}^4P + 2\ {}^2P]$$
$$- (p^3\ {}^4S) + (s^2\ {}^1S) + (sp)[9/2\ {}^3P + 3/2\ {}^1P] + 3(p^2\ {}^3P) - 2(s\ {}^2S) - 3(p\ {}^2P),$$

$$W_3(s^2p^3\ {}^2D) = (s^2p^2)[3/2\ {}^3P + 3/2\ {}^1D] + (sp^3)[3/2\ {}^3D + 1/2\ {}^1D] - 3(s^2p\ {}^2P)$$
$$- (sp^2)[2\ {}^4P + 3\ {}^2D + {}^2P] - (p^3\ {}^2D) + (s^2\ {}^1S) + (sp)[9/2\ {}^3P + 3/2\ {}^1P]$$
$$+ (p^2)[3/2\ {}^3P + 3/2\ {}^1D] - 2(s\ {}^2S) - 3(p\ {}^2P),$$

$$W_3(s^2p^3\ {}^2P) = (s^2p^2)[3/2\ {}^3P + 5/6\ {}^1D + 2/3\ {}^1S] + (sp^3)[3/2\ {}^3P + 1/2\ {}^1P] - 3(s^2p\ {}^2P)$$
$$- (sp^2)[2\ {}^4P + {}^2P + 5/3\ {}^2D + 4/3\ {}^2S] - (p^3\ {}^2P) + (s^2\ {}^1S)$$
$$+ (sp)[9/2\ {}^3P + 3/2\ {}^1P] + (p^2)[3/2\ {}^3P + 5/6\ {}^1D + 2/3\ {}^1S] - 2(s\ {}^2S) - 3(p\ {}^2P).$$

The lower approximations can be found also for these configurations but since they can be obtained in the straightforward way described above for p^4 they are not given here.

Of the six electron configurations we consider sp^5, p^6 and s^2p^4. The energies of the various multiplets of these in terms of the energies of the higher ions, with all energies measured to the core beneath, are given in the following relations.

sp^5 $$W_4(sp^5\ {}^3P) = (p^5\ {}^2P) + (sp^4)[8/3\ {}^4P + 1/3\ {}^2P + 5/3\ {}^2D + 1/3\ {}^2S] - (p^4)[3\ {}^3P + 5/3\ {}^1D + 1/3\ {}^1S]$$
$$- (sp^3)[5/3\ {}^5S + 1/3\ {}^3S + 25/6\ {}^3D + 5/6\ {}^1D + 5/2\ {}^3P + 1/2\ {}^1P]$$
$$+ (p^3)[2\ {}^4S + 5\ {}^2D + 3\ {}^2P] + (sp^2)[14/3\ {}^4P + 4/3\ {}^2P + 10/3\ {}^2D + 2/3\ {}^2S]$$
$$- (p^2)[6\ {}^3P + 10/3\ {}^1D + 2/3\ {}^1S] - (sp)[4\ {}^3P + {}^1P] + 5(p\ {}^2P) + (s\ {}^2S),$$

$$W_4(sp^5\ {}^1P) = (p^5\ {}^2P) + (sp^4)[3\ {}^2P + 5/3\ {}^2D + 1/3\ {}^2S] - (p^4)[3\ {}^3P + 5/3\ {}^1D + 1/3\ {}^1S]$$
$$- (sp^3)[2\ {}^3S + 5/2\ {}^3D + 5/2\ {}^1D + 3/2\ {}^3P + 3/2\ {}^1P] + (p^3)[2\ {}^4S + 5\ {}^2D + 3\ {}^2P]$$
$$+ (sp^2)[2\ {}^4P + 4\ {}^2P + 10/3\ {}^2D + 2/3\ {}^2S] - (p^2)[6\ {}^3P + 10/3\ {}^1D + 2/3\ {}^1S]$$
$$- (sp)[3\ {}^3P + 2\ {}^1P] + 5(p\ {}^2P) + (s\ {}^2S),$$

p^6 $$W_4(p^6\ {}^1S) = 6(p^5\ {}^2P) - (p^4)[9\ {}^3P + 5\ {}^1D + {}^1S] + (p^3)[4\ {}^4S + 10\ {}^2D + 6\ {}^2P]$$
$$- (p^2)[9\ {}^3P + 5\ {}^1D + {}^1S] + 6(p\ {}^2P),$$

s^2p^4 $W_4(s^2p^4\,{}^3P) = (s^2p^3)[4/3\,{}^4S+5/3\,{}^2D+{}^2P]+(sp^4)[4/3\,{}^4P+2/3\,{}^2P]$
$-(p^4\,{}^3P)-(s^2p^2)[4\,{}^3P+5/3\,{}^1D+1/3\,{}^1S]-(sp^3)[5/3\,{}^5S+{}^3S+5/2\,{}^3D+5/6\,{}^1D$
$+3/2\,{}^3P+1/2\,{}^1P]+4(s^2p\,{}^2P)+(p^3)[4/3\,{}^4S+5/3\,{}^2D+{}^2P]$
$+(sp^2)[16/3\,{}^4P+8/3\,{}^2P+10/3\,{}^2D+2/3\,{}^2S]-(s^2\,{}^1S)-(p^2)[4\,{}^3P+5/3\,{}^1D+1/3\,{}^1S]$
$-(sp)[6\,{}^3P+2\,{}^1P]+2(s\,{}^2S)+4(p\,{}^2P),$

$W_4(s^2p^4\,{}^1D) = (s^2p^3)[3\,{}^2D+{}^2P]+2(sp^4\,{}^2D)-(p^4\,{}^1D)-(s^2p^2)[3\,{}^3P+8/3\,{}^1D+1/3\,{}^1S]$
$-(sp^3)[9/2\,{}^3D+3/2\,{}^1D+3/2\,{}^3P+1/2\,{}^1P]+4(s^2p\,{}^2P)+(p^3)[3\,{}^2D+{}^2P]$
$+(sp^2)[4\,{}^4P+2\,{}^2P+16/3\,{}^2D+2/3\,{}^2S]-(s^2\,{}^1S)-(p^2)[3\,{}^3P+8/3\,{}^1D+1/3\,{}^1S]$
$-(sp)[6\,{}^3P+2\,{}^1P]+2(s\,{}^2S)+4(p\,{}^2P),$

$W_4(s^2p^4\,{}^1S) = 4(s^2p^3\,{}^2P)+2(sp^4\,{}^2S)-(p^4\,{}^1S)-(s^2p^2)[3\,{}^3P+5/3\,{}^1D+4/3\,{}^1S]-(sp^3)[6\,{}^3P+2\,{}^1P]$
$+4(s^2p\,{}^2P)+4(p^3\,{}^2P)+(sp^2)[4\,{}^4P+2\,{}^2P+10/3\,{}^2D+8/3\,{}^2S]$
$-(s^2\,{}^1S)-(p^2)[3\,{}^3P+5/3\,{}^1D+4/3\,{}^1S]-(sp)[6\,{}^3P+2\,{}^1P]+2(s\,{}^2S)+4(p\,{}^2P).$

For the configuration (s^2p^5) we have

s^2p^5 $W_5(s^2p^5\,{}^2P) = (s^2p^4)[3\,{}^3P+5/3\,{}^1D+1/3\,{}^1S]+(sp^5)[3/2\,{}^3P+1/2\,{}^1P]-(s^2p^3)[2\,{}^4S+5\,{}^2D+3\,{}^2P]$
$-(sp^4)[4\,{}^4P+2\,{}^2P+10/3\,{}^2D+2/3\,{}^2S]-(p^5\,{}^2P)+(s^2p^2)[6\,{}^3P+10/3\,{}^2D+2/3\,{}^2P]$
$+(sp^3)[5/2\,{}^5S+3/2\,{}^3S+15/2\,{}^3D+5/2\,{}^1D+9/2\,{}^3P+3/2\,{}^1P]$
$+(p^4)[3\,{}^3P+5/3\,{}^1D+1/3\,{}^1S]-5(s^2p\,{}^2P)-(sp^2)[8\,{}^4P+4\,{}^2P+20/3\,{}^2D+4/3\,{}^2S]$
$-(p^3)[2\,{}^4S+5\,{}^2D+3\,{}^2P]+(s^2\,{}^1S)+(sp)[15/2\,{}^3P+5/2\,{}^1P]$
$+(p^2)[6\,{}^3P+10/3\,{}^1D+2/3\,{}^1S]-2(s\,{}^2S)-5(p\,{}^2P).$

IIIb. Inter-Multiplet Separations

Relations have been developed above to give the absolute values of energy states in terms of those of higher ions. It is frequently the case among known energy states that the absolute values of several ions in succession are not known. Still it is desirable to know the relative separations in such cases. These can be obtained easily and directly for all the configurations which are studied above by subtraction of relations for states of the same configuration. Due to the equality of the sums of the coefficients for each configuration which occurs, these difference relations can always be written in terms of the energy differences between multiplets in the higher ions.

It is also useful to have these difference relations in lower approximation. For example, the direct differences of the relations given above for sp^4 give the separation of two multiplets in terms of multiplet differences in sp^3, p^4, sp^2, p^3, sp and p^2. A lower approximation can be found which gives the same separation in terms of the same differences in sp^3, p^4, sp^2 and p^3. We find the coefficients as in section IIb.

$$W_3'(ABCDE) = 2/3\sum W(\alpha\beta\gamma\delta) - 1/3\sum W(\alpha\beta\gamma) + 1/3\sum W(\alpha). \tag{30}$$

If we subtract two such expressions for different multiplets of the same configuration we find that the actual differences are the same as in the next higher approximation but all are multiplied by the coefficients in (30). The difference relations for the various configurations discussed above are collected below. Since the differences are all given from the lowest level of the configuration any other difference can be obtained by one subtraction. Some of the other differences give much simpler relations.

p^3 $(p^3)[^4S-{}^2D]=(p^3)3/2\ (^3P-{}^1D)$,

$(p^3)[^4S-{}^2P]=(p^3)[5/6\ (^3P-{}^1D)+2/3\ (^3P-{}^1S)]$,

sp^2 $(sp^2)[^4P-{}^2P]=(sp)3/2\ [^3P-{}^1P]$,

$(sp^2)[^4P-{}^2D]=(p^2)[^3P-{}^1D]+(sp)1/2\ [^3P-{}^1P]$,

$(sp^2)[^4P-{}^2S]=(p^2)[^3P-{}^1S]+(sp)1/2\ [^3P-{}^1P]$

p^4 $(p^4)[^3P-{}^1D]=(p^3)4/3\ [^4S-{}^2D]-(p^2)[^3P-{}^1D]$,

$(p^4)[^3P-{}^1S]=(p^3)[4/3\ (^4S-{}^2P)+5/3\ (^2D-{}^2P)]-(p^2)[^3P-{}^1S]$.

Next lower approximation:

$(p^4)[^3P-{}^1D]=1/2\ (p^3)4/3\ [^4S-{}^2D]$,

$(p^4)[^3P-{}^1S]=1/2\ (p^3)[4/3\ (^4S-{}^2P)+5/3\ (^2D-{}^2P)]$,

sp^3 $(sp^3)[^5S-{}^3S]=(sp^2)8/3\ [^4P-{}^2P]-(sp)2[^3P-{}^1P]$,

$(sp^3)[^5S-{}^3D]=(p^3)[^4S-{}^2D]+(sp^2)[1/6\ (^4P-{}^2P)+3/2\ (^4P-{}^2D)]$
$-(p^2)3/2\ [^3P-{}^1D]-(sp)1/2\ [^3P-{}^1P]$,

$(sp^3)[^5S-{}^1D]=(p^3)[^4S-{}^2D]+(sp^2)[3/2\ (^4P-{}^2P)+3/2\ (^4P-{}^2D)]$
$-(p^2)3/2\ [^3P-{}^1D]-(sp)3/2\ [^3P-{}^1P]$,

$(sp^3)[^5S-{}^3P]=(p^3)[^4S-{}^2P]+(sp^2)[1/6\ (^4P-{}^2P)+5/6\ (^4P-{}^2D)+2/3\ (^4P-{}^2S)]$
$-(p^2)[5/6\ (^3P-{}^1D)+2/3\ (^3P-{}^1S)]-(sp)1/2\ [^3P-{}^1P]$,

$(sp^3)[^5S-{}^1P]=(p^3)[^4S-{}^2P]+(sp^2)[3/2\ (^4P-{}^2P)+5/6\ (^4P-{}^2D)+2/3\ (^4P-{}^2S)]$
$-(p^2)[5/6\ (^3P-{}^1D)+2/3\ (^3P-{}^1S)]-(sp)3/2\ [^3P-{}^1P]$.

The next lower approximation is obtained from the above by dropping those terms in two electrons (sp and p^2) and multiplying the terms in three electrons by a factor 1/2. For example, for $^5S-{}^3D$ we have

$$(sp^3)[^5S-{}^3D]=1/2\ (p^3)[^4S-{}^2D]+1/2\ (sp^2)[1/6\ (^4P-{}^2P)+3/2\ (^4P-{}^2D)],$$

s^2p^2 $(s^2p^2)[^3P-{}^1D]=(sp^2)[4/3\ (^4P-{}^2D)+2/3\ (^2P-{}^2D)]-(p^2)[^3P-{}^1D]$,

$(s^2p^2)[^3P-{}^1S]=(sp^2)[4/3\ (^4P-{}^2S)+2/3\ (^2P-{}^2S)]-(p^2)[^3P-{}^1S]$.

For the next lower approximation drop the terms in p^2 and multiply those in sp^2 by 1/2.

sp^4 $(sp^4)[^4P-{}^2P]=(sp^3)[5/4\ (^5S-{}^3S)+5/4\ (^3D-{}^1D)+3/4\ (^3P-{}^1P)]$
$-(sp^2)3[^4P-{}^2P]+(sp)3/2\ [^3P-{}^1P]$,

$(sp^4)[^4P-{}^2D]=(p^4)[^3P-{}^1D]+(sp^3)[1/4\ (^3P-{}^1P)+1/12\ (^3S-{}^3D)+3/4\ (^5S-{}^1D)$
$+1/2\ (^5S-{}^3D)]-(p^3)4/3\ [^4S-{}^2D]-(sp^2)[(^4P-{}^2D)+2/3\ (^4P-{}^2P)]$
$+(p^2)[^3P-{}^1D]+(sp)1/2\ [^3P-{}^1P]$.

$(sp^4)[^4P-{}^2S]=(p^4)[^3P-{}^1S]+(sp^3)[5/3\ (^3D-{}^3P)+1/3\ (^5S-{}^3P)+11/12\ (^5S-{}^1P)$
$+1/12\ (^3S-{}^1P)]-(p^3)[4/3\ (^4S-{}^2P)+5/3\ (^2D-{}^2P)]$
$-(sp^2)[2/3\ (^4P-{}^2P)+(^4P-{}^2S)]+(p^2)[^3P-{}^1S]+(sp)1/2\ [^3P-{}^1P]$.

To obtain the next lower approximation drop the terms in sp and p^2 and multiply those in p^4 and sp^3 by 2/3 and those in p^3 and sp^2 by 1/3. For the lowest approximation drop the terms in p^3 and sp^2 as well and multiply those in p^4 and sp^3 by 1/3.

$$s^2p^3 \quad (s^2p^3)[^4S-{}^2D]=(s^2p^2)3/2\,[^3P-{}^1D]+(sp^3)[5/4\,(^5S-{}^3D)+1/4\,(^3S-{}^3D)+1/2\,(^3S-{}^1D)]$$
$$-(sp^2)[2(^4P-{}^2D)+(^2P-{}^2D)]-(p^3)[^4S-{}^2D]+(p^2)3/2\,[^3P-{}^1D],$$
$$(s^2p^3)[^4S-{}^2P]=(s^2p^2)[5/6\,(^3P-{}^1D)+2/3\,(^3P-{}^1S)]+(sp^3)[5/4\,(^5S-{}^3P)+1/4\,(^3S-{}^3P)$$
$$+1/2\,(^3S-{}^1P)]-(sp^2)[5/3\,(^4P-{}^2D)+1/3\,(^4P-{}^2S)+(^2P-{}^2S)]$$
$$-(p^3)[^4S-{}^2P]+(p^2)[5/6\,(^3P-{}^1D)+2/3\,(^3P-{}^1S)].$$

Follow the same procedure as for sp^4 to obtain the lower approximations.

$$sp^5 \quad (sp^5)[^3P-{}^1P]=(sp^4)8/3\,[^4P-{}^2P]-(sp^3)[5/3\,(^5S-{}^3S)+5/3\,(^3D-{}^1D)+(^3P-{}^1P)]$$
$$+(sp^2)8/3\,[^4P-{}^2P]-(sp)[^3P-{}^1P].$$

To obtain the next lower approximation drop the two electron terms and multiply all five electron terms by 3/4, all four electron terms by 1/2 and all three electron terms by 1/4. For the next approximation drop the three electron terms as well and multiply the five electron terms by 1/2 and the four electron terms by 1/6. For the lowest approximation drop the four electron terms also and multiply the five electron terms by 1/4.

$$s^2p^4 \quad (s^2p^4)[^3P-{}^1D]=(s^2p^3)4/3\,[^4S-{}^2D]+(sp^4)[4/3\,(^4P-{}^2D)+2/3\,(^2P-{}^2D)]-(p^4)[^3P-{}^1D]$$
$$-(s^2p^2)[^3P-{}^1D]-(sp^3)[5/3(^5S-{}^3D)+1/3\,(^3S-{}^3D)+2/3\,(^3S-{}^1D)]$$
$$+(p^3)4/3\,[^4S-{}^2D]+(sp^2)[4/3\,(^4P-{}^2D)+2/3\,(^2P-{}^2D)]-(p^2)[^3P-{}^1D],$$
$$(s^2p^4)[^3P-{}^1S]=(s^2p^3)[4/3\,(^4S-{}^2P)+5/3\,(^2D-{}^2P)]+(sp^4)[4/3\,(^4P-{}^2S)+2/3\,(^2P-{}^2S)]$$
$$-(p^4)[^3P-{}^1S]-(s^2p^2)[^3P-{}^1S]-(sp^3)[5/3\,(^5S-{}^3P)+(^3S-{}^3P)$$
$$+3/2\,(^3D-{}^1P)+(^3D-{}^3P)+5/6\,(^1D-{}^3P)]+(p^3)[4/3\,(^4S-{}^2P)+5/3\,(^2D-{}^2P)]$$
$$+(sp^2)[4/3\,(^4P-{}^2S]+2/3\,(^2P-{}^2S)]-(p^2)[^3P-{}^1S].$$

To obtain the lower approximations follow the same procedure as for sp^5.

IV. Examples

(a) The relations developed in the preceding section IIIa express the energy of a given state of an atom or ion in terms of the energy states of the higher ions. In these relations we may use the values of the calculated energies[4] or we may use experimentally known states and from them determine other states. It is the latter application which is most useful since the energies have, for the greater part, been calculated only to the first order by the perturbation method and in general do not agree very well with the observed states. The examples considered here will be confined to the elements O, N and C largely because the beautiful work of Edlén[5] has made the energy states of these elements so fully and accurately known. Table XII gives the energies of various states of O, N and C relative to the $1s^2$ core, as taken from the work of Edlén. The spin-orbit separations have been reduced to the center of gravity.

Three electrons

Let us consider the state $2s2p^2\,{}^2P$. From Table VII we find the following relation

[4] For example, if the Slater relations are known for two electrons they can be found for several electrons by using the relations which give the many electron energies in terms of those of two electrons.

[5] B. Edlén, Zeits. f. Physik **84**, 746 (1933). This is a condensed work. For complete information see Nova Acta Regiae Societatis Scientiarum Upsaliensis, Series IV, Vol. 9, No. 6.

TABLE XII. *Energies to the $1s^2$ shell for oxygen, nitrogen and carbon.*

Configuration and State	O	N	C	Configuration and State	O	N	C
$s^2p^4\ ^3P$	3,492,650			$p^4\ ^3P$	2,815,781		
^1D	3,476,859			^1D	2,801,355		
^1S	3,458,934			^1S	2,756,342		
$sp^3\ ^3P^o$	3,369,401			$s^1p\ ^3P^o$	2,656,580	1,796,546	1,102,954
$^1P^o$							
				$sp^3\ ^4P$	2,585,463	1,739,779	1,059,945
$s^2p^3\ ^4S^o$	3,382,889	2,152,548		^2P	2,476,194	1,650,703	992,344
$^2D^o$	3,356,073	2,133,325		^2D	2,529,895	1,695,636	1,028,064
$^2P^o$	3,342,422	2,123,708		^2S	2,492,471	1,665,659	1,006,502
$sp^4\ ^4P$	3,262,959	2,064,415		$p^3\ ^4S^o$	2,425,562	1,610,257	960,952
^2P	3,170,240			$^2D^o$	2,401,669	1,593,583	952,531
^2D	3,216,898			$^2P^o$	2,367,817	1,566,255	934,252
^2S	3,187,179						
				$s^1\ ^1S$	2,032,441	1,414,037	906,337
$s^2p^2\ ^3P$	3,099,440	2,035,246	1,193,783				
^1D	3,079,374	2,020,019	1,183,619	$sp\ ^3P^o$	1,950,515	1,347,114	853,969
^1S	3,056,461	2,002,648	1,172,164	$^1P^o$	1,873,643	1,283,342	803,825
$sp^3\ ^5S^o$	3,039,750	1,988,667	(1,159,500)	$p^2\ ^3P$	1,819,006	1,238,794	768,912
$^3S^o$	2,902,558	1,880,205	1,088,013	^1D	1,800,719	1,225,152	760,463
$^3D^o$	2,979,606	1,943,091	1,129,724	^1S	1,744,532	1,178,667	723,818
$^1D^o$	2,912,595	1,891,146					
$^3P^o$	2,957,258	1,926,115	1,118,557	$s\ ^2S$	1,114,009	789,538	520,178
$^1P^o$	2,889,186	1,868,569					
				$p\ ^2P^o$	1,017,280	708,901	455,523

TABLE XIII. *Three electron configurations. Absolute values to normal state of next ion.*

Configuration and State	O			N			C		
	Calc.	Obs.	Diff.	Calc.	Obs.	Diff.	Calc.	Obs.	Diff.
$2s^22p\ ^2P$	617,295	624,139	6,844	374,365	382,509	8,144	187,067	196,617	9,550
$2s2p^3\ ^4P$	539,026	553,022	13,996	311,645	325,742	14,097	139,289	153,608	14,319
^2P	423,717	443,753	20,036	215,987	236,666	20,679	64,073	86,007	21,934
^2D	482,302	497,454	15,152	266,117	281,599	15,482	105,768	121,728	15,960
^2S	426,115	460,030	33,915	219,632	251,622	31,990	69,123	100,165	31,042
$2p^3\ ^4S$	372,737	393,121	20,384	175,642	196,220	20,578	33,830	54,615	20,785
^2D	345,305	369,228	23,923	155,179	179,546	24,367	21,155	46,194	24,039
^2P	307,850	335,376	27,524	124,189	152,218	28,029	−3,272	27,915	31,187
$(2s^2)2p^3\ ^4S$	261,376	283,244	21,868	94,803	117,214	22,411			
^2D	231,271	256,428	25,157	71,961	97,991	26,030			
^2P	216,001	242,777	26,776	60,382	88,374	27,992			

$$(sp^2)\ ^2P=(p^2)\ ^3P+(sp)[1/2\ ^3P+3/2\ ^1P]$$
$$-2(p)\ ^2P-(s)\ ^2S.$$

If we use this relation to determine the state $(sp^2)\ ^2P$, then we insert the correct energies on the right side from Table XII. For O IV we find $(sp^2)\ ^2P=2{,}456{,}158$ cm^{-1} with respect to the $1s^2$ shell while the observed energy is 2,476,194 cm^{-1}. The discrepancy between the two is 20,036 cm^{-1}. This appears to be a rather small error compared to the total energy to the shell beneath and it is even fairly small compared to the interaction energy of the three electrons, 672,375 cm^{-1}. Under the usual criteria for a perturbation problem this would be declared to be a good approximation. Unfortunately, however, we are seldom interested in the total energy but rather in the "absolute energy" to the normal state of the next ion. This absolute value calculated is 423,717 and observed 443,753 cm^{-1}. This error in the calculated value is due to the omission of the triple energy and we may therefore expect the discrepancy for the three electron cases to be greater than for more electrons where the triple energies are included. The results for configurations $2s^22p$, $2s2p^2$, $2p^3$ and $(2s^2)2p^3$ (i.e., $2p^3$ outside a closed $2s^2$ shell), giving the calculated and observed absolute values to the normal state of the next ion and their differences, are presented in Table XIII. The difference between the calculated and observed values (the triple energy) for a given state is nearly constant[6] with

[6] The regularities of the pair and triple energies as well as the total electrostatic interaction as a function of Z will be discussed in a later paper.

TABLE XIV. *The four electron configurations. Absolute values to normal state of next ion.*

Configuration and State	O			N			C		
	Calc.	Obs.	Obs.-Calc.	Calc.	Obs.	Obs.-Calc.	Calc.	Obs.	Obs.-Calc.
$2s^22p^3\ {}^3P$	440,345	442,602	2257	235,965	238,584	2619	88,155	90,786	2631
^1D	420,342	422,536	2194	220,707	223,357	2650	77,910	80,622	2712
^1S	401,681	399,623	−2058	207,238	205,986	−1252	71,431	69,167	−2264
$2s2p^4\ {}^5S$	382,399	382,912	513	191,449	192,005	556	55,894	——	——
^1S	244,756	245,720	964	81,456	83,543	2087	−24,412	−14,984	9428
^3D	322,816	322,768	−48	146,062	146,429	367	26,053	26,727	674
^1D	253,993	255,757	1764	91,066	94,484	3418	−14,027	——	——
^3P	301,469	300,420	−1049	129,740	129,453	−287	17,827	15,560	−2267
^1P	232,648	232,348	−300	74,744	71,907	−2837	−22,326	——	——
$2p^4\ {}^3P$	158,228	158,943	715	18,191	——				
^1D	144,657	144,517	−140	9,603	——				
^1S	99,288	99,504	216	−25,896	——				
$(2s^2)2p^4\ {}^3P$	108,516	109,761	1245						
^1D	92,827	93,970	1143						
^1S	74,787	76,045	1258						

Z. Thus if an adjacent element is known the actual correction (triple energy) can be extrapolated with considerable accuracy.

Four electrons

Since the triple energies are included in the relations for four electrons we expect them to agree better with the experimentally determined states and indeed this proves to be the case. Table XIV gives the absolute energies (to the normal state of the next ion) of the various multiplets of the configurations $2s^22p^2$, $2s2p^3$, $2p^4$ and $(2s^2)2p^4$ as determined from the relations developed above and as observed, together with their differences. The discrepancy for s^2p^2 in the absolute values is about 2500 cm^{-1}. The relative value $^3P-{}^1D$ is, however, within 100 cm^{-1} for all three elements. The $^1D-{}^1S$ separation has a larger discrepancy than the absolute values. It is interesting to note how the differences (observed minus calculated) decrease with increasing Z, with the exception of ^1S for N. The configuration sp^3 fits better than s^2p^2 except for one or two multiplets in N and C which are not far from the ionization limit. In general we can expect these relations to hold best for the low terms of high multiplicity since the higher orders are not as important.[7] In C, the $sp^3\ {}^5S$ state, which is important as the lowest tetravalent state, has been predicted at 55,894 cm^{-1}. This is 34,994 cm^{-1} or 4.32 electron-volts above the normal state of C. The multiplets of p^4 (O III) agree somewhat better than either of the other configurations and for $(2s^2)2p^4$ (normal state of O I), the absolute values are all about 1200 cm^{-1} too small, thus making the separations check with a maximum error of about 100 cm^{-1}. The error of only 15 cm^{-1} in the $^3P-{}^1S$ separation is certainly fortuitous.

Five and six electrons

The ordinary absolute values with respect to the normal state of the next ion, of the multiplets of configurations $2s^22p^3$ of O and N and of $2s2p^4$ and $2s^22p^4$ of O, determined by the methods above, the values obtained experimentally, and the differences between these are presented in Table XV. It has been pointed out

TABLE XV. *Five and six electron configurations. Absolute values to normal state of next ion.*

Configuration and State	O			N		
	Calc.	Obs.	Obs.-Calc.	Calc.	Obs.	Obs.-Calc.
$2s^22p^2\ {}^4S$	283,121	283,244	123	117,640	117,214	−426
^2D	256,019	256,428	409	98,583	97,991	−592
^2P	241,802	242,777	975	86,558	88,374	1816
$2s2p^4\ {}^4P$	162,775	163,314	539			
^2P	68,964	70,595	1631			
^2D	115,860	117,253	1393			
^2S	85,804	87,534	1730			
$2s^22p^4\ {}^3P$	111,038	109,761	−1277			
^1D	95,472	93,970	−1502			
^1S	78,465	76,045	−2420			

that the methods used here are more accurate the more electrons there are considered: thus p^4 is better than p^3. This does not go on indefinitely, however, since as more electrons are

[7] It is possible to apply these relations to the determination of the energy states of negative ions. The higher orders, however, may be important and the results therefore may not be very accurate. For example, one finds that O should have an electron affinity in the $2p^3$ state of about 8000 cm^{-1} or about 1 e. volt, whereas Lozier (Washington meeting 1934) gives 2.2±0.2 e. volts.

added the 0th approximation recedes further from the actual problem and higher orders become larger. The percentage error on the total energy measured to the closed shell beneath will continue to decrease but the actual error may not. There are also other perturbing effects due to spin-orbit interaction which become apparent in these higher approximations. The absolute energies calculated for $2s^22p^4$ of O I are enough greater than the energies obtained when only the $2p^4$ group was considered that the differences between the observed and calculated values have negative signs, and indeed the deviations are not as small as they are for $2p^4$. This is a case in which the actual size of the first term not considered in the approximation is higher for s^2p^4 than for p^4, in spite of the fact that the former is a higher approximation.

The atomic energy relations developed here have been used in the examples given above to calculate the absolute energies of atoms and ions in terms of the energies of higher ions. The spectroscopist is generally interested in the reverse process and these relations can be used as well for this purpose. Let us consider $(2s^2)2p^4$ of O I and suppose that we wish to find the absolute value of $2s^22p\,^3P$ in O IV. The energies of all the states which were used in the relations for $2p^4$ were with respect to the $2s^2$ shell but if we do not know the O IV states we would know the states of the lower ions only with respect to $2s^22p\,^3P_1$. Using energies to this limit (indicated by a prime) we can rewrite the relation for $(2s^2)2p^4\,^3P$ in the following way:

$$4(s^2p)^3P-3(s^2p)\,^3P_1=(s^2p)\,^2P-2\Delta\,^2P=(s^2p^4)\,^3P'$$
$$-(s^2p^3)[4/3\,^4S'+5/3\,^2D'+{}^2P']$$
$$+(s^2p^3)[4\,^3P'+5/3\,^1D'+1/3\,^1S'], \quad (31)$$

where $\Delta\,^2P$ is[8] the separation $^2P_1-{}^2P_{1\frac{1}{2}}$, assuming the interval rule. If we neglect this correction we find

$$(s^2p)\,^2P : 624{,}611\ \text{cm}^{-1}, \quad \text{observed} : 624{,}139\ \text{cm}^{-1}.$$

If we know the ^2P separation (as we do here) we would find a value $(s^2p)\,^2P=625{,}384\ \text{cm}^{-1}$ which does not agree so well. The error in the corrected absolute value (1245) is about the same as the error for the normal state of O I, but the percentage error is very much smaller due to the large ionization potential.

Let us consider the configuration s^2p^3. If we rewrite the relation for $s^2p^3\,^4S$ so that the energies (indicated with a prime) are all measured to $(s)\,^2S_{\frac{1}{2}}$ for the case in which absolute values in the highest ion are unknown, we find

$$3(p)\,^2P-2(s)\,^2S_{\frac{1}{2}}=(p)\,^2P-2\nu(^2S_{\frac{1}{2}}-{}^2P_{1\frac{1}{2}})+\Delta\,^2P$$
$$=-(s^2p^3)\,^4S'+3(s^2p^2)\,^2P'+(sp^3)[5/4\,^5S'+3/4\,^3S']$$
$$-3(s^2p)\,^2P'-(sp^3)[4\,^4P'+2\,^2P']-(p^3)\,^4S'+(s^2)\,^1S'$$
$$+(sp)[9/2\,^3P'+3/2\,^1P']+3(p^3)\,^2P', \quad (32)$$

[8] This complication is removed, of course, if Δ^2P is known.

where $\nu(^2S_{\frac{1}{2}}-{}^2P_{1\frac{1}{2}})$ is one of the resonance lines. Thus if we know the states in the lower ions and this one spectral line we can (neglecting $\Delta\,^2P$) immediately get the absolute values. For O we have

$$(p)\,^2P-2\nu(^2S_{\frac{1}{2}}-{}^2P_{1\frac{1}{2}})+\Delta\,^2P=823{,}693\ \text{cm}^{-1},$$
$$\nu_{\text{obs.}}=96{,}907.7\ \text{cm}^{-1}, \quad (p)\,^2P+\Delta\,^2P=1{,}017{,}508;$$
$$\text{observed} : 1{,}017{,}280\ \text{cm}^{-1}.$$

Using the observed $\Delta\,^2P$ we find

$$(p)\,^2P=1{,}016{,}975, \quad \text{error} : 305\ \text{cm}^{-1}.$$

If we did not know this one line it would still be possible to eliminate either $(s)\,^2S$ or $(p)\,^2P$ between relations for two different configurations, e.g., s^2p^3 and sp^4, and solve finally for both.

For the examples in O, N and C considered here, only those states have been considered which involve electrons with total quantum number $n=2$. For these elements the states which have an electron with higher n value such as $2s^22p^24s$ are not suited to this method since the electrostatic interaction of the inner electrons may easily be larger than the energy of the outer electron in the central field. In such a case the multiplets which arise from the same state in the ion lie very close together. The separation of the different groups built on different states in the ion can be found directly from the distance of these basis states in the ion.

(b) In section III(b) it was shown that expressions could be found for the differences of energy states within a configuration, in terms of the differences found in higher ions. To use these expressions absolute values are not necessary. The various multiplet separations of $2p^3$, $(2s^2)2p^3$ and $2s2p^3$ determined from these relations and observed for the elements O, N and C, are presented, together with their differences, in Table XVI. The differences between the observed and calculated values are roughly constant with Z, as they were for the absolute values. The errors for the three electron configurations are rather large but their regularity for different Z makes a much closer prediction possible if an adjacent element is known.

The differences calculated and observed for the four electron configurations $2s^22p^2$, $2s2p^3$, $2p^4$ and $(2s^2)2p^4$ are presented in Table XVII. For four electrons we have two approximations for the differences. The higher one (marked II) determines the separations in terms of differences in the three and two electron ions, and the lower one uses only the three electron ions. It is interesting to notice that certain separations [for example $2s^22p^2(^3P-{}^1D)$] are quite close in the lower approximation while other differences $2s^22p^2(^1D-{}^1S)$ are much more in error. The

TABLE XVI. *Three electron configurations. Inter-multiplet separations.*

Configuration and States	O			N			C		
	Calc.	Obs.	Obs.-Calc.	Calc.	Obs.	Obs.-Calc.	Calc.	Obs.	Obs.-Calc.
$2p^3\ {}^4S-{}^2D$	27,430	23,893	−3537	20,463	16,674	−3789	12,673	8,421	−4,252
${}^2D-{}^2P$	37,458	33,852	−3606	30,997	27,328	−3669	24,430	18,279	−6,151
${}^4S-{}^2P$	64,888	57,745	−7143	51,460	44,002	−7458	37,103	26,700	−10,403
$(2s^2)2p^3\ {}^4S-{}^2D$	30,099	26,816	−3283	22,840	19,223	−3617			
${}^2D-{}^2P$	15,275	13,651	−1624	11,581	9,617	−1964			
${}^4S-{}^2P$	45,374	40,467	−4907	34,421	28,840	−5581			
$2s2p^3\ {}^4P-{}^2P$	115,308	109,269	−6039	95,658	89,076	−6582	75,216	67,601	−7,615
${}^4P-{}^2D$	56,723	55,568	−1155	45,528	44,143	−1385	33,521	31,881	−1,640
${}^2D-{}^2P$	58,585	53,701	−4884	50,130	44,933	−5197	41,695	35,720	−5,975
${}^2D-{}^2S$	56,187	37,424	−18,763	46,485	29,977	−16,508	36,645	21,562	−15,083

TABLE XVII. *Four electron configurations. Inter-multiplet separations.*

Configuration and States	O			N			C		
	Calc.	Obs.	Obs.-Calc.	Calc.	Obs.	Obs.-Calc.	Calc.	Obs.	Obs.-Calc.
II $2s^22p^2\ {}^3P-{}^1D$	20,002	20,066	64	15,260	15,227	−33	10,245	10,164	−81
${}^1D-{}^1S$	18,661	22,913	4252	13,469	17,371	3902	6,479	11,455	4976
${}^3P-{}^1S$	38,663	42,979	4316	28,729	32,598	3869	16,724	21,619	4895
I $2s^22p^2\ {}^3P-{}^1D$	19,145	20,066	921	14,452	15,227	775	9,347	10,164	817
${}^1D-{}^1S$	37,424	22,913	−14,511	29,977	17,371	−12,606	21,562	11,455	−10,107
${}^3P-{}^1S$	56,569	42,979	−13,590	44,429	32,598	−11,831	30,809	21,619	−9190
II $2s2p^3\ {}^4S-{}^2S$	137,640	137,192	−448	109,992	108,462	−1530			
${}^4S-{}^2D$	59,590	60,144	554	45,388	45,576	188			
${}^4S-{}^2P$	80,933	82,492	1559	61,708	62,552	844			
${}^2D-{}^2P$	21,343	22,348	1005	16,320	17,076	756	8,224	11,167	2943
${}^2D-{}^2D$	68,820	67,011	−1809	54,996	51,945	−3051			
${}^2P-{}^2P$	68,820	68,072	−748	54,996	57,546	2550			
I $2s2p^3\ {}^4S-{}^2S$	145,692	137,192	−8500	118,768	108,462	−10,306			
${}^4S-{}^2D$	62,728	60,144	−2584	48,869	45,576	−3293			
${}^4S-{}^2P$	92,129	82,492	−9637	72,524	62,552	−9972			
${}^2D-{}^2P$	29,401	22,348	−7053	23,655	16,976	−6679			
${}^2D-{}^2D$	72,846	67,011	−5835	59,384	51,945	−7439			
${}^2P-{}^2P$	72,846	68,072	−4774	59,384	57,546	−1838			
II $2p^4\ {}^3P-{}^1D$	13,570	14,426	856						
${}^1D-{}^1S$	45,369	45,013	−356						
${}^3P-{}^1S$	58,939	59,439	500						
I $2p^4\ {}^3P-{}^1D$	15,928	14,426	−1502						
${}^1D-{}^1S$	50,778	45,013	−5765						
${}^3P-{}^1S$	66,706	59,039	−6767						
II $(2s^2)2p^4\ {}^3P-{}^1D$	15,688	15,791	103						
${}^1D-{}^1S$	18,040	17,925	−115						
${}^3P-{}^1S$	33,728	33,716	−12						
I $(2s^2)2p^4\ {}^3P-{}^1D$	17,877	15,791	−2086						
${}^1D-{}^1S$	20,476	17,925	−4551						
${}^3P-{}^1S$	38,353	33,176	−4637						

II denotes highest approximation; I next highest.

higher orders are apparently more important for the latter, or put another way, the ${}^1S$ is probably perturbed by adjacent levels. It is also interesting to notice that there are certain ratios of the separations holding for the lower approximation which still hold for the higher approximation. For example in $2s2p^3$, $({}^5S-{}^3S)$ is twice as large as either $({}^3D-{}^1D)$ or $({}^3P-{}^1P)$ in the lower approximation.[9] The same relation holds in the higher approximation.

[9] This same ratio is obtained (See M. H. Johnson, Phys. Rev. **39**, 209 (1932)) from the Slater-Condon relations. One cannot conclude from the apparent validity of these ratios in this and similar configurations, that first order calculations should be expected to hold.

The multiplet differences for the configuration, $2s^22p^3$, of O and N and for $2s2p^4$ and $2s^22p^4$ for O are presented in Table XVIII. For the five electron configurations there are three approximations, III being the highest. Again $({}^4S-{}^2D)$ of $2s^22p^3$ is good in the lowest approximation but the other separations of that configuration are not. Agreement closer than 200 or 300 cm^{-1} must be regarded as fortuitous and it is doubtful

TABLE XVIII. *Five and six electron configurations. Inter-multiplet separations.*

Element	Configuration and States	Obs.	Calc. III	Obs.-Calc. III	Calc. II	Obs.-Calc. II	Calc. I	Obs.-Calc. I
O	$2s^2\,2p^3\ {}^4S-{}^2D$	26,816	27,102	−286	26,891	−75	27,000	−184
	${}^2D-{}^2P$	13,651	14,209	−558	12,418	1233	20,167	−6516
	${}^4S-{}^2P$	40,467	41,311	−844	39,309	1158	47,167	−6700
N	$2s^2 2p^3\ {}^4S-{}^2D$	19,223	19,054	169	19,403	−180	19,540	−317
	${}^2D-{}^2P$	9,617	12,026	−2409	9,790	−173	16,111	−6494
	${}^4S-{}^2P$	28,840	31,080	−2240	29,193	−353	35,651	−6811
O	$2s2p^4\ {}^4P-{}^2P$	92,719	93,808	−1089	94,935	−2216	102,103	−9384
	${}^4P-{}^2D$	46,061	46,913	−852	47,218	−1157	50,154	−4093
	${}^2D-{}^2S$	29,719	30,060	−341	28,908	811	37,618	−7899
	${}^4P-{}^2S$	75,780	76,973	−1193	75,793	−18	87,772	−11,992
O	$2s^2 2p^4\ {}^3P-{}^1D$	15,791	15,907	−116	15,973	−182	16,516	−725
	${}^1D-{}^1S$	17,925	17,592	333	16,261	1664	25,098	−7173
	${}^3P-{}^1S$	33,716	33,499	217	32,234	1482	41,614	−7898
		Calc. IV (${}^3P-{}^1D$) 15,568; (${}^1D-{}^1S$) 17,002; (${}^3P-{}^1S$) 32,560						
		Obs.-Calc. 223; 923; 1146						

For s^2p^3 and sp^4, III denotes the highest approximation, II next highest, I lowest.
For s^2p^4 there are four approximations: IV highest, III next highest, etc.

whether the greater error in the highest approximation for ${}^4S-{}^2D$ of $2s^22p^3$ has any significance. For $2s^22p^4$ the greater error in the highest approximation indicates that it is better to consider only the $2p^4$ outside the closed $2s^2$ shell. There are four approximations available for $2s^22p^4$ and $({}^3P-{}^1D)$ is not bad even in the lowest.

APPENDIX I

The relations developed here will now be examined by using the methods of the perturbation theory. For three electrons with coordinates x_1, x_2 and x_3, the Hamiltonian has the following form:

$$H(x_1x_2x_3)=H_0+v(x_1x_2x_3)=H_0+v(x_1x_2)+v(x_1x_3)+v(x_2x_3) \tag{33}$$

where H_0 includes the central field due to the nucleus and $v(x_1x_2x_3)$ is the interaction of the three electrons.

Let us consider the three electron state which is characterized by the quantum numbers A, B and C for the three electrons. Let $\Psi(ABC)$ represent the normalized wave function of this state including the first order terms. We can expand this $\Psi(ABC)$ in terms of the infinite set of one electron wave functions which are themselves properly normalized.

$$\Psi(ABC)=\frac{1}{\sqrt{6}}\begin{vmatrix} A(x_1) & B(x_1) & C(x_1) \\ A(x_2) & B(x_2) & C(x_2) \\ A(x_3) & B(x_3) & C(x_3) \end{vmatrix} + \sum_{a,b,c}{}' \kappa(abc)\frac{1}{\sqrt{6}}\begin{vmatrix} a(x_1) & b(x_1) & c(x_1) \\ a(x_2) & b(x_2) & c(x_2) \\ a(x_3) & b(x_3) & c(x_3) \end{vmatrix}, \tag{34}$$

where

$$\kappa(abc)=\frac{V(ABC/abc)}{E_0(ABC)-E_0(abc)}$$

and $a(x_1)$ is the wave function of the state a of the one electron problem which has the same central field and the prime on the sum indicates that the term ABC is omitted. $E_0(ABC)$ is the energy of the state ABC of the three electron problem if the interaction of the electrons is completely neglected.

$$E_0(ABC)=E(A)+E(B)+E(C).$$

The change in the energy of the state ABC due to the electrostatic interaction, including terms of the first and second order, can be written

$$E(ABC)=\int \Psi(ABC)v(x_1x_2x_3)\Psi^*(ABC)dx_1dx_2dx_3. \tag{35}$$

There will be no terms in $E(ABC)$ in which the quantum numbers of the antisymmetric combination of one electron wave functions will differ for more than two electrons. On this basis the energy $E(ABC)$ may be written in three parts,

$$E(ABC)=E_1(ABC)+E_2(ABC)+E_3(ABC) \tag{36}$$

where $E_1(ABC)$, $E_2(ABC)$ and $E_3(ABC)$ contain only terms which differ in zero, one and two electrons, respectively.

For $E_1(ABC)$, $E_2(ABC)$ and $E_3(ABC)$ in terms of the expanded wave functions, we find

$$E_1(ABC)=V(ABC/ABC) \tag{37}$$

$$E_2(ABC)=\sum_n\{\kappa^*(ABn)V(ABC/ABn)+\kappa(ABn)V(ABn/ABC)+\kappa^*(AnC)V(ABC/AnC)+\kappa(AnC)V(AnC/ABC)+\kappa^*(nBC)V(ABC/nBC)+\kappa(nBC)V(nBC/ABC)\}$$

$$=\sum_n\{2\kappa(ABn)V(ABC/ABn)+2\kappa(AnC)V(ABC/AnC)+2\kappa(nBC)V(ABC/nBC)\}, \tag{38}$$

$$E_3(ABC)=\sum_{m,n}\{2\kappa(Amn)V(ABC/Amn)+2\kappa(mnC)V(ABC/mnC)+2\kappa(mBn)V(ABC/mBn)\}, \tag{39}$$

where
$$V(ABC/Amn)=1/6\int\begin{vmatrix}A(x_1)&B(x_1)&C(x_1)\\A(x_2)&B(x_2)&C(x_2)\\A(x_3)&B(x_3)&C(x_3)\end{vmatrix}v(x_1x_2x_3)\begin{vmatrix}A(x_1)&m(x_1)&n(x_1)\\A(x_2)&m(x_2)&n(x_2)\\A(x_3)&m(x_3)&n(x_3)\end{vmatrix}dx_1dx_2dx_3.$$

Since we wish to examine certain relations between the energies of the three electron problem and those of the two electron problem we must now study the latter. The central field will be taken as the same as that for the three electron problem so that if the interaction of the electrons is neglected, the energy states for a single electron are the same for both cases. The change in energy of the state AB due to the electrostatic interaction may again be written in three parts.

$$E(AB)=E_1(AB)+E_2(AB)+E_3(AB), \tag{40}$$

where $E_1(AB)$, $E_2(AB)$ and $E_3(AB)$ contain only terms which differ in zero, one and two electrons, respectively. In terms of the expanded wave functions of the two electron problem (the λ's are the expansion coefficients), we find

$$E_1(AB)=V(AB/AB), \tag{41}$$

$$E_2(AB)=\sum_n\{2\lambda(AB/An)V(AB/An)+2\lambda(AB/nB)V(AB/nB)\}, \tag{42}$$

$$E_3(AB)=\sum_{m,n}\{2\lambda(AB/mn)V(AB/mn)\}, \tag{43}$$

where
$$V(AB/mn)=1/2\int\begin{vmatrix}A(x_1)&B(x_1)\\A(x_2)&B(x_2)\end{vmatrix}v(x_1x_2)\begin{vmatrix}m(x_1)&n(x_1)\\m(x_2)&n(x_2)\end{vmatrix}dx_1dx_2$$

and
$$\lambda(AB/mn)=\frac{V(AB/mn)}{E_0(AB)-E_0(mn)}.$$

We find that the V's of the three electron problem can be written in terms of those of two electrons due largely to Eq. (44).

$$v(x_1x_2x_3)=v(x_1x_2)+v(x_1x_3)+v(x_2x_3), \tag{44}$$

$$V(ABC/ABC)=V(BC/BC)+V(AC/AC)+V(AB/AB), \tag{45}$$

$$V(ABC/ABn)=V(BC/Bn)+V(AC/An), \tag{46}$$

$$V(ABC/Amn)=V(BC/mn). \tag{47}$$

Using the above relations between the V's we can find the κ's in terms of the λ's.

$$\kappa(Amn)=\lambda(BC/mn), \tag{48}$$

$$\kappa(ABn)=\lambda(BC/Bn)+\lambda(AC/An). \tag{49}$$

These relations enable us to write the electrostatic energies of the three electron problem in terms of those of the two electron problem.

$$E_1(ABC)=V(AB/AB)+V(AC/AC)+V(BC/BC)=E_1(AB)+E_1(AC)+E_1(BC). \tag{50}$$

This is a relation between the first order terms of the electrostatic interaction. If we include the energy in the central field we find

$$W^1(ABC)=W^1(AB)+W^1(AC)+W^1(BC)-W(A)-W(B)-W(C). \tag{51}$$

Since this is the same as Eq. (4), this shows that (4) is exact to the first order terms. For $E_2(ABC)$ and $E_3(ABC)$ we find

$$E_2(ABC)=\sum_n\{2[\lambda(BC/Bn)+\lambda(AC/An)][V(BC/Bn)+V(AC/An)]+2[\lambda(AB/An)+\lambda(BC/nC)]\times[V(AB/An)+V(BC/nC)]+2[\lambda(AB/nB)+\lambda(AC/nC)][V(AB/nB)+V(AC/nC)]\}, \tag{52}$$

$$E_3(ABC)=E_3(AB)+E_3(AC)+E_3(BC)+\text{cross terms in (52)}, \tag{53}$$

$$E_3(ABC)=\sum_{m,n}\{2\lambda(BC/mn)V(BC/mn)+2\lambda(AB/mn)V(AB/mn)+2\lambda(AC/mn)V(AC/mn)\},$$

$$E_3(ABC)=E_3(BC)+E_3(AB)+E_3(AC). \tag{54}$$

If it were not for the cross terms in (52) we would again get Eq. (4) when (53) and (54) are added to (51). Except for the cross terms in (52), Eq. (4) would hold up to the second order. We conclude that Eq. (4) which relates the energies

of the three, two and one electron problems, is exact up to the first order and holds also for parts of the second order.

Let us now consider four electrons in the same central field. The Hamiltonian of the problem will have the form

$$H(x_1x_2x_3x_4)=H_0(x_1x_2x_3x_4)+\sum_{i>j=1}^{4} v(x_ix_j), \tag{55}$$

where the central field is included in H_0. The wave function (including first order terms) of the state which is characterized by the quantum numbers A, B, C and D for the four electrons may be written

$$\Psi(ABCD)=\frac{1}{\sqrt{24}}\begin{vmatrix} A(x_1) & B(x_1) & C(x_1) & D(x_1)\\ A(x_2) & B(x_2) & C(x_2) & D(x_2)\\ A(x_3) & B(x_3) & C(x_3) & D(x_3)\\ A(x_4) & B(x_4) & C(x_4) & D(x_4)\end{vmatrix}+\sum_{mnop}{}' \mu(mnop)\frac{1}{\sqrt{24}}\begin{vmatrix} m(x_1) & n(x_1) & o(x_1) & p(x_1)\\ m(x_2) & n(x_2) & o(x_2) & p(x_2)\\ m(x_3) & n(x_3) & o(x_3) & p(x_3)\\ m(x_4) & n(x_4) & o(x_4) & p(x_4)\end{vmatrix}. \tag{56}$$

where $\mu(mnop)=\dfrac{V(ABCD/mnop)}{E_0(ABCD)-E_0(mnop)}=0$ if $mnop$ differs from $ABCD$ in the quantum numbers of more than two electrons.

The change in the energy $E(ABCD)$ due to the electrostatic interaction, including second order terms, may be split into three parts as before.

$$E(ABCD)=E_1(ABCD)+E_2(ABCD)+E_3(ABCD). \tag{57}$$

For $E_1(ABCD)$, $E_2(ABCD)$ and $E_3(ABCD)$ we find

$$E_1(ABCD)=V(AB/AB)+V(AC/AC)+V(AD/AD)+V(BC/BC)+V(BD/BD)+V(CD/CD),$$

$$E_1(ABCD)=E_1(ABC)+E_1(ABD)+E_1(ACD)+E_1(BCD)-E_1(AB)-E_1(AC)-E_1(AD)-E_1(BC)-E_1(BD)-E_1(CD), \tag{58}$$

$$\begin{aligned}E_2(ABCD)=\sum_n\{&2\mu(ABCn)[V(AD/An)+V(BD/Bn)+V(CD/Cn)]\\&+2\mu(ABnD)[V(AC/An)+V(BC/Bn)+V(CD/nD)]+2\mu(AnCD)[V(AB/An)+V(BC/nC)+V(BD/nD)]\\&+2\mu(nBCD)[V(AB/nB)+V(AC/nC)+V(AD/nD)]\},\end{aligned}$$

$$E_2(ABCD)=E_2(ABC)+E_2(ABD)+E_2(ACD)+E_2(BCD)-E_2(AB)-E_2(AC)-E_2(AD)-E_2(BC)-E_2(BD)-E_2(CD), \tag{59}$$

$$\begin{aligned}E_3(ABCD)=\sum_{m,n}\{&2\mu(ABmn)V(CD/mn)+2\mu(AmCn)V(BD/mn)+2\mu(mBCn)V(AD/mn)\\&+2\mu(mBnD)V(AC/mn)+2\mu(AmnD)V(BC/mn)+2\mu(mnCD)V(AB/mn)\},\end{aligned}$$

$$E_3(ABCD)=E_3(ABC)+E_3(ABD)+E_3(ACD)+E_3(BCD)-E_3(AB)-E_3(AC)-E_3(AD)-E_3(BC)-E_3(BD)-E_3(CD). \tag{60}$$

If we include the energy of the unperturbed problem we find for the total energy in second order.

$$\begin{aligned}W^2(ABCD)=&W^2(ABC)+W^2(ABD)+W^2(ACD)+W^2(BCD)-W^2(AB)-W^2(AC)-W^2(AD)-W^2(BC)\\&-W^2(BD)-W^2(CD)+W(A)+W(B)+W(C)+W(D).\end{aligned} \tag{61}$$

This relation is the same as Eq. (7) so we conclude that (7) is exact up to and including the second order. It is very probable that (7) holds for parts of the third and higher orders. Up to the second order one can verify the relations for more than four electrons in the same way, although the equations become somewhat lengthy. Inclusion of the third and higher orders, however, greatly increases the complication.

Appendix II

In the configuration p^2 consider the two states with $M_S=0$, $M_L=1$. We know that these two states together give ^3P and ^1D, each being some linear combination of the two. In order to find this linear combination, let us consider in Table IV for p^2 the two states which are ^3D alone. These two states must have the same pair energy. If we write the pair energy of two electrons as $w(m_s\ m_l\ \ m_s'\ m_l')$ and the total pair energy for ^3D as $w(^3D)$ we have the following relations

$$w(^3D)=\underset{^3P}{w(1/2\ 1,\ 1/2\ 0)}+\underset{^1D}{w(1/2\ 1,\ -1/2\ 1)}+w(1/2\ 0,\ -1/2\ 1), \tag{62}$$

$$w(^3D)=\underset{^1D}{w(1/2\ 1,\ -1/2\ 1)}+w(1/2\ 1,\ -1/2\ 0)+\underset{^3P}{w(-1/2\ 1,\ -1/2\ 0)}. \tag{63}$$

In (62), the first pair energy is that of ^3P of p^2 (compare Table II) and the second that of ^1D. In (63), the first is ^1D and the last ^3P. Since the pair energies must be equal in both cases we have (64)

$$w(1/2\ 0,\ -1/2\ 1)=w(1/2\ 1,\ -1/2\ 0). \tag{64}$$

If we go back now to the two states of p^2 having $M_S=0$ and $M_L=1$, we see that (64) shows they have the same pair energy and hence the two states must have the same linear combination of ^3P and ^1D. The two states together give $^3P+{}^1D$ so each state is $1/2\ {}^3P+1/2\ {}^1D$.

Let us consider the three states with $M_S=0$ and $M_L=0$ from the configuration p^2. We know that these three states together give ^3P, ^1D and ^1S. If we go to Table VIII for configuration p^4 there are four states which are uniquely $p^4\,^3P$. Since these must have the same pair energy Eqs. (65), (66) and (67) result.

$$w(p^4\,^3P)=w(1/2\ 1,\ 1/2\ 0)+w(1/2\ 1,\ 1/2-1)+w(1/2\ 1,\ -1/2\ 1)+w(1/2\ 0,\ 1/2-1)+w(1/2\ 0,\ -1/2\ 1)+w(1/2-1,\ -1/2\ 1), \quad (65)$$

$$w(p^4\,^3P)=w(1/2\ 1,\ 1/2\ 0)+w(1/2\ 1,\ 1/2-1)+w(1/2\ 1,\ -1/2\ 0)+w(1/2\ 0,\ 1/2-1)+w(1/2\ 0,\ -1/2\ 0)+w(1/2-1,\ -1/2\ 0), \quad (66)$$

$$w(p^4\,^3P)=w(1/2\ 1,\ 1/2\ 0)+w(1/2\ 1,\ 1/2-1)+w(1/2\ 1,\ -1/2-1)+w(1/2\ 0\ \ 1/2-1)+w(1/2\ 0,\ -1/2-1)+w(1/2-1,\ -1/2-1). \quad (67)$$

Utilizing knowledge of the pair energies of other states of p^2, and noting that if the signs of all the quantum numbers in a pair are changed the pair energy is unchanged, we get the following relations:

$$w(1/2\ 0,\ -1/2\ 0)=1/2\ w(^1D)-1/2\ w(^3P)+w(1/2\ 1,\ -1/2-1), \quad (68)$$

$$w(1/2-1,\ -1/2\ 1)=w(1/2\ 1,\ -1/2-1). \quad (69)$$

In addition the three states together give ^3P, ^1D and ^1S.

$$w(1/2\ 0,\ -1/2\ 0)+2w(1/2\ 1,\ -1/2-1)=w(^3P)+w(^1D)+w(^1S). \quad (70)$$

Hence we have (71) and (72)

$$w(1/2\ 1,\ -1/2-1)=1/2\ w(^3P)+1/6\ w(^1D)+1/3\ w(^1S), \quad (71)$$

$$w(1/2\ 0,\ -1/2\ 0)=2/3\ w(^1D)+1/3\ w(^1S). \quad (72)$$

This means that in the set $M_S=0$, $M_L=0$ the first and third states are $1/2\ ^3P+1/6\ ^1D+1/3\ ^1S$ and the second is $2/3\ ^1D+1/3\ ^1S$.

Eqs. (64) and (69) indicate that the division into multiplets is the same for two states which differ either in the signs of all the m_s or all the m_l. The state which differs from another state in the signs of all the m_s and all the m_l is simply the corresponding state from the half of the Pauli table with $M_S+M_L<0$ and also has the same division into multiplets.

p^3

From the configuration p^3 there are multiplets ^4S, ^2D and ^2P. In the set with $M_S=1/2$ and $M_L=1$ (see Table IV), we find that each of the states has the same pair energy and hence each state is given by $1/2\ ^2D+1/2\ ^2P$ since the two together give $^2P+^2D$. The same is true for the set with $M_S=-1/2$, and $M_L=1$.

In the set with $M_S=1/2$ and $M_L=0$ there are three states which together give ^4S, ^2D and ^2P. Since we know that the pair energies of a state (ABC) must be the same as for $(AB)+(AC)+(BC)$, we have

$$w(ABC)=w(AB)+w(AC)+w(BC), \quad (73)$$

where $w(ABC)$ is used here to represent the pair energies of (ABC). Utilizing (73), we find from the states which are already known in Table IV the following relations

$$w(p^3\,^4S)=3w(p^2\,^3P), \quad (74)$$

$$w(p^3\,^2D)=3/2\ w(p^2\,^3P)+3/2\ w(p^2\,^1D), \quad (75)$$

$$w(p^3\,^2P)=3/2\ w(p^2\,^3P)+5/6\ w(p^2\,^1D)+2/3\ w(p^2\,^1S). \quad (76)$$

From the three states with $M_S=1/2$ and $M_L=0$ we have

$$w(1/2\ 1,\ 1/2\ 0,\ -1/2-1)=2w(p^2\,^3P)+2/3\ w(p^2\,^1D)+1/3\ w(p^2\,^1S), \quad (77)$$

$$w(1/2\ 1,\ 1/2-1,\ -1/2\ 0)=2w(p^2\,^3P)+w(p^2\,^1D), \quad (78)$$

$$w(1/2\ 0,\ 1/2-1,\ -1/2\ 1)=2w(p^2\,^3P)+2/3\ w(p^2\,^1D)+1/3\ w(p^2\,^1S). \quad (79)$$

We wish to find $w(1/2\ 1,\ 1/2\ 0,\ -1/2-1)$, $w(1/2\ 1,\ 1/2-1,\ -1/2\ 0)$ and $w(1/2\ 0,\ 1/2-1,\ -1/2\ 1)$ in terms of $w(p^3\,^4S)$, $w(p^3\,^2D)$ and $w(p^3\,^2P)$ so that all the Eqs. (74) to (79) are satisfied simultaneously. If we solve (74), (75) and (76) for $w(p^2\,^3P)$, $w(p^2\,^1D)$ and $w(p^2\,^1S)$ and substitute these values in (77), (78) and (79), we get the following

$$w(1/2\ 1,\ 1/2\ 0,\ -1/2-1)=1/3\ w(p^3\,^4S)+1/6\ w(p^3\,^2D)+1/2\ w(p^3\,^2P), \quad (80)$$

$$w(1/2\ 1,\ 1/2-1,\ -1/2\ 0)=1/3\ w(p^3\,^4S)+2/3\ w(p^3\,^2D), \quad (81)$$

$$w(1/2\ 0,\ 1/2-1,\ -1/2\ 1)=1/3\ w(p^3\,^4S)+1/6\ w(p^3\,^2D)+1/2\ w(p^3\,^2P). \quad (82)$$

The relations (80), (81) and (82) for the pair energies give the proper linear combinations found in Table IV for the three states of the set $M_S=1/2$, $M_L=0$.

It may seem that this is somewhat involved, but it is nearly always possible, with a little practice, to determine the coefficients immediately from inspection. For example, in the last case it is apparent since $p^3\,^2P$ occurs (see Table IV, last column) only with $p^3\,^1S$, that it will occur in the first and third states of the set with coefficient 1/2. The second state

has a ^1D in the multiplets from pairs but no ^2P in the p^3 multiplets, so ^2D must occur with the coefficient 2/3. The first and third states must have the same linear combination and the sum of the ^2D coefficients is unity so ^2D occurs in the first and third states with coefficient 1/6. Since for each state the sum of the coefficients must be unity, the coefficient of ^4S is 1/3 for each state.

It is not necessary to know the exact linear combination of all the states of Table IV in order to find the energies of the various multiplets but the information is useful in finding the linear combinations in more complicated configurations.

sp^2

From the configuration sp^2 there are multiplets ^4P, ^2P, ^2D and ^2S. Each of the states in Table V with $M_S=3/2$ is assigned to ^4P alone and those with $M_L=2$ belong to ^2D. In the set with $M_S=1/2$ and $M_L=1$ three of the possible four states will be represented, ^4P, ^2P and ^2D. Using (73) and the information available about ^4P and ^2D we find

$$w(sp^2\,{}^4P)=w(p^2\,{}^3P)+2w(sp\,{}^3P), \tag{83}$$

$$w(sp^2\,{}^2D)=w(p^2\,{}^1D)+3/2\,w(sp\,{}^3P)+1/2\,w(sp\,{}^1P), \tag{84}$$

Considering the whole set $M_S=1/2$, $M_L=1$ we have

$$w(sp^2\,{}^4P)+w(sp^2\,{}^2D)+w(sp^2\,{}^2P)=2w(p^2\,{}^3P)+w(p^2\,{}^1D)+4w(sp\,{}^3P)+2w(sp\,{}^1P). \tag{85}$$

With (83) and (84) this gives

$$w(sp^2\,{}^2P)=w(p^2\,{}^3P)+1/2\,w(sp\,{}^3P)+3/2\,w(sp\,{}^1P). \tag{86}$$

From the individual states of the $M_S=1/2$, $M_L=1$ set, we have

$$w(1/2,\,1/2\;1,\,-1/2\;0)=w(1/2,\,1/2\;0,\,-1/2\;1)=1/2\,w(p^2\,{}^3P)+1/2\,w(p^2\,{}^1D)+3/2\,w(sp\,{}^3P)+1/2\,w(sp\,{}^1P), \tag{87}$$

$$w(1/2,\,1/2\;1,\,1/2\;0)=w(p^2\,{}^3P)+w(sp\,{}^3P)+w(sp\,{}^1P). \tag{88}$$

If now we solve (83), (84) and (86) for $w(p^2\,{}^3P)$, $w(sp\,{}^3P)$ and $w(sp\,{}^1P)$ in terms of $w(sp^2\,{}^4P)$, $w(sp^2\,{}^2D)$, $w(sp^2\,{}^2P)$ and $w(p^2\,{}^1D)$ and put them into (87) and (88) we find

$$w(1/2,\,1/2\;1,\,-1/2\;0)=w(1/2,\,1/2\;0,\,-1/2\;1)=1/3\,w(sp^2\,{}^4P)+1/2\,w(sp^2\,{}^2D)+1/6\,w(sp^2\,{}^2P), \tag{89}$$

$$w(1/2,\,1/2\;1,\,1/2\;0)=1/3\,w(sp^2\,{}^4P)+2/3\,w(sp^2\,{}^2P). \tag{90}$$

These relations for the pair energies give the linear combinations for the three states with $M_S=1/2$ and $M_L=1$ found in Table V.

In the set of states with $M_S=1/2$ and $M_L=0$ all four possible multiplets, ^4P, ^2P, ^2D, and ^2S, are represented. Considering the whole set together we have

$$w(sp^2\,{}^4P)+w(sp^2\,{}^2P)+w(sp^2\,{}^2D)+w(sp^2\,{}^2S)=2w(p^2\,{}^3P)+w(p^2\,{}^1D)+w(p^2\,{}^1S)+11/2\,w(sp\,{}^3P)+5/2\,w(sp\,{}^1P). \tag{91}$$

With the help of (83), (84) and (86) we find from (91)

$$w(sp^2\,{}^2S)=w(p^2\,{}^1S)+3/2\,w(sp\,{}^3P)+1/2\,w(sp\,{}^1P) \tag{92}$$

For the four states we get the following relations for the pair energies

$$w(1/2,\,1/2\;1,\,-1/2-1)=w(1/2,\,1/2-1,\,-1/2\;1)=1/2\,w(p^2\,{}^3P)+1/6\,w(p^2\,{}^1D)+1/3\,w(p^2\,{}^1S)+3/2\,w(sp\,{}^3P)+1/2\,w(sp\,{}^1P), \tag{93}$$

$$w(1/2,\,1/2\;0,\,-1/2\;0)=2/3\,w(p^2\,{}^1D)+1/3\,w(p^2\,{}^1S)+3/2\,w(sp\,{}^3P)+1/2\,w(sp\,{}^1P), \tag{94}$$

$$w(-1/2,\,1/2\;1,\,1/2-1)=w(p^2\,{}^3P)+w(sp\,{}^3P)+w(sp\,{}^1P). \tag{95}$$

Solving (83), (84), (86) and (92) for $w(p^2\,{}^3P)$, $w(p\,{}^1S)$, $w(sp\,{}^3P)$ and $w(sp\,{}^1P)$ in terms of $w(sp^2\,{}^4P)$, $w(sp^2\,{}^2P)$, $w(sp^2\,{}^2D)$, $w(sp^2\,{}^2S)$ and $w(p^2\,{}^1D)$ as above and putting them in (93), (94) and (95) we find

$$w(1/2,\,1/2\;1,\,-1/2-1)=w(1/2,\,1/2-1,\,-1/2\;1)=1/3\,w(sp^2\,{}^4P)+1/6\,w(sp^2\,{}^2P)+1/6\,w(sp^2\,{}^2D)+1/3\,w(sp^2\,{}^2S), \tag{96}$$

$$w(1/2,\,1/2\;0,\,-1/2\;0)=1/3\,w(sp^2\,{}^2S)+2/3\,w(sp^2\,{}^2D), \tag{97}$$

$$w(-1/2,\,1/2\;1,\,1/2-1)=1/3\,w(sp^2\,{}^4P)+2/3\,w(sp^2\,{}^2P). \tag{98}$$

The relations (96), (97) and (98) give the proper linear combinations found in Table V. For this configuration the inspection method gives the coefficients almost immediately.

No further particular examples are worked out here in detail as we believe the method is amply illustrated above. The coefficients can nearly always be found most easily by the inspection method for which a certain amount of familiarity with the Pauli tables is indeed helpful. There are numerous regularities to guide one which unfortunately cannot be pointed out here in detail.

The Infrared Spectrum of Methyl Chloride

A. H. NIELSEN AND E. F. BARKER, *Department of Physics, University of Michigan*

(Received September 19, 1934)

Certain new infrared absorption bands of CH_3Cl were mapped in the region from 0.7μ to 7.0μ. In each case the bands show the structure predicted by the theory of the symmetry properties of molecules having three equal atoms. It is also predicted that every third line in the $\perp$ bands shall be enhanced. This was observed in the present investigation as well as previously by Bennett and Meyer. Several new intervals between the lines in the $\perp$ bands were observed which may be of value with regard to a theoretical interpretation of this anomalous spacing. Two absorption regions, observed here, appear to give evidence of an interaction between the levels ν_1 and $2\nu_4$ thought to exist in some of the methyl compounds. These bands are $\nu_3+(\nu_1, 2\nu_4)$ at 5900 cm^{-1} and $\nu_3+(\nu_1, 2\nu_4)$ at 4200 cm^{-1}. A few lines of ν_3 in the P branch near the center were resolved. The Q branch proved to be much more pronounced than Bennett and Meyer's work shows.

I. INTRODUCTION

THE infrared vibration-rotation spectrum of the methyl halides was measured by Bennett and Meyer[1] who found that the $\perp$ bands showed an anomalous spacing of the lines. This effect, they suggested was due to an interaction between the vibration and the rotation of the molecule. A pair of $\parallel$ bands, separated by 85 cm^{-1}, was also found at 3.2μ which have recently been interpreted as $(\nu_1, 2\nu_4)$.[2] Normally the levels ν_1 and $2\nu_4$ would lie very close together. It is thought that in a number of methyl compounds they interact as in the case of the CO_2[3] molecule and that the observed separation is a result of this interaction. This resonance also serves to increase the intensity of the $\parallel$ component of $2\nu_4$ so that it is comparable with ν_1. Only in the case of ν_3 for CH_3F was resolution obtained by Bennett and Meyer so that the moments of inertia of the remaining molecules are unknown. The line of further investigation pointed out by the previous observations is as follows: (1) to acquire more experimental data on the anomalous spacing of the lines in the $\perp$ bands; (2) to obtain more experimental evidence of the supposed interaction between ν_1 and $2\nu_4$; (3) to determine, if possible, the moments of inertia $A=B$ from the resolution of one of the $\parallel$ bands; (4) to obtain experimental data on the complex structure of the harmonics and combination bands of $\perp$ vibrations predicted by the theory of molecules having three equivalent particles.[4]

Two infrared spectrometers, one of the Pfund[5] type designed by J. D. Hardy, and another designed by C. F. Meyer[6] were available for this investigation. Three gratings ruled with 7200 lines per inch, 4800 lines per inch and 2400 lines per inch were used for the 1.5μ–3.0μ, 4.0μ, and the 7.0μ regions, respectively. In addition, a concave grating of 15,000 lines per inch in a Paschen mounting was used in the photographic region. For the bolometric measurements a 25.4 cm cell closed with rocksalt windows, and a 1.5 meter cell having glass windows were used. In the photographic region the equivalent length of the absorption cell was 100 meters at atmospheric pressure.

II. EXPERIMENTAL RESULTS

The 1.6μ region

Two $\perp$ bands and one $\parallel$ band were found as shown in Fig. 1. The lowest frequency $\perp$ band occurs alone while the other $\perp$ one overlaps the $\parallel$ band. The predicted structure of the second harmonic of a $\perp$ vibration is a pair of close bands of $\parallel$ and $\perp$ character. This is just what is observed in curves *b*, *c*, Fig. 1, hence this pair has been designated as $2\nu_2$. The spacing of the lines in the $\perp$ component is 12.0 cm^{-1}. The zero branch of the $\parallel$ component is quite sharp and

[1] Bennett and Meyer, Phys. Rev. **32**, 888 (1928).
[2] The bracket $(\nu_1, 2\nu_4)$ indicates that the wave functions representing the two perturbed levels are linear combinations of the wave functions of the levels ν_1 and $2\nu_4$.
[3] D. M. Dennison, Phys. Rev. **41**, 304 (1932).
[4] D. M. Dennison, Rev. Mod. Phys. **3**, 338 (1931).
[5] A. H. Pfund, J. Opt. Soc. Am. and Rev. Sci. Inst. **15**, 69 (1927).
[6] E. F. Barker and C. F. Meyer, Trans. Farad. Soc. **25**, 913 (1929).

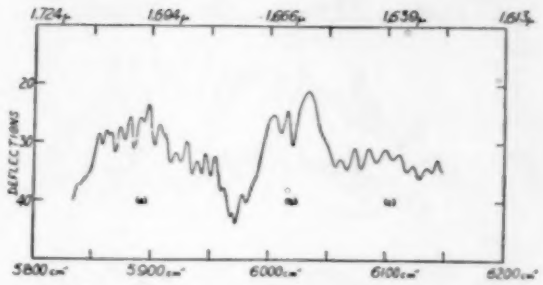

FIG. 1. Curve (*a*) shows the perpendicular structure of the band $\nu_2+(\nu_1, 2\nu_4)$. Curves (*b*) and (*c*) show the splitting up of the parallel, and perpendicular components of $2\nu_3$.

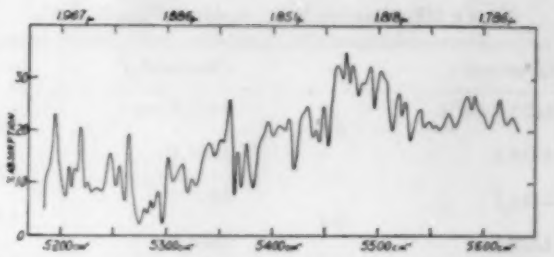

FIG. 2. Perpendicular structure to which no interpretation can at present be given.

more intense than any found by Bennett and Meyer (with the exception of ν_3). The other ⊥ band is thought to be $\nu_2+(\nu_1, 2\nu_4)$ involving the two resonance levels. This identification would indicate that the two ∥ components of $\nu_2+2\nu_4$ are much weaker than the two ⊥ components since the region shows only ⊥ structure. The data on this region are given in Tables I and II. For this region the 25.4 cm cell was used, and, since the background was free from atmospheric absorption, galvanometer deflections were plotted against cm^{-1}.

TABLE I. (*Data on the ∥ bands.*)

P branch	*Q* branch	*R* branch	$\nu_P-\nu_R$
4025.7 cm^{-1}	4047.1 cm^{-1}	4056.3 cm^{-1}	30.6 cm^{-1}
4078.0	4089.5	4106.3	24.3
4213.8	4230.6	4245.9	32.1
6003.4	6015.2	6034.0	30.6

TABLE II. (*Data on curves a and c, Fig. 1.*)

Observed ν	$\Delta\nu$	Observed ν	$\Delta\nu$
5855.1 cm^{-1}		5920.4 cm^{-1}	
	6.7		9.1
5861.8		5929.5	
	4.5		9.0
5866.3		5938.5	
	6.7		7.0
5873.0		5945.5	
	8.9		9.2
5881.9		5954.7	
	9.0		6.9
5890.9		5961.6	
	6.8		6.9
5897.7		5968.5	
	9.0		9.3
5906.7		5977.8	
	6.0		
5912.7			
	7.7		
6048.3		6110.7	
	11.9		12.2
6060.2		6122.9	
	12.0		11.0
6072.2		6133.9	
	12.0		8.6
6084.2		6142.5	
	14.4		
6098.6			
	12.1		

The 1.8μ region

The absorption in this region is shown in Fig. 2. The band is essentially of the ⊥ variety, but it is so complex that no interpretation can at present be given to it. The absorption is considerably weaker here than at 1.6μ necessitating the use of the 1.5 meter cell. The curve is plotted in percent absorption because the background is complicated by the strong water vapor absorption. The complex appearance of this region is no doubt partly due to distortion by the water vapor lines.

The 2.4μ region

A. Fig. 3 shows the highest frequency absorption of the group of bands in the region of 2.4μ. Its structure is ⊥ throughout. This absorption is believed to be composed of two overlapping ⊥ bands, namely, $\nu_2+\nu_3$ having its center at 4383.8 cm^{-1} and $\nu_2+2\nu_5$ with its center at 4478.5 cm^{-1}. Theoretically both $\nu_2+\nu_3$, and $\nu_2+2\nu_5$ would be single ⊥ bands, and this seems to agree with observation in that the edges of the region have sharply defined lines but the middle is distorted from overlapping. The average spacing of the lines in Table III is seen to be 8.5 cm^{-1}. The curves show clearly that every third line is enhanced as predicted by the theory of systems having three equivalent nuclei each with a spin angular momentum of $\frac{1}{2}(h/2\pi)$. As in the 1.6μ region the 25.4 cm cell was used and galva-

TABLE III. (*Data on the ⊥ bands of Figs. 3, 4, 6.*)

Observed ν	$\Delta\nu$	Observed ν	$\Delta\nu$
4323.9 cm^{-1}		4441.6 cm^{-1}	
	9.5		8.5
4333.4		4449.1	
	8.3		8.8
4341.7		4457.9	
	8.4		8.8
4350.1		4466.7	
	8.3		8.8
4358.4		4475.5	
	6.0		7.7
4364.4		4483.2	
	7.2		9.0
4371.6		4492.2	
	8.5		8.9
4380.1		4501.1	
	7.3		9.0
4387.4		4510.1	
	9.8		10.4
4397.2		4520.5	
	7.3		10.3
4404.5		4530.8	
	8.6		7.9
4413.1		4538.7	
	10.5		6.5
4423.6		4545.2	
	10.5		
4434.1			
	7.5		

Mean spacing of lines in low frequency side of band = 8.4 cm^{-1}.
Mean spacing of lines in high frequency side of band = 8.6 cm^{-1}.

4123.9 cm^{-1}		4182.3 cm^{-1}	
	12.8		4.9
4136.7		4187.2	
	11.3		5.0
4148.0		4192.2	
	9.7		6.6
4157.7		4198.8	
	3.3		6.7
4161.0		4205.5	
	4.3		8.3
4165.3		4213.8	
	3.8		
4169.1			
	13.2		

2389.7 cm^{-1}		2456.9 cm^{-1}	
	8.1		9.5
2397.8		2466.4	
	9.8		9.8
2407.6		2476.2	
	10.6		10.2
2418.2		2486.4	
	9.7		9.7
2427.9		2496.1	
	9.5		10.1
2437.4		2506.2	
	9.6		
2447.0			
	9.9		

Mean spacing of lines = 9.7 cm^{-1}.

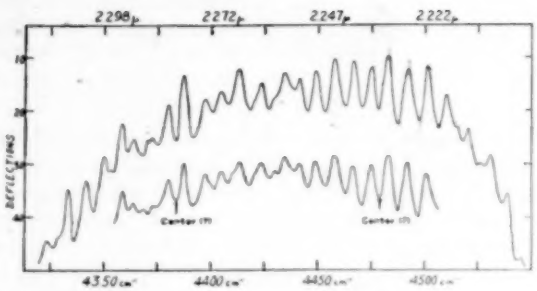

FIG. 3. Two overlapping perpendicular bands, $\nu_2+\nu_3$ and $\nu_2+2\nu_1$.

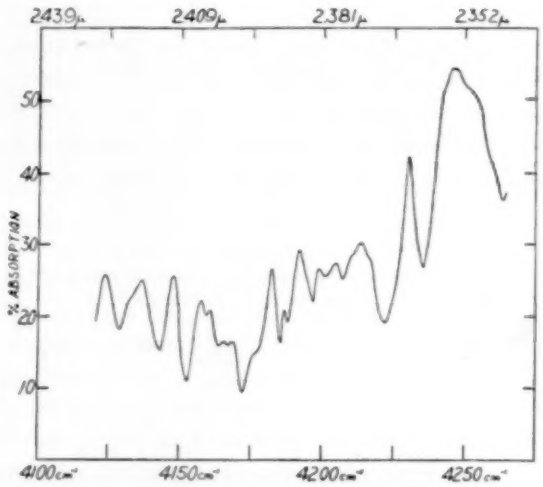

FIG. 4. Perpendicular and parallel structure showing the separation of the bands $\nu_3+(\nu_1, 2\nu_4)$.

nometer deflections were plotted against cm^{-1}. The slit widths included 1.6 cm^{-1} and readings were taken at intervals of 1.2 cm^{-1}.

B. At somewhat longer wave-lengths a pair of bands were observed of which one is ∥ and the other ⊥. These bands, shown in Fig. 4, have been designated as $\nu_3+(\nu_1, 2\nu_4)$ which is the second observed group thought to contain the resonance pair of levels. This identification is made because the separation of these bands is just the separation expected for a combination of some other level with the pair $(\nu_1, 2\nu_4)$. Theoretically $\nu_3+\nu_1$ is a ∥ band, and $\nu_3+2\nu_4$ is composed of a ∥ and a ⊥ component lying close together. This is in agreement with observation since one ∥ band is found, and the ⊥ structure shows such distortion as might be expected from overlapping. Again in this case the zero branch of the parallel band is very sharp and strong, in

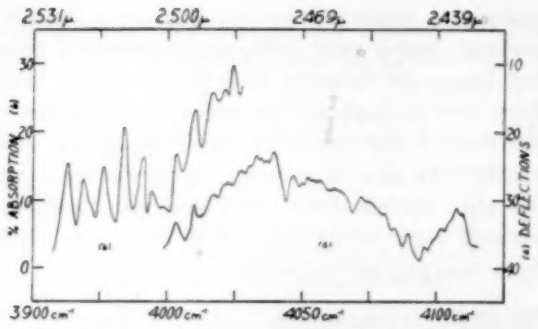

FIG. 5. One perpendicular and two parallel bands comprising $\nu_2+\nu_6$.

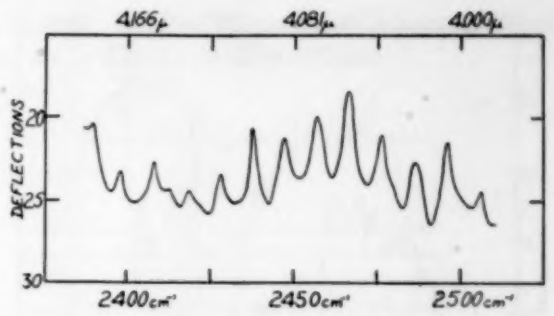

FIG. 6. The perpendicular structure of $\nu_8+2\nu_5$.

contrast to Bennett and Meyer's observations. The absorption was observed with the aid of the 1.5 meter cell and the curve was plotted in percentage absorption because of some strong atmospheric lines. The slits included 1.5 cm^{-1} and readings were taken at intervals of 1.6 cm^{-1}. Table III gives the frequencies of the lines in the $\perp$ band, while Table I contains the data on the $\parallel$ one.

C. The lowest frequency portion of the group at 2.4μ is shown in Fig. 5 and is composed of a $\perp$ and two $\parallel$ bands all overlapping to some extent. This group has been identified as $\nu_2+\nu_6$ since the character of the observed band agrees with that predicted for such a combination. The three bands are all of about the same intensity, but since the perpendicular part was plotted in percent absorption the ordinates are not directly comparable. Due to intense water vapor lines in the region, the authenticity of this band was for a time doubted. However, the gas was dried so carefully and such precautions were taken as to remove this doubt. Table IV shows the close agreement of some of the CH_3Cl lines with water vapor lines.[7] Another evidence indicating that the lines are due to CH_3Cl is the fact that every third line shows the characteristic enhancement. The zero branches of the parallel bands chosen to lie at 4047.1 cm^{-1} and at 4089.5 cm^{-1} are not very well defined. The region was measured with the 25.4 cm cell and the slit widths included 1.4 cm^{-1}, readings being taken at intervals of 1 cm^{-1}.

TABLE IV. (*Data on curve b of Fig. 5.*)

Observed ν (cm^{-1})	H_2O lines (cm^{-1})	$\Delta\nu$	Observed ν (cm^{-1})	H_2O lines (cm^{-1})	$\Delta\nu$
3963.0	3962.8	−0.2	3994.1	3995.7	1.6
3968.9	3970.3	0.14	4003.1		
3976.3	3976.6	0.3	4010.6	4009.3	−1.3
				4020.7	4.0
3983.7	3983.6	−0.1	4016.7		
				4012.2	−4.5
3991.1	3991.2	0.1	4024.2	4026.7	2.5

The 4.0μ region

Only the one $\perp$ band shown in Fig. 6, was found in this region. It is very clean throughout giving clearly an average spacing between lines of 9.7 cm^{-1}. The 1–1–2 intensity characteristic is shown more clearly in this band than in any other found. This band is believed to be $\nu_8+2\nu_5$ which according to theory must be a single $\perp$ band and should lie more free from overlapping than any other band in this region. The frequencies of the lines are given in Table III. Mapping of this band was accomplished with the 25.4 cm cell and the slits were set to include 2.5 cm^{-1}. Galvanometer readings taken at intervals of 1 cm^{-1} were plotted against cm^{-1}.

The 7.0μ region

Resolution of ν_3 would give the moments of inertia $A=B$ of the molecule. As Fig. 7 shows, this was not wholly successful despite the refinements in modern apparatus. Only a few lines in the negative branch near the center of the band were resolved giving a spacing of 1.3 cm^{-1}. These provide insufficient information for a reliable determination of the moments of inertia.

[7] Plyler and Sleator, Phys. Rev. 37, 1493 (1931).

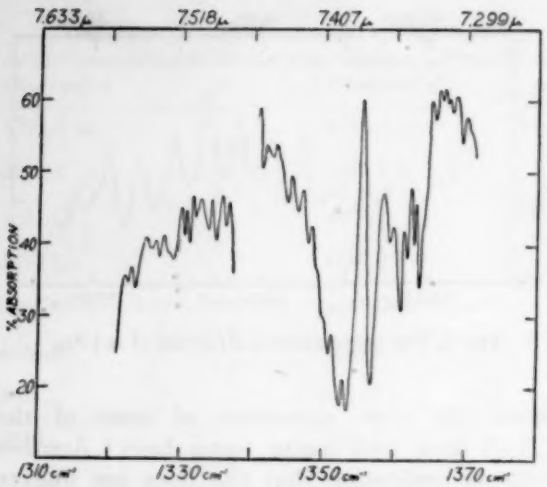

FIG. 7. This curve shows the result of the new attempt to resolve ν_3.

It is believed that the failure is due partly to the isotope effect in this vibration, partly to strong water vapor absorption and partly to inadequate resolving power. The zero branch, however, has a very different appearance from that found by Bennett and Meyer, being very sharp and as high as the positive and negative branches of the band. Its position agrees very exactly with that determined in the earlier work. The slits include 0.67 cm^{-1} and galvanometer readings were taken every 0.35 cm^{-1}. The final curve was plotted in percent absorption.

TABLE V. (*Data on photographic bands.*)

Observed ν	$\Delta\nu$	Observed ν	$\Delta\nu$
9992.6 cm^{-1}		10061.4 cm^{-1}	
	5.8		16.8
9998.4		10078.2*	
	3.3		6.9
10001.7		10085.1*	
	7.4		6.8
10009.1		10091.9*	
	9.2		8.7
10018.3		10100.6*	
	7.0		6.3
10025.3		10106.9*	
	7.8		4.0
10032.1		10110.9	
	7.7		2.4
10039.8		10113.3	
	4.0		7.4
10043.8		10120.7	
	8.5		3.9
10052.3		10124.6	
	5.1		
10057.4			
	4.0		

Mean spacing of lines = 6.7 cm^{-1}.
* Lines most accurately measured.

13772.7 cm^{-1}		13816.9 cm^{-1}	
	5.9		10.7
13778.6		13827.6	
	28.0		9.7
13806.6		13837.3	
	10.3		

The photographic region

Two bands were found photographically at 0.72μ and at 1.0μ, both apparently of the $\perp$ type. Prints of these do not reproduce well and are omitted here, but the frequencies of the lines are given in Table V. The lines marked with an asterisk were most accurately measured and given a spacing of 6.7 cm^{-1}. No interpretation of the 0.72μ band can satisfactorily be given at this time, but the one at 1.0μ is believed to be $\nu_4+3\nu_1$, a single $\perp$ band.

TABLE VI.

Observed ν	Identification	Character of observed bands	Predicted character
2967.0 cm⁻¹	(ν_1, $2\nu_4$)	$\parallel$, $\parallel$	$\parallel$, $\perp$, $\parallel$
2879.6 cm⁻¹			
3047.2	ν_2	$\perp$	$\perp$
1355.3	ν_3	$\parallel$	$\parallel$
1459.6	ν_4	$\perp$	$\perp$
732.3	ν_5	$\parallel$	$\parallel$
1019.9	ν_6	$\perp$	$\perp$
2461.8	$\nu_6+2\nu_5$	$\perp$	$\perp$
3981.0			
4047.9	$\nu_2+\nu_6$	$\perp$, $\parallel$, $\parallel$	$\perp$, $\parallel$, $\parallel$
4089.6			
4175.8			
4230.6	$\nu_3+(\nu_1, 2\nu_4)$	$\perp$, $\parallel$	$\perp$, $\parallel$, $\perp$
4383.8	$\nu_2+\nu_3$	$\perp$	$\perp$
4453.5	$\nu_2+2\nu_6$	$\perp$	$\perp$
5400.0	?	$\perp$	–
5900.0	$\nu_2+(\nu_1, 2\nu_4)$	$\perp$	$\parallel$, $\perp$, $\perp$, $\parallel$, $\parallel$
6050.0	$2\nu_2$	$\parallel$, $\perp$	$\parallel$, $\perp$
10000.0	$\nu_4+3\nu_1$	$\perp$	$\perp$
13800.0	?	$\perp$	–

In conclusion we submit Table VI giving the centers of the observed bands, and the present interpretation of them. The character of these bands as observed is compared with that predicted by the theory of such molecules which have three equivalent particles.

Absorption Spectra of the Samarium Ion in Solids. V. The Absorption Spectrum and Energy Levels of the Sm^{+++} Ion as It Exists in Monoclinic Crystals of $Sm_2(SO_4)_3 \cdot 8H_2O$

FRANK H. SPEDDING AND RICHARD S. BEAR, *Chemical Laboratory, University of California*

(Received October 11, 1934)

The absorption spectrum and energy levels indicated therein for the samarium ion in crystalline monoclinic $Sm_2(SO_4)_3 \cdot 8H_2O$ are shown to be similar to those of $SmCl_3 \cdot 6H_2O$, which is also a monoclinic salt. Absorption lines of the sulfate at temperatures between 20°K and room temperature are used to prove the existence of several low-lying levels separated from the basic one by 160, 188 and 225 cm^{-1}. These levels are of particular interest in view of heat capacity and magnetic studies of this salt.

IN previous papers of this series[1] we have described the absorption spectra of the samarium ion for monoclinic crystals of $SmCl_3 \cdot 6H_2O$ and for hexagonal ones of $Sm(BrO_3)_3 \cdot 9H_2O$, $Sm(C_2H_5SO_4)_3 \cdot 9H_2O$ and $SmI_3 \cdot 9H_2O$. The chloride spectrum was found to be distinctly different from those of the hexagonal group in that its individual multiplets were spread out somewhat more and frequently contained more lines. These results were in agreement with those of Spedding and Nutting[2] for the corresponding gadolinium compounds, i.e., the extension within multiplets and the number of components of each of the multiplets of the rare earth ions seem to depend more on the positions of surrounding atoms or ions in the crystal and less on the chemical composition of the compound, except insofar as the composition affects the crystal structure.

This paper describes the spectrum of a second monoclinic salt, $Sm_2(SO_4)_3 \cdot 8H_2O$. The magnetic susceptibility[3] and heat capacity[4] of this solid have already been measured over a wide temperature range, and a spectroscopic determination of the energy levels will be useful in attempting to understand the results of these other investigations. Here we present only the experimental facts. In a later paper we shall introduce a discussion of the relation between the physical and chemical properties of samarium salts and their energy levels.

[1] Spedding and Bear, Phys. Rev. **42**, 58, 76 (1932); **44**, 287 (1933); **46**, 308 (1934).
[2] Spedding and Nutting, Phys. Rev. **38**, 2294 (1931); J. Am. Chem. Soc. **55**, 496 (1933).
[3] Freed, J. Am. Chem. Soc. **52**, 2702 (1930).
[4] Ahlberg and Freed, Phys. Rev. **39**, 540 (1932).

Experimental Part

Because of the difficulty of obtaining the moderately soluble sulfate as large single crystals, conglomerate absorption has been used exclusively. However, the constituent crystals were of sufficient size to escape the description "powdered" and were of approximately the same individual dimensions as the material used in preparing the former conglomerates. Groth[5] states that the crystals are monoclinic in external symmetry, with axial ratios $a : b : c = 3.0030 : 1 : 2.0022$, $\beta = 118° 16'$.

Two different preparations (however, from the same ultimate source) gave identical results. One was secured by recrystallization of sulfate of high degree of purity as originally supplied by the Wellsbach Company; the other was obtained from the same material after precipitation of the samarium as the oxalate, ignition to the oxide, solution in HCl, evaporation and reconversion to the sulfate by the method described by Freed[4] (double decomposition between H_2SO_4 and the chloride in alcoholic solution and digestion of the solid sulfate with water). Crystals finally used were grown by slow evaporation of saturated solutions.

Even more than in the chloride investigation was it difficult to choose the proper thickness of absorbing layer. Because of the magnitude of the separation between the basic state and the excited lower levels, rather thick conglomerates are required to bring out the high-temperature lines, i.e. those increasing in intensity as the temperature is raised. The extreme thickness

[5] Groth, *Crystallography*, Vol. 2, p. 458.

in turn offers trouble with increased complexity of spectra and makes longer exposures necessary. The sulfate has the additional inconvenience of showing rather diffuse lines. In obtaining the photographs with the sulfate, however, the same thicknesses, from 5 to 10 mm, have been found most satisfactory.

Investigation of only the visible region of the spectrum has been done. The equipment described before was used to obtain the photographs at low temperatures.

Results

In Fig. 1 are shown the spectra of the sulfate as transmitted at 20°, 78°, 169° and 298°K by a conglomerate of 5 mm thickness. In addition is shown a 10 mm layer photograph as it appears at 78°. Table I gives measurements and roughly estimated intensities of the absorption lines and bands observed at those temperatures.

Close examination of the photographs at low temperatures of the thin- and thick-layer spectra shows a marked tendency for the thicker layer to produce doublets from lines which are apparently single in the thin-layer case. In some instances the lines can be observed to be double for both thin and thick layers and then the effect is noticed as a widening of the separation between the two peaks of intensity.

This behavior suggests that the double lines themselves are not completely resolved. If they were composed of very fine lines of varying intensities, with the strongest located on the inner side (with respect to the doublet) of each component, one would understand how the widening occurred. Increase in layer thickness would enlarge the apparent separation of the doublet components by increasing the number of fine lines that are able to absorb strongly the light. The fine unresolved lines composing the doublet components could possibly be results of Stark splitting of the resolvable lines by the crystal field, but one is more inclined to suppose

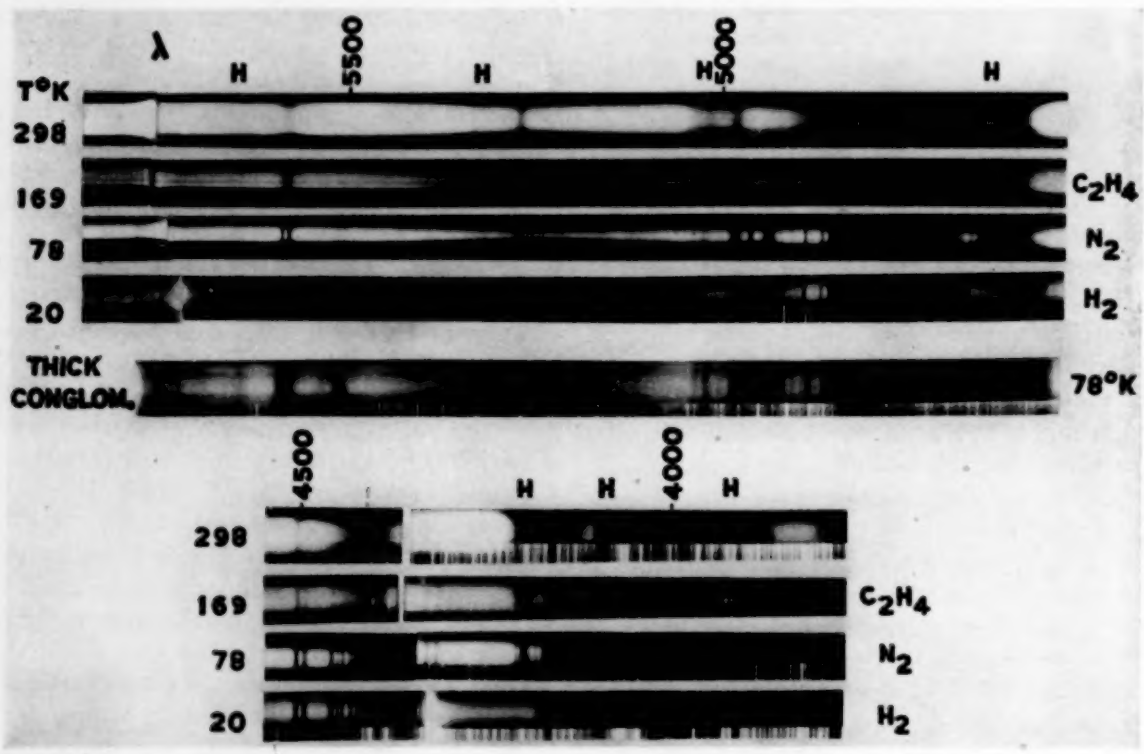

FIG. 1. Conglomerate absorption of $Sm_2(SO_4)_3 \cdot 8H_2O$. The substances at whose boiling points the spectra were photographed are indicated on the right, the corresponding temperatures on the left. *H* is placed above regions wherein the most prominent high-temperature lines are located.

TABLE I. *Conglomerate absorption lines and bands of* $Sm_2(SO_4)_3 \cdot 8H_2O$.

H (type) = high-temperature line; L (type) = low-temperature line; HL (type) = probably both types overlap; R.T., E.T., N.T. and H.T. = columns for measurements at room, ethylene, nitrogen and hydrogen temperatures, respectively; Int. = columns of intensity and character of the lines, completely filled only for hydrogen temperature. Intensity is estimated very roughly on a scale of 10, with very faint lines given as 0; *s, vs* indicate degrees of increasing sharpness; *ws* signifies that a line is somewhat broader than a single one would be expected to be but has fairly sharp edges; *nd, d, vd* indicate degrees of increasing diffuseness; *b* = broad line or band, used most frequently with bands; "2," "3" possibly double or triple, respectively. Primed values represent band edges, *c*, centers where otherwise the figure might be mistaken for a band edge. ‡ stands before lines or bands that have required extremely thick conglomerates to bring them out, *x* before lines or bands that are quoted from plates obtained with the same thick conglomerate but are also visible distinctly on plates of thinner conglomerates. The last type of line is given as it appears for thick conglomerates because of widening or greater complexity made evident therein and may be roughly compared in many cases with its appearance in a thin conglomerate by looking at the figures given for hydrogen temperature, all of which are for a thin 5 mm conglomerate.

R.T. ν(cm^{-1})	E.T. ν(cm^{-1})	Type	N.T. ν(cm^{-1})	Int.	H.T. λ(A)	H.T. ν(cm^{-1})	Int.
		H	17049				
	‡ 17131	L	17126		5837.1	17127	5*vs*
	Ends of plates. Presence uncertain, doubtful.	H	17177				
		L	17203		5810.6	17205	3*d*
		L	17256		5793.3	17256	5*d*
		H?	‡ 17348	0			
		H?	‡ 17382	0			
		H?	‡ 17404	0			
	‡ 17485	L	17483		5718.9	17481	3*d*
	‡ 17665′, 17676′	H	17667	1*d*			
	‡ 17696′, 17707′	H	17692*c*, 17702*c*	1*d*, 1*d*			
17715′	‡ 17726′, 17736′	H	17732	2*d*			
17755′	‡ 17753′, 17765′	H	17753′, 17764′	1*d*			
		H	‡ 17785	0			
	‡ 17805′, 17819′	H	‡ 17804′, 17819′, 17826′	0			
	‡ 17836′, 17850′	H	‡ 17834*c*, 17847′, 17857′	0, 0			
		?	‡ 17863	0			
		?	‡ 17878	0			
17877′	17887′	L	*x* 17886′, *x* 17888.7		5588.6′, 5588.0S	17889′, 17890.4	10*s*
		L	*x* 17894.3				
	17897′		17898′		5587.5′	17892′	
17907′	17913′		17912′		5579.7′	17917′	
	x	L	*x* 17915.9		5578.85	17919.9	10*ws* "2"
		L	*x* 17923.4		5578.1′	17922′	
17927′	17928′		17928′				
		L	17934		5574.9	17933	3*d*
		L	17947		5570.7	17946	1*d*
		L	17957		5567.6	17956	1*d*
		L	‡ 17967		5564.2	17967	1*d*
		L	‡ 17976		5561.8	17975	1*d*
			17989′				
	‡ 17996′	L	17995		5556.6*c*	17992*c*	0
		L	18003		5553.5	18002	0
	18009′		18009′		5551.0*c*	18010*c*	0
		L	18021		5547.8	18020	1*d*
		L	18028′		5545.7′	18027′	0
			18038′		5540.7′	18043′	
	18048′		18052′		5539.3′	18048′	
		L	18059		5536.9′	18056′	0
	‡	L	18067*c*		5533.2′	18068′	
		L	18080		5530.0	18080	0
	18092′	L	‡ 18096		5524.9	18095	0

R.T. ν(cm^{-1})	E.T. ν(cm^{-1})	Type	N.T. ν(cm^{-1})	Int.	H.T. λ(A)	H.T. ν(cm^{-1})	Int.
		L	‡ 18109		5520.6	18109	0
		L	18118′		5517.6*c*	18119*c*	0
		L	18133		5513.5	18132	1*d*
			18145′		5510.6′	18142′	
	18151′		18151′		5507.9′	18115′	
		L	18154		5507.1	18153	3*d*
	‡	L	18163				
			18167′		5503.1′	18166′	
	18176′	L	18178		5499.5	18179	2*d*
		L	‡ 18190		5496.2	18189	1*d*
		L	18206		5491.0	18206	1*d*
		L	‡ 18222		5486.1	18223	1*d*
		L	18238		5481.6	18238	1*d*
		L	18263		5474.0	18263	1*d*
		L?	‡ 18291				
18720′	18720′	H	18718′	1*d* "2"			
18735′	18723′		18726′				
	‡ 18763′	H	18755′	1*d*			
	18779′		18769′				
18784′	‡ 18786′	H	18780′	1*d*			
18805′	18798′		18795′				
		L	18890		5292.4	18890	1*d*
	‡ 18918	L	18917		5285.10	18915.8	2*nd*
	18941′	L	18943.9		5277.50	18943.1	10*s*
18943′			18951′		5276.1′	18948′	
	x 18951′	L	*x* 18955	"2"	5275.25	18951.3	10*ws*
18960′	18959′		18960′		5274.4′	18954′	
			18984′		5266.9′	18981′	
	‡ 18993	L	18993′		5264.1′	18991′	0
	‡ 19002.8	L	19000.5		5262.00	18998.9	1*s*
		L?	‡ 19009				
		L	‡ 19016.5*c*		5257.35	19015.8	2*nd*
	‡ 19021.3	L	‡ 19019.0*c*				
	‡ 19034.0	L	‡ 19031.0		5253.50	19029.6	1*s*
		L	19055				
	‡ 19070.4	L	19068.5		5243.25	19067.0	8*s*
		L?	‡ 19083				
	‡ 19098	L	19100		5234.70	19098.0	2*s*
	‡ 19118	L	‡ 19121				
		L	‡ 19132		5226.7	19127	0
	‡ 19158′, 19172′	L	19165		5216.8	19163	2*d*
		L?	‡ 19188′				
			19208′				
		L?	‡ 19233′				
			19263′				
		L?	‡ 19293				
		L?	‡ 19325				
		L?	‡ 19521				
		L	19550		5114.45	19547.0	1*s*
		L?	‡ 19559				

TABLE I—(*Continued.*)

R.T. ν(cm⁻¹)		E.T. ν(cm⁻¹)	Type		N.T. ν(cm⁻¹)	Int.	H.T. λ(A)	H.T. ν(cm⁻¹)	Int.
19820′		19822′	H	‡	19811				
			H		19815	1*d*			
19842′		19840′			19831	3*d*			
					19835′				
					19858′				
		19867′	H		19868	2*d*			
					19870′				
					19878′				
19883′			H		19883	3*d*			
			H		19895	2*d*			
		19904′			19897′				
19915′			H?	‡	19911	0			
		19942′	H		19942	1*d*			
	‡		H		19963′	1*d*			
		19974′			19973′				
					20005′				
			L	‡	20009		4996.2	20009	1*d*
			L				4994.0	20018	1*d*
20029′		20032′			20037′		4992.3′	20025′	
	x		L				4989.05*c*	20038.3*c*	10*nd*
		20048′	L		20045′		4987.80*c*	20043.3*c*	10*nd*
					20050′				
20061′	*x*	20058	L	*x*	20060′		4984.95	20054.8	10*ws*
			L		20072′		4981.9	20067	3*d*
			L	‡	20083		4977.4	20085	0
20095′			L	‡	20097		4974.7	20096	0
			L				4972.0	20107	00
					20115′		4969.6′	20117′	
		20124′	L	*x*	20124′		4967.7′	20124′	
20133′		20136′			20137′		4965.5′	20133′	9*d*
							4962.7′	20145′	
			L		20154		4960.4	20154	0
					20169′				
			L	‡	20171		4956.15	20171.3	2*nd*
	‡	20177′	L	‡	20182		4953.40	20182.5	2*nd*
20198′		20192′	L	‡	20193		4951.00	20192.3	2*nd*
					20201′				
		20206′	L		20204		4948.1	20204	6*d*
			L		20214		4945.7	20214	8*d*
20224′		20222′			20223′				
	x		L		20226		4943.0	20225	9*d*
		20233′			20228′				
		20242′			20239′		4940.3′	20236′	
	x		L				4938.5′	20243′	10*d*
		20250′			20248′		4936.8′	20250′	
			L				4934.20	20261.1	0*s*
	‡	20268′	HL				4931.7′	20271′	0
20283′		20280′					4929.2′	20282′	
		20295′			20293′		4926.1′	20294′	
			HL		20299				0
20308′		20306′			20302′		4922.2′	20310′	
		20339′	L				4918.0	20328	0
20354′	*x*	20355′	HL		20343		4915.9′	20337′	0
	x	20366	H	‡	20361		4910.9′	20357′	
		20388′	L	‡	20387		4903.9	20386	1*d*
	HL		L	‡	20397		4901.1	20398	1*d*
20407′		20408′	L				4897.6	20413	0
					20423′				
20430′		20431	L		20429		4894.00	20427.5	10*s*
20444′					20431′				
		20451′	H	‡	20456				
		20465′							
			H?	‡	20479				
20512′		20512′	L		20522.2		4871.70	20521.1	10*s*
20524		20527′							

R.T. ν(cm⁻¹)	E.T. ν(cm⁻¹)	Type		N.T. ν(cm⁻¹)	Int.	H.T. λ(A)	H.T. ν(cm⁻¹)	Int.
		L	‡	20544		4866.2	20544	1*d*
20555	20562′	L		20569		4860.40	20568.7	10*ws*
	20573′							
		L				4856.10	20586.9	1*s*
		L				4854.35	20594.4	1*s*
20602′		L		20598′		4851.80	20605.2	2*s*
						4850.1′	20613′	
		L		20615′		4849.2	20616	10*d*
	20621	L		20621		4847.5	20624	10*d*
				20626′		4846.5′	20628′	
		L		20640		4843.9	20639	9*d*
		L				4841.0	20651	2*d*
	20659′	L		20655′		4839.7′	20657′	
	20672′			20673′		4835.0′	20677′	10*db*
	20689′	L		20689′		4831.7′	20691′	
20698′	20707′			20708′		4826.2′	20714′	10*db*
	20738′	L		20733′		4821.6′	20734′	
	20753′			20756′		4816.8′	20755′	10*db*
	20771′	L		20776′		4813.5′	20769′	
	20789′			20789′		4808.0′	20793′	10*db*
	20820′			20817		4804.4′	20808′	
20852′	20851′	L		20842′				
20880′	20882′			20878′				
20919′	20917′	L		20924′				10*db*
20942′	20944′			20955′				
20992′	20983′	L		20983′				
21028′	21010′			21010′		4755.2′	21024′	
	21041′	L		21039′		4753.1′	21033′	
	21061′			21050′		4749.8′	21048′	8*db*
	21089′	L		21084′		4743.2′	21077′	
	21101′			21096′		4738.2′	21099′	10*db*
21138′	21141′			21140′		4732.1′	21127′	
		L		21147				
	21154′			21149′				
	21165′			21165′				
		L		21173				10*db*
21178′	21179′			21181′		4719.9′	21181′	
21210′	21209′			21206′		4716.0′	21199′	
		L		21212				
	21227′	L		21227				10*db*
21232′				21235′		4706.8′	21240′	
	21293	L		21291′		4695.9′	21289′	
				21301′		4693.1′	21302′	8*db*
21332′	21331′	H(L)		21328′	3*d*	4687.6*c*	21327*c*	
21362′	21348′			21341′		4683.9′	21344′	1*d*
		H(L)		21391′	3*d*	4674.5′	21387′	
21400′	21405			21404′		4670.7′	21404′	1*d*
21429′						4666.4′	21424′	
		L				4663.0′	21439′	0
21451′	21450′	H(L)		21454′		4660.3′	21452′	
	21471′			21466′	8*db*	4656.0′	21472′	0
21487′		L				4654.10	21480.4	1*s*
		L				4651.10	21494.3	1*s*
21508′	21506′	L		21513′		4648.55	21506.1	2*vs*
		H(L)			8*db*	4646.2	21517	2*d*
21548′	21532′	L		21523′		4644.05	21526.9	1*vs.*
						4638.3′	21554′	
	21566	L		21563		4635.8′	21565′	8*db*
		L				4631.0	21588	2*d*
21622′				21620′		4625.4′	21614′	
	21628	L		21625				9*db*
				21629′		4622.4′	21628′	
				21645′		4619.3′	21642′	
21649′	21648	L		21649				8*db*
				21653′		4616.8′	21654′	

TABLE I—(*Continued.*)

R.T. ν(cm⁻¹)	E.T. ν(cm⁻¹)	Type	N.T. ν(cm⁻¹)	Int.	H.T. λ(A)	H.T. ν(cm⁻¹)	Int.
21677′	21671′	L	21668′		4614.2′	21666′	8*db*
	21682′		21674		4610.7′	21683′	
	21693′	L	21692′		4607.5′	21698′	9*db*
21708′	21706′		21717′		4603.8′	21715′	
					4601.6′	21725′	
		L	21737		4598.9′	21738′	2*d*
					4596.3′	21750′	
		L	21759		4593.8′	21763′	2*d*
					4591.5′	21773′	
	‡ 21777	L	21779		4589.4′	21783′	2*d*
					4586.7′	21796′	
	‡ 21802	L	21804		4584.2′	21808′	2*d*
					4581.3′	21822′	
	‡ 21828	L	21830		4579.5′	21830′	1*d*
					4576.8′	21843′	
		L			4574.5′	21854′	0
	‡ 21862′				4572.7′	21863′	
	21879′	L	21873		4569.8′	21877′	1*d*
		?	‡ 21906	0			
	21915′	L	21931		4560.6′	21921′	1*db*
21951′	x 21950′				4556.1′	21943′	
	21970	H	‡ 21966	1*d*	4550.1′	21971′	
21983′		L	‡ 21982	0	4546.4′	21989′	0
22007′	22014′	H	‡ 22014	1*d*			
		L	22022′		4538.55	22027.4	1*nd*
22033′	22036′		x 22039′				
		?	‡ 22052	1*d*			
22072′	22070′	H	‡ 22068′	1*d*			
	22088′		22082′				
22101′		H	‡ 22094	1*d*			
		H	‡ 22112′	0			
			22127′				
		H	‡ 22149′	0			
			22165′				
			22181′				
22186′	22185′	L	x 22186		4505.9*c*	22187*c*	10*d*
	x "2"	L	x 22196		4504.9*c*	22192*c*	10*d*
22202′	22200′		22200′				
22236′			22234′				
		L	x 22237		4495.40	22238.8	10*s*
	22240	L	x 22241				
			22244′				
22258′	22255	L	22254.6		4492.30	22254.1	10*s*
		H	‡ 22281	1*d*			
	‡ 22303′	H	22300	2*d*			
22314′	‡ 22324′	H	‡ 22321	1*d*			
22342′	‡ 22334′	H	22341	1*d*			
	22348′						
	22370′	H	‡ 22360′				
	‡ 22385′	H	x 22379′	1*d* "2"			
	22397′		22392′	1*d* "2"			
			22416′				
22421′	22420′	L	x 22420		4459.3′	22419′	10*d*
	x	L	x 22430		4457.9′	22426′	
	22435′		22437′		4456.1′	22435′	
22448′		L			4453.7	22447	0
22466′	22470	L	22468.3		4449.60	22467.6	10*s*
22501′	22501	L	22500.0		4443.15	22500.4	10*s*
22531′	22539′						
	x 22554′	L	22549		4433.5	22549	8*d*
22562′	‡ 22566	L	22566.5		4430.05	22566.8	8*s*
		L	22583		4426.7	22584	3*d*
		L			4424.0	22598	3*d*

R.T. ν(cm⁻¹)	E.T. ν(cm⁻¹)	Type	N.T. ν(cm⁻¹)	Int.	H.T. λ(A)	H.T. ν(cm⁻¹)	Int.
22609′	22609′				4421.7′	22609′	
		L	22616′		4420.4′	22616′	10*db*
	22628′		22625′		4417.7′	22630′	
22650′	22642′		22646′		4414.7′	22645′	10*db*
		L			4413.5′	22652′	
	22656′				4412.6′	22656′	10*db*
		L	22663′		4410.4′	22667′	
					4408.2′	22679′	
22722′	‡ 22732′	L	22731′		4398.6′	22728′	9*db*
	22744′		22743′		4395.4′	22745′	
	‡ 22766′	L	22765′		4392.3′	22761′	9*db*
22776′	22780′		22776′		4387.3′	22787′	
		L	22823′		4380.1′	22824′	9*db*
			22835′		4378.1′	22835′	
			22859′		4374.2′	22855′	9*db*
		L	22865′		4371.4′	22870′	
			22894′		4366.7′	22894′	
			22932′		4359.9′	22930′	
	‡ 22945	L	22940′		4356.9′	22946′	8*db*
			22949′				
			22962′		4354.3′	22959′	
	‡ 22971	L	22972′		4351.5′	22974′	10*db*
	‡ 23003	L	23001		4347.0	22998	9*d*
23015′		L			4343.1	23018	0
23055′	23045	L	23043		4338.8	23041	10*d*
23072′	23079*c*	L	23075		4332.7	23074	9*d*
	23088*c*	L	23086		4330.5	23086	9*d*
23113′	23107	L	23104		4327.2	23103	7*d*
		L	23121		4323.7	23122	0
23152′			23154′		4318.3′	23151′	
23175′	23160	L	23160′		4315.8′	23164′	8*db*
	23305.7	L	23300.6		4290.75	23299.3	3*ns*
23645′			23660′				
		H?	‡ 23680′	0			
		H?	‡ 23690	0			
23712′	23720′	H	‡ 23723	1*d*			
	23747′		23747′				
23759′	23758′	H	23753′	7*d*			
	23785′	H	23782′	9*d*			
	23800′		23796′				
23812′	23812′	H	23808′	9*d*			
	23826′		23820′				
23853′	23850′		23846′				
23880′	23883′						
23918′	23907′	L	23900		4183.15	23898.7	10*ns*
23965′			23964′		4172.3′	23961′	
	23969′	L			4171.1	23968	10*d*
	23985′				4168.6	23982	10*d*
23990′			23986′		4167.5′	23988′	
		L			4166.4	23995	0
		L			4162.8	24015	1*d*
		L	24031		4160.52	24028.7	10*s*
24040′	24056′		24050′		4157.8′	24045′	
24067′	24074′	L	24075′				
24094′	24094′		24098′				
24137′	24152′	L					
24196′	24186′		24182′				10*db*
		L	24213′				
			24234′				
		L	24257′				
	24276′		24289′		4116.0′	24289′	
		?	24299	1*d*			
24325′		L	24319	6*d*	4110.4	24321	9*d*
	24337	H	24333	4*d*			
		L			4105.7	24350	7*d*

TABLE I—(*Continued.*)

R.T. ν(cm⁻¹)	E.T. ν(cm⁻¹)	Type	N.T. ν(cm⁻¹)	Int.	H.T. λ(A)	H.T. ν(cm⁻¹)	Int.
	24362	H	24357	3*d*			
		L	24368	3*d*	4102.5	24369	7*d*
24387′	24386′	H	24389*c*	7*d*			
	24401′	HL	24397*c*	7*d*	4097.5	24398	2*d*
	24415′	L	24412*c*	7*d*	4095.2	24412	9*d*
	24429′	H	24422*c*	7*d*			
		L			4090.9	24438	7*d*
	24443′	H	24445*c*	7*d*			
	24460′	H	24452*c*	7*d*			
		L			4087.2	24060	2*d* "2"
	24477	H	24477	6*d*			
		L			4082.8	24486	4*d*
24486′		H	24494	3*d*			
	24522′	?	24513	0	4079.0′	24509′	"2"
24550′	24546′	L	24545′		4072.5	24548	10*d*
	24554						
	24566	L			4069.6	24565	9*d*
	24572′		24570′				
24580′	24584	L	24583		4066.9*c*	24582*c*	10*d*
		L	24599		4064.3	24598	4*nd*
	24612	L	24611		4062.1	24611	10*d*
	24637	L	24636		4058.1	24635	10*d*
24655′	24650	L	24651		4055.4	24651	10*d*
	24665′	L	24668*c*		4053.0	24666	10*d*
	24681′	L	24677*c*		4050.5	24681	10*d*
	24697′	L			4048.2	24695	1*d*
			24702′		4046.0′	24709′	
					4034.4′	24780′	
		L	24845′				
			24880′				
		L	24930′				
			24960′				
25135′	25160′		25155′				
	25181	L	25177′				
			25189′				
			25204′				
25215′	25215	L	25222′				10*b*
25255′	25240	L	25234′				
			25255′				
		L	25272				
		L	25293				
	25310	L	25311				
	25345	L	25342		3945.1	25341	Too Intense for Intensity Estimation
			25360′				
25377	25369	L	25370′		3941.2	25366	
					3940.1′	25373′	
		L			3937.1	25392	
	25413′	L	25413		3933.6	25415	
H 25431′	25432′	L	25440		3929.6	25440	
25462′		L			3927.2	25456	
25475′	25478′	L	25485		3923.2	25482	
	25500′	L	25499		3920.7	25498	
25520′		L	25528		3916.4	25527	
		L	25561		3912.7′	25551′	
25574′			25571′				
	25584	L	25590′				
	25605	L	25598′				
25619′			25617′				
			25640′				
	25646	L	25650′				
		L	25659				
	25676	L	25676				
		L	25686				
25708′	25700	L	25702				
	25724	L	25720′				
			25729′				
	25745	L	25742′				
25764′			25749′		3880.3′	25764′	

R.T. ν(cm⁻¹)	E.T. ν(cm⁻¹)	Type	N.T. ν(cm⁻¹)	Int.	H.T. λ(A)	H.T. ν(cm⁻¹)	Int.
			25792′		3876.7′	25788′	
25800	25797	L	25800′		3874.4′	25803′	
25816′	25820′		25819′				
		L	25822		3871.7	25821	
		L	25837		3868.8	25840	
25843′	25839′		25839′				
	25858	L	25858		3866.1	25859	
	‡ 25902	?					
25920′	25928′		25924′		3857′	25920′	
	‡ 25953′	L	25950′		Absorption		
25963′	25967′	L	25971		too		
	‡ 25992′	L	25987		strong.		
	‡ 26006′	L	26014				
26026′	26027′						
	‡ 26043	?					
	26052′		26057′				
26086′	26074′	L	26079′				
	‡ 26214	H					
	‡ 26254′						
26280′	26285′	H					
	26335′						
	‡ 26370′	H					
	‡ 26397	H?					
26415′		L	26414*c*				
	26419	L	26420*c*				
		L	26434				
		L	26449				
	26451′		26480′				
	26500′		Abs.				
	26530′		too				
	26580′		strong.				
	26603′						
	26630′						
	26655′						
	26695′						
	26815′						
	26860						
	26890						
26940′	26926						
	26967						
27040′	27010						
27132′	27130′						
27165′	27150′						
27200′	27190′						
27235′	27218′						
27330′	27350′						
	27380′						
	27420′						
	27470′						
	27545′						
	27660′						
	27695′						
27925′	27920′						
	‡ 27953′						
	27980′						
	28004′						
28055′	‡ 28061						
	‡ 28081						
	28100′						
	x 28126′						
28185′	28193						
28210′							
28280′	28280						
28310′	28300						
28318′	28330						
28342′							

that they are due to magnetic interactions between samarium ions because of the extreme smallness of the effect. This phenomenon is not entirely absent in the chloride spectrum but it is interesting that this peculiarity should be most pronounced with the sulfate, whose spectrum in other ways seems to be that resulting from a crystalline field which is even stronger than that of the chloride.

It seems reasonable to assume that the easily distinguishable lines composing a multiplet group are the ones that reflect the separations between levels arising from electric splitting of a highly excited level which would be single and degenerate in the absence of the crystal field. Smaller separations between lines within a multiplet may indicate small electric separations (of the order of 10 cm^{-1} or less) of the well-shielded basic $^6H_{5/2}$ level, while the variability in apparent position of individual lines indicates that a further, possibly magnetic, perturbation affects the levels. This division of the experimentally observed effects cannot be proved at present, however, since both electric and magnetic phenomena would produce qualitatively identical results, i.e., with stronger or less homogeneous fields the magnitudes of both types of splitting would be greater. If the above explanation of the behavior of the lines is correct, one would expect that greater spectroscopic resolution, and perhaps lower temperatures, will reveal important facts concerning the nature of energy levels in solids. The longer exposures required for this procedure (they are already from 30 to 60 hours in length) would raise extreme difficulties at 20°K or lower.

In spite of the trouble in locating the exact position of the individual components of the doublets, it has been found possible to determine pretty definitely the situation of the lower levels that are most important spectroscopically. This has been done by working with centers of doublets and diffuse lines or bands. The results for the most clear multiplets (the same ones previously diagrammed for the chloride) are given in Fig. 2, though many of the less important faint *low-temperature lines* of these regions are not included. All of the most intense *high-temperature lines* in these multiplets can be explained by the use of the levels 0, 160, 188 and 225 cm^{-1}. Evidence from other more complex portions of the spectrum supports these values in general. Again *both constant energy separations* and *proper temperature behavior of intensity* have been made the requirements for the location of the lines in the diagram.

There is some evidence at higher temperatures for the existence of another level at approximately 245 cm^{-1} from the basic one. This is most apparent at about 23,600 to 23,800 cm^{-1}, where no other simple explanation of the reddest ends of the bands observed at ethylene and room temperatures seems possible. The faint bands, which extend 300 and more cm^{-1} from the nearest low-temperature line in the chloride spectrum and which probably require levels of corresponding separations, are not visible in the sulfate spectrum. This may be related to the general displacement of the sulfate levels to higher energy values, a shift perhaps just able to eliminate possibility of observing transitions from these levels.

In the foregoing consideration it is assumed that the basic levels of the ions of the two salts are similar ($^6H_{5/2}$) and that the 145, 160, 204 and 217 levels of the chloride are related, respectively, to the 160, 188, 225 and 245 ones of the sulfate. In this connection it is interesting that though the chloride lines arising from the levels 160 and 217 seem to be most conspicuous, in the sulfate the 160 and 225 lines are most noticeable. This suggests a reversal of the relation just given within the doublets of levels.

The multiplet on the long wave-length end of the spectrum at 17,000 to 17,300 cm^{-1} is one that offers some rather puzzling features. In the chloride, ethylsulfate and bromate spectra nothing of certainty could be gathered from it, hence it could not be used to determine the energy levels. The corresponding sulfate lines, however, do seem to indicate the presence of another level by the existence of two high-temperature satellites 78 cm^{-1} from their respective low-temperature companions. It is not justifiable to base the existence of a level, whose Boltzmann population should allow it to be made more evident elsewhere in the spectrum, upon such isolated cases. Though the evidence at hand is inconclusive, it would not be surprising to have such a level be demonstrated eventually.

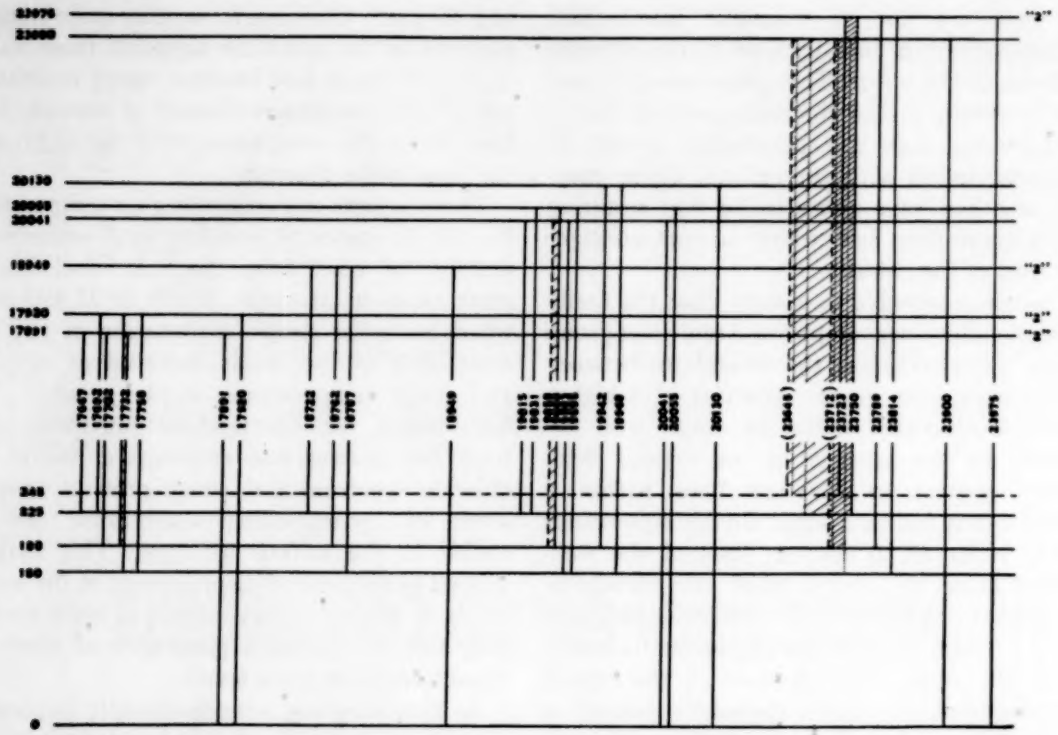

FIG. 2. Energy levels of $Sm_2(SO_4)_3 \cdot 8H_2O$. Shaded areas represent bands. Figures in parentheses denote band edges measured at ethylene temperature. All other figures are from plates taken at 78°K. Levels which are actually probably double are indicated by "2."

It may be anticipated that the bromide spectrum also has a possible level at 58 cm^{-1}, evidence for which is based on similar scanty evidence in this region, beside the proper "monoclinic" levels somewhat higher.

Table II shows how well the lines agree with the level diagram assumed. In many other places on the plates the existence of the new lines brought into evidence at low temperatures by the lessened thermal agitation of the crystal and the higher population in the basic state makes it impossible to pick out satisfactorily the location of the high-temperature satellites. However, at ethylene temperature (169°K), when the fainter low-temperature lines have been "washed out," one is often able to locate additional confirmation of the postulated levels.

The most important relations between the sulfate and chloride spectra in other types of behavior are the following. The sulfate shows practically the same amount of displacement in the positions of lines upon changing the temperature from 298° to 20°K. At any given temperature the sulfate multiplets are shifted to shorter wave-lengths from the corresponding ones in the chloride spectrum, though only by about 10 to 20 cm^{-1}. On the other hand it will be recalled that the bromate acted in a different manner, manifesting slightly greater shifts with temperature change and possessing multiplets located 50 to 100 cm^{-1} toward longer wave-lengths than

TABLE II. *Prominent low-temperature lines and their high-temperature satellites (78°K).*

L.-t. line	Satellite *A*		Satellite *B*		Satellite *C*	
ν(cm^{-1})	ν(cm^{-1})	$\Delta\nu_A$	ν(cm^{-1})	$\Delta\nu_B$	ν(cm^{-1})	$\Delta\nu_C$
17891	17732	159	17702	189	17667	224
17919	17758	161	17732	187	17692	227
18949	18787	162	18762	187	18722	227
20041	19882	159	Too diffuse		19815	226
20056	19895	161	19868	188	19831	225
20130	19968	163	19942	188		
20522	20361	161				
20621	20456	165				
22190	22030	160			21966	224
22239	22074	163	22052	187	22014	225
22255	22094	161				
23975	23814	161	23789	186	23750	225

those of the chloride. The ethylsulfate of samarium resembled the bromate in these respects.

Conclusions

Again, this time in the sulfate spectrum, is proved the existence of more than three lower levels which are of importance in determining the absorption spectrum of the samarium ion. It seems impossible that crystal splitting of the basic $^6H_{5/2}$ level could account for them all, since only three new levels $(J+\frac{1}{2})$ can be expected when electric perturbations remove the degeneracy of such a state. A possible explanation of these levels has been advanced by one of us.[6]

Magnetic interactions between samarium ions could increase the number of levels resulting from the $^6H_{5/2}$ one, but it is unlikely that these could be of sufficient magnitude since the magnetic moment of a samarium ion is so small. We have indicated that magnetic effects are probably responsible for the diffuseness and variability in appearance of certain of the absorption lines, an effect so small as to be unresolvable on the present plates.

[6] Spedding, J. Am. Chem. Soc. **54**, 2593 (1932).

DECEMBER 1, 1934 PHYSICAL REVIEW VOLUME 46

Elastic Electron Scattering in Potassium

J. Howard McMillen,* *Palmer Physical Laboratory, Princeton, New Jersey*

(Received July 2, 1934)

A method was developed for the measurement of slow electron scattering in vapors. Angular distribution curves from 25° to 160° were obtained for 5, 10, 15, 25, 50, 75, 100 and 150 volt electrons elastically scattered by potassium atoms. All curves contained a large peak near 100°. The scattering curves fell off rapidly for angles up to about 60° and rose rapidly for angles greater than about 130°. The position of the peak was found to shift to larger and then smaller angles as the energy of the colliding electrons was decreased. Henneberg's calculations which employ the Thomas-Fermi atomic field were found to give scattering curves whose general shapes agree quite well with the experimental curves. Best agreement occurred for the 5 and 50 volt electrons. When the potassium and argon experimental curves were compared it was found that the curves were quite similar for electron energies of 50 volts or more. For slower electrons the curves became more dissimilar.

Introduction

THE angular distribution curves for electrons scattered elastically by gaseous atoms generally contain a set of maxima and minima. These are referred to as diffraction patterns and are attributed to the diffraction of the associated de Broglie waves in their passage through the field of the atom.[1]

If exchange effects are neglected the nature of these patterns is seen to depend almost entirely upon the electrons' distance of closest approach as taken from the classical theory and the magnitude of the field at that distance. Considerable progress has been made in our understanding of the relations between these factors by the comparison of diffraction patterns for various gases and for various energies of the scattered electrons.

So far scattering measurements have been made on several important groups of atoms, namely, the inert gases,[2, 3] the halogens,[4] and three elements from the third column of the periodic table, zinc,[5] cadmium,[6] and mercury.[7, 8] The longest unbroken sequence of increasing

* National Research Fellow.

[1] For general discussion of theory, see Mott and Massey, *Theory of Atomic Collisions*, Oxford Press (1933).

[2] F. L. Arnot, Proc. Roy. Soc. **A133**, 615 (1931).

[3] Hughes, McMillen and Webb, Phys. Rev. **41**, 154 (1932).

[4] F. L. Arnot, Proc. Roy. Soc. **A144**, 360 (1934).

[5] E. C. Childs and H. S. W. Massey, Proc. Roy. Soc. **A141**, 473 (1933).

[6] E. C. Childs and H. S. W. Massey, Proc. Roy. Soc. **A142**, 509 (1933).

[7] F. L. Arnot, Proc. Roy. Soc. **A140**, 334 (1933).

[8] E. B. Jordan and R. B. Brode, Phys. Rev. **43**, 112 (1933).

atomic number is that made up of phosphorus, sulphur, chlorine and argon.[9]

It was deemed advisable to extend the data pertaining to electron diffraction patterns by obtaining curves for one of the alkalis. Of this group potassium was considered the most important, as it extends the phosphorus-argon series mentioned above. It was also hoped that because of its hydrogen-like structure the experimental data would be of considerable theoretical interest.

Apparatus

Electron scattering in a vapor was first accomplished by Childs and Massey.[6] They concentrated the vapor at the scattering center by utilizing an undefined jet. A similar arrangement was attempted by the author but abandoned because of the following difficulties. It was found first of all that the background scattering (scattering current observed with the oven cooled) formed too large a portion of the scattering from the vapor.[10] Increasing the effective pressure within the jet by raising the temperature of the oven so reduced the life of the charge as to prohibit any improvement in this direction. Consideration of the possibility of lengthening the collision path was abandoned because of the non-uniformity of pressure throughout the jet included in this path. Over the collision path the pressure within the jet varies as $\cos^2 \varphi$ where φ is the angular spread of the jet. This variation in pressure is negligible as long as the collision path is very short or the oven far away. Both these latter requirements seriously reduce the magnitude of the scattered current.

These difficulties were overcome by constructing a collision chamber that was practically molecule-tight for low pressures and which was capable of being raised to about 150°C, a temperature which gives a pressure of about 0.001 mm of mercury. A small slit in the chamber permitted the passage of the scattered electrons to the collector and at the same time accounted for very little loss of the vapor. Within this chamber was rotated the electron gun. This was accomplished by suspending the gun from the lid of the chamber and then rotating the lid while the lid's own weight kept it in place. With this method as high a pressure as was desired could be maintained and with a much less expenditure of energy than in the jet method.

Details of the apparatus are shown in Fig. 1. A large brass base plate P, a cylindrical wall W and a disk K formed a chamber in which was placed the oven-collision chamber A and the electron energy filter F. Electrons from a tungsten filament leave the electron gun G and enter the collision chamber A. Those scattered at a particular angle θ pass out of the chamber through S to the electron energy filter F and from there to the collector C.

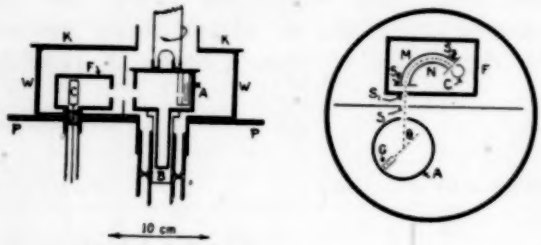

Fig. 1. Apparatus.

The collision chamber was a thick walled chamber, made of nichrome IV alloy. This alloy is non-magnetic and gave no evidence of reacting with the potassium. The lower part of A held the charge of potassium and fitted into a lavite furnace B which was wound with heating wire. The chamber was supported in a glass tube which was waxed into a base plate P. The chamber was well insulated from losses by heat conduction by using small wire stays and glass as supports. To reduce the radiation losses the chamber was polished. Water jackets served to cool the rest of the apparatus in the proximity of the oven.

The electron gun was made of thin wall nichrome IV and fastened rigidly to the top of the chamber A. By means of a ground glass joint the top of A could be rotated.

The electron energy filter separated the electrons of various energies through the use of a radial electrostatic field. The details of this

[9] C. B. O. Mohr and F. H. Nicoll, Proc. Roy. Soc. **A138**, 469 (1932).

[10] This may be the surface ionization effect observed by Childs and Massey, reference 5, when they attempted to scatter electrons from potassium in the apparatus which they subsequently used for cadmium and zinc.

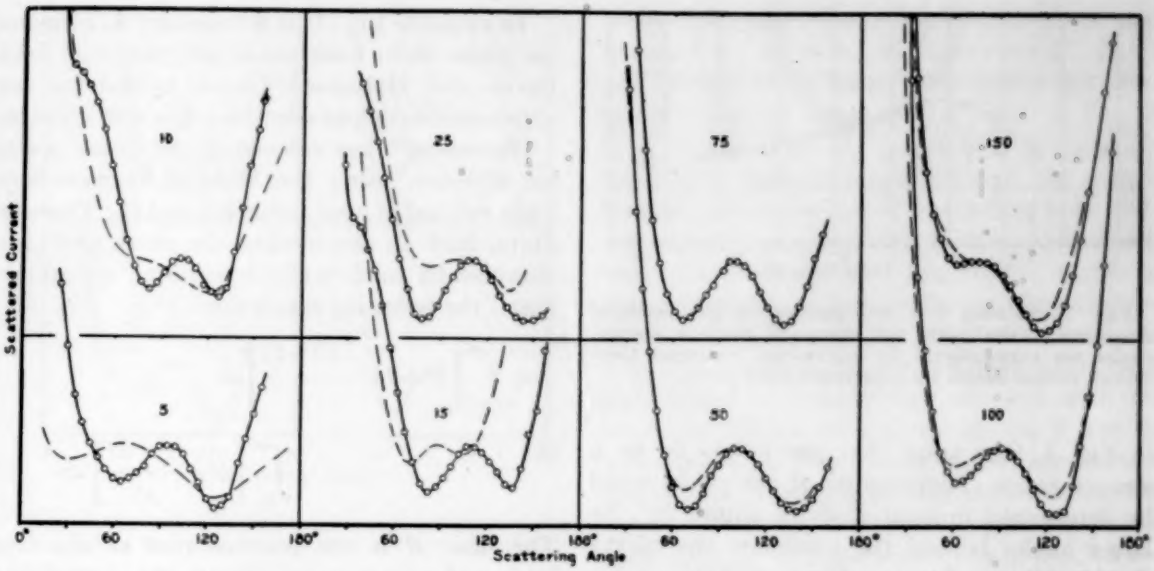

FIG. 2. Angular distribution curves for electrons of various energies: *continuous line* for potassium, *broken line* for argon.

method have been discussed in earlier reports.[11, 12] In this experiment the parts were contained in a brass box. The box was supported on a brass tube which ran out through the base plate. The filter was electrically insulated from the rest of the apparatus and it was possible to lower or increase the energy of the electrons before entering the filter. The resolution of the electron energy filter was such as to filter out the electrons suffering the first inelastic loss (1.6 volts) if the energy of the elastically scattered electrons was 50 volts or less. Hence in studying the scattering of electrons of energy greater than 50 volts they were retarded to 50 volts energy, by appropriately adjusting the potential of F, before the electrons entered the electron energy filter.

The pressure in the oven was determined from thermocouple readings of its temperature. The pressure was kept low enough to insure single collisions. At the temperatures used the vapor was 99.95 percent monatomic.[13]

Readings were taken before and after the oven had been heated to measure the scattering from the walls of the apparatus. These readings were negligible in all cases except that in which 5 volts electrons were used. For this case the background scattering had to be subtracted. Every set of readings was checked by repeating on both sides of the zero angle.

The following dimensions may be of interest: Slit S, 8×4 mm; slits S_1, S_2 and S_3, 1×10 mm; diameter of holes in gun, 1 mm; distance between S_1 and S_2, 10 mm; diameter of deflection plates M and N, 24 mm and 30 mm; cross section of electron gun, 3 mm by 11 mm.

EXPERIMENTAL RESULTS

Elastic scattering data was obtained for 5, 10, 15, 25, 50, 75, 100 and 150 volt electrons over an angular range extending from 25° to 160°. (See Fig. 2.)

All curves show a peak or maximum in the vicinity of 100°. This peak shifts to larger angles and then retreats to smaller angles as one goes from higher colliding electron energies to lower ones. The peaks for electrons of energies less than 100 volts are symmetrical about their center and their positions quite easily ascertained. In the 150 volt curve, however, the peak is not well defined and its position is somewhat difficult to determine. The position of the peak is given as a function of colliding electron energy

[11] A. L. Hughes and V. Rojansky, Phys. Rev. **34**, 284 (1929).
[12] A. L. Hughes and J. H. McMillen, Phys. Rev. **34**, 291 (1929).
[13] F. W. Loomis and R. E. Nusbaum, Phys. Rev. **39**, 89 (1932).

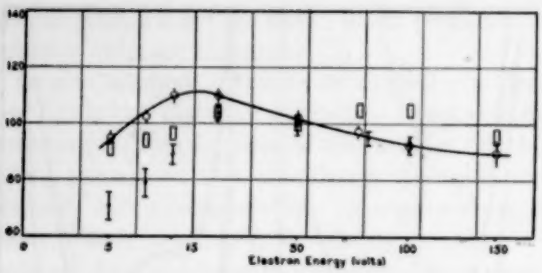

FIG. 3. Showing how the position of the principal maximum varies with the scattered electron energy: *circles* are experimental for potassium, *rectangles* theoretical, *vertical dashes* are experimental for argon.

in Fig. 3. One notes that the points lie on a smooth curve. The position of the peaks could be determined in most cases to within $2\frac{1}{2}°$. At larger angles beyond the maximum the curves rise rapidly, indicating large probability for backward scattering. On the 10, 15 and 25 volt curves there is an indication of a second peak somewhere in the neighborhood of 40°. Its exact position is very difficult to determine, however, as it is superimposed on a very steep part of the curve. At small angles the scattering falls off less rapidly for slower electrons, as has been found to be the case in the investigations of other gases.

DISCUSSION

The wave theory of elastic electron scattering is embodied in the following expression:[14]

$$f(\theta)=k^{-2}d\omega\sum_{l,\,l'=0}^{\infty}(2l+1)(2l'+1)P_l(\cos\theta)\times P_{l'}(\cos\theta)\sin\gamma_l\sin\gamma_{l'}\cos(\gamma_l-\gamma_{l'}),\quad(1)$$

where $d\omega$ is the increment of solid angle P_l is the Legendre polynomial of the lth degree, l and l' the orbital angular momentum quantum numbers, and γ_l the phase shifts brought about by the scattering field of the atom. Both exchange effects and the possibility of polarization have been neglected in arriving at this expression. Neither become important until colliding electron energies approach magnitudes comparable with those of the ionization potentials. Just how necessary it is to take into account these effects is still very uncertain.

[14] P. M. Morse, Rev. Mod. Phys. **4**, 577 (1932).

To evaluate Eq. (1) it is necessary to compute the phase shifts from the atom's potential field. Faxen and Holtsmark[15] have carried out an approximate computation for argon and krypton.

Henneberg[16] has calculated the phase shifts for mercury, using the Wentzel-Kramers-Brillouin method of approximation and the Thomas-Fermi field. In this method the phase shifts are obtained by numerically integrating (in atomic units) the following expression:

$$\gamma_l=\int_R^{\infty}\left[k^2+2V-\frac{l(l+1)}{r^2}\right]^{\frac{1}{2}}dr-\int_{R_0}^{\infty}\left[k^2-\frac{l(l+1)}{r^2}\right]dr.\quad(2)$$

The limit R is the positive root of the first integrand and corresponds to the *distance of closest approach* on the particle theory of scattering. The limit R_0 is the positive root of the second integrand and in the particle theory is known as the *impact parameter*. Phase shifts for mercury are given by Henneberg as a function of l for various values of k^2. Now a very important feature of Henneberg's theory lies in the fact that these phase shifts as calculated for mercury are applicable to any other scattering atom. To obtain a set of phase shifts for an

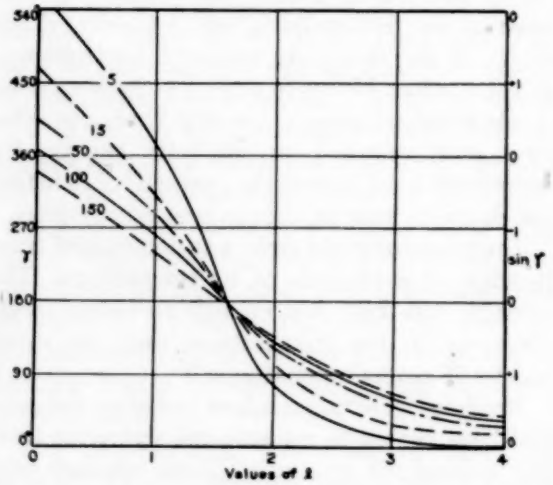

FIG. 4. Showing potassium phase shifts and their sines for various l values and electron energies.

[15] H. Faxen and J. Holtsmark, Zeits. f. Physik **45**, 307 (1927).

[16] W. Henneberg, Zeits. f. Physik **83**, 555 (1933).

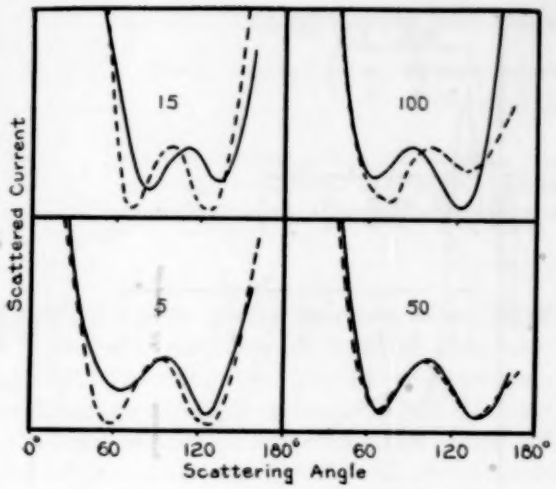

FIG. 5. *Continuous line* indicates experimental scattering curve, *broken lines* refer to the calculated curves of Henneberg.

atom of atomic number Z one first defines a variable q as:

$$q=(Z'/Z)^{\frac{1}{2}},$$

where Z' represents the atomic number of mercury. The new phase shift is then given by:

$$\gamma_Z(k)=q^{-1}\gamma_{Z'}(q^2k)$$

and the new l values by:

$$l_Z=q^{-1}(l_{Z'}+\tfrac{1}{2})-\tfrac{1}{2}.$$

Using these relations, it was possible to obtain a set of phase shifts for potassium. A few of these are plotted in Fig. 4.

Now Henneberg also pointed out that to duplicate the main features of the slow electron scattering curves it was necessary to employ only the first few terms in expansion of Eq. (1). It turns out that for the higher terms the values of $(2l+1)(\sin\gamma_l)$ change so slowly with l that the sum of all these terms gives a curve which falls off monotonically. Hence the characteristics of the curves for slow electrons other than those of falling off monotonically will be given by the first few Legendre coefficients whose sin γ values change rapidly with l. These large changes in the values of sin γ come about for values of γ_l greater than $\pi/2$ and from Fig. 4 we see that for potassium they include values of l equal to and less than 2.

We have used these phase shift values and summed the six terms which involve P_0, P_1, P_2 and their combinations. These curves are compared with the experimental ones in Fig. 5. One observes that the agreement is surprisingly good. The main characteristics of the experimental curves, namely, a maximum near 100°, are reproduced. The shift of the experimental maximum to large and then smaller angles as one reduces the energy of the colliding electron is also in evidence in the calculated curves. In Fig. 3 the position of the calculated maximum does not always agree any too well with the experimental, except perhaps in the 5 and 50 volt curves. Another feature of the experimental curves that is entirely lacking in the theoretical curves is that of the second maximum in the vicinity of 40° which is present in the 10, 15 and 25 volt curves. It is quite evident that Henneberg's calculations gives the correct form of the scattering curves and that the curves shift with colliding electron energies in the proper manner. However, these same calculated curves would fit the experimental argon curves almost as well. Whether this lack of precision is due to the crudeness of the Thomas-Fermi field employed or whether it is due to the approximation of the method is difficult to say. Deviation between theory and experiment for the slower electron energies can of course be safely attributed to the neglect of exchange considerations.

As argon lies next to potassium in the periodic table, it is of interest to compare curves of argon[17] with those of potassium. This can be done by inspecting Fig. 2. In the first place one notices that their diffraction patterns are of the same type, namely, that of a maximum in the vicinity of 100°. Moreover, one notices that the 50, 100 and 150 volt curves agree quite well, the only discrepancy being that the position of the maximum is at slightly smaller angles in the case of argon. For energies less than 50 volts, however, the curves become more discordant.

This tendency of scattering curves for faster electrons to be similar, and slower electrons to

[17] The 25, 50, 100 and 150 volt curves for argon were taken from unpublished data furnished through the kindness of A. L. Hughes and G. M. Webb. The 5 and 10 volt curves are those of Ramsauer and Kollath, Ann. d. Physik **5**, 529 (1932). The 15 volt curve is that of Nicoll and Mohr, Proc. Roy. Soc. **A142**, 320 (1933).

be dissimilar, when curves of atoms differing very little in atomic number are compared, was first observed by Mohr and Nicoll by comparing molecular H_2S and PH_3 curves with the atomic argon curve.[9] Their comparison was based on the assumption that the sulphur and phosphorus atoms were largely responsible for the shape of the molecular scattering curve. That we have verified this effect with atomic potassium bears out their assumption. The explanation for this effect is simply that fast electrons are scattered in the inner shells of the atom where the fields are very much alike and hence give rise to similar scattering curves. Slow electrons, however, are scattered in the valence electron shells and there encounter very much different fields, thus giving scattering curves of different patterns.

To show just what part of the atom is most influential in determining the form of the scattering curve, we have superimposed on the density distribution curve of argon[18] the two distances R and R_0. See Fig. 6. On the particle theory it is between these two distances that the particle experiences the greatest deviation as it passes through the central field of the atom. On the wave theory one finds that the magnitude of the phase shift as computed by Eq. (2) is largely accounted for by the integration between these two distances R and R_0. Since our curves are predominantly of the P_2 type one is interested in these radial distances for the case in which the l value is 2. We see from the figure that it is electrons of energy less than 50 volts that are influenced by the composition of potassium's valence electron shell. One also

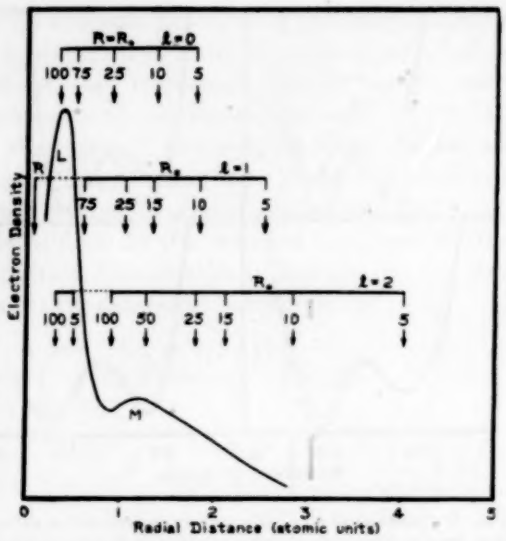

FIG. 6. Electron density distribution for argon's L and M shell with arrows indicating the R and R_0 distances for various colliding electron energies and l values.

notes that the part played by this valence electron shell increases for the slower electrons just as the difference between the experimental curves for these two atoms increases for slower electrons.

Here again, however, one has an alternative explanation of the relation between the curves for these two gases, namely, the effect of electron exchange. For it is just in this energy range, that is, for energies near that of the ionization potentials, that one expects the exchange effects to enter. Unfortunately there is nothing in the experimental curves to suggest that one or the other of these explanations is the more proper.

The author wishes to express his appreciation of the facilities offered him while carrying on this work in the Palmer Physical Laboratory, and to thank Professor R. Ladenburg for the interest shown in this work.

[18] Hartree's distribution curve for argon was used, since the one for potassium was not available. It is also important to bear in mind that the R and R_0 values were calculated with the Thomas-Fermi field of potassium.

The Spectrum and Ionization Potential of Radium

HENRY NORRIS RUSSELL, *Carnegie Institution of Washington, Mount Wilson Observatory*

(Received October 15, 1934)

A new interpretation of the connection between the two groups of terms in Ra I found by Rasmussen is suggested and confirmed by new observations which he has courteously communicated. Certain term-designations are altered. The first ionization potential is 5.252 volts.

RASMUSSEN, in his admirable analysis of the arc spectrum of radium[1] has conclusively identified two groups of lines—one resulting from transitions from ^3D and ^1D terms to higher odd levels and the other from $^3P^0$ and $^1P^0$ to higher even levels and the ground-term $^1S_0$. Absolute term-values for the first group are well determined from a series of four $^3F^0$ terms. The only series available in the other consists of two ^3S terms, and gives but a rough limit. Connection between the two groups should occur through the ultraviolet line λ3101.80 which must arise from the ^1S level. Rasmussen assigns this as $1^1S_1-3^1P_1$.[2] The combination $3^1D_2-3^1P_1$ should lie in the red and he adopts the strongest unclassified line at 6336.90. All terms are thus referred to an accurately known limit, giving $1^1S_0=41{,}949.19$ and 5.176 volts for the ionization potential: but this arrangement is not confirmed by any other combinations. An independent determination of the term-values for the P^0 terms and those which combine with them may be made by combining the low ^1S and the two higher ^3S terms in a single series. This apparently crazy method—first suggested to the writer some time ago by Professor A. G. Shenstone in connection with another spectrum—works very well, as is illustrated by Table I which gives the Rydberg denominators n^* for the other alkaline earths.

The progression of these values is very regular and leads to the estimates for Ra I given in the corresponding line. The estimated tolerances represent the probable limit of error provided that the progression remains regular. The "observed" values are discussed below. With Rasmussen's value $^1S_0=41{,}950$ the values of Δn^* come out 1.070 ($^1S-^3S$) and 1.145 ($^3S-^3S$). Increasing the assumed limit by 500 reduces these to 1.036 and 1.066; by 200 more, to 1.024 and 1.036. The two estimated values of Δn^* for Ra I therefore require the additions of 683±80 and 606±20 to Rasmussen's limit,—or, in the mean, 630±30. With the new value of $^1S_0$, the term which combines with it to give λ3101 comes out 10,350±30.

TABLE I. *Rydberg denominators for alkaline earths.*

Term	1^1S_0		2^3S_1		3^3S_1
Element	n^*	Δn^*	n^*	Δn^*	n^*
Be	1.208	0.971	2.179	1.026	3.205
Mg	1.334	0.981	2.315	1.031	3.346
Ca	1.492	0.993	2.485	1.040	3.525
Sr	1.546	1.003	2.549	1.044	3.593
Ba	1.616	1.014	2.630	1.045	3.675
Ra(est.)		1.025 ± 0.005		1.050 ± 0.003	
Ra(obs.)	1.605	1.028	2.633	1.047	3.680

Now Rasmussen has already identified a level $dp^3D_1^0$ at 10,347.38. The corresponding level in Ba I combines strongly with $^1S_0$, and it appears very probable that the radium line is homologous. Upon communicating this suggestion to Dr. Rasmussen the writer received a cordial letter stating he had found upon his plates another ultraviolet line which confirms the new arrangement; λ2955.65, intensity 2. As the further investigation upon this spectrum, which he plans, may take some time, he generously suggested that this evidence should be presented in the present paper. The new combination, together with some others whose interpretation has been altered, are exhibited in Table II. The intensities are given before the wave numbers, and the differences of the observed and computed values below. It is evident that the true connection between the two parts of the spectrum has been found. Retaining Rasmussen's values for the

[1] Rasmussen, Zeits. f. Physik **87**, 607 (1934).

[2] These serial numbers are "Laufzahlen" beginning with 1, 2, 3, 4 for the *S*, *P*, *D* and *F* series. They are retained here for comparison with Rasmussen's tables.

TABLE II. *Term values in Ra I.*

		3^1D_2 25495.95	3^3D_3 27870.00	3^3D_2 28583.38	3^3D_1 28861.50	1^1S_0 42577.35
$dp^3D_1^0$	10347.38	(3) 15148.55 −0.02		(8) 18236.03 +0.03	(10) 18514.07 −0.05	(6) 32230.02 +0.05
$dp^3P_2^0$	8194.44	(5) 17301.40 −0.11	(6) 19675.58 +0.02	(4) 20389.00 +0.06	(3) 20667.06 0.00	
$^3P_1^0$	8753.65			(5) 19829.62 −0.11	(5) 20107.96 +0.11	(2) 33823.65 −0.05
$^3P_0^0$	8794.94				(4) 20066.56 (0.00)	

first set (3^3D, etc.) those of his second set (given in his Table IV) should be increased by 627.66. The corresponding values of n^* for the S terms are given in the last line of Table I.

The ionization potential corresponding to the new data is *5.252 volts*.

The adoption of the term $dp^3P_1^0$, as here given, accounts for the unclassified line at λ4982 ($^3D_1 - {}^3P_0$) and removes from the list Rasmussen's doubtful level at 5431.68 combining with 2^3P^0. His levels at 10,702.91 and 11,014.06 may then be interpreted as $3^3P_2^0$ and $3^3P_1^0$. The isolated line at λ5755.45 ($\nu = 17{,}370.03$) then gives $3^3P_0^0 = 11{,}491.47$. This interpretation differs from Rasmussen's mainly in the choice between alternatives which he mentioned as possible. It puts dp^3P^0 higher than dp^3D^0, as in the case of Ca, Sr and Ba, and 3^3P^0 between dp^3F^0 and dp^3D^0, as is true in Ca and Sr (but not in Ba, where the limits of the normal and displaced series are closer together). Apart from some effects of this difference, the similarity of the spectra of the alkaline earths is remarkably detailed. For example, dp^1D^0 is superposed on dp^3F^0 in all four spectra, and the separation $dp(^3P_1^0 - {}^3P_0^0)$ is abnormally small in every case.

Some revision of the assignments of the high level even terms appears also to be desirable. Table III gives the new and old term-values and

TABLE III. *Term values and designations.*

Old		New	
2^3P_0	28,871.25	$2^3P_0^0$	29,498.91
2^3P_1	27,950.31	$2^3P_1^0$	28,577.97
2^3P_2	25,261.15	$2^3P_2^0$	25,888.81
2^1P_1	21,233.98	$2^1P_1^0$	21,861.64
dd^3P_1	9948.87	4^3D_1	10,576.53
4^3D_2	9956.28	4^3D_2	10,583.94
4^3D_3	9752.41	4^3D_3	10,380.07
4^3D_1	10,701.08	$p^2\,{}^3P_1$	11,328.74
....	9008.56	$p^2\,{}^3P_2$	9636.22
....	9734.85	$p^2\,{}^1D_2$	10,362.51

designations. The slight inversion of 4^3D_1 appears preferable to the very large interval demanded by the old assignment. The outstanding levels are attributed to the p^2, rather than the d^2, configuration, since the former is lower in Ca and Sr (which resemble Ra more closely than Ba does). Which of the last two levels is $^3P_2$ is doubtful: the present assignment assumes that the difference $^3P_2 - {}^3P_1$ is likely to be large. Further identifications must be postponed till the fainter lines have been more fully observed.

In conclusion, the writer desires to express his hearty thanks to Dr. Rasmussen for his generous communication of the new data and his permission to refer to them here.

The Effect of Hydrogen on the Afterglow in Mercury Vapor

M. M. MANN* AND WALTER M. NIELSEN, *Duke University*

(Received July 6, 1934)

Observations have been made on the change in intensity of the radiation in the mercury afterglow when hydrogen was introduced into the luminous vapor stream. It has been found that with no potential applied to a grid embedded in the vapor stream, the introduction of hydrogen to a pressure of 4×10^{-4} mm of Hg (at the point of observation) decreases slightly but definitely the intensity of the afterglow. With higher hydrogen pressures but with other conditions the same the lines increase in density. With grid potentials of from 3.5 to 4 volts (positive with respect to the anode) additional excitation takes place in the vicinity of the grid and the introduction of hydrogen to a pressure of 4×10^{-4} mm of Hg brings about a marked reduction in the intensity of the lines emitted in the afterglow. It is suggested that the intensity of the lines in the mercury afterglow when excited under these conditions is in part dependent upon the concentration of atoms in the $6\,^3P_{012}$ states.

IT is generally assumed that the nature of the spectrum emitted in the afterglow of mercury vapor under ordinary conditions of excitation, pressure etc., is typical of recombination spectra.[1] Such spectra are characterized by an abnormally high intensity of the lines originating in high energy levels compared with lines having their origin in lower energy states. The work of Miss Hayner[1] on mercury vapor and of Kenty[2] on the afterglow in argon indicate that recombination between positive ions and electrons is of greater likelihood when the temperature of the electrons is small. The variation of recombination light as a function of electron energy in mercury vapor as observed by Miss Hayner, and particularly by Webb and Sinclair, shows a much more rapid decrease with increase in electron energy than can be accounted for on the generally accepted views of the recombination process. From their work Webb and Sinclair concluded that their results could be accounted for by assuming that recombination takes place in two stages, (a) capture of an electron into a high energy level, and (b) transitions to lower levels with the emission of series lines. In order to account for the rapid decrease in intensity of the visually observed afterglow they assumed that such highly excited atoms might suffer a collision with a relatively high energy electron and be re-ionized, and from their results attempted to evaluate the critical energy necessary to carry through such re-ionization processes.

We had initially planned to study the distribution of energy among the lines of the Balmer series of hydrogen recombination spectra and to compare it with the theoretical expectation from a knowledge of the recombination coefficients[3] and transition probabilities.[4] The observations reported in this note are an outgrowth of some observations made in an attempt to observe such spectra in the luminous stream diffusing from an arc struck in a stream of hydrogen and mercury vapor.[5] In some of the initial experiments with no added hydrogen in the arc region or vapor stream, the intensities of some of the lines varied under different conditions (to be described later) in such a way as to suggest that processes other than recombination were playing an effective rôle. There are reasons[6] for believing that the concentrations of excited atoms in the lowest $^3P_{012}$ states of mercury are under certain conditions intimately connected with the character of the spectral radiation in the mercury discharge, and so it seemed that the effect on the afterglow of hydrogen introduced into the luminous stream might be of interest.

EXPERIMENTAL

The tube used was similar to and of approximately the same dimension as that of Webb and

* Based in part on a thesis submitted by the junior author for the M.A. degree at Duke University.

[1] Lord Rayleigh, Proc. Roy. Soc. **A108**, 262 (1925); **A112**, 14 (1926); Miss Hayner, Zeits. f. Physik **35**, 365 (1926); Webb and Sinclair, Phys. Rev. **37**, 182 (1931).

[2] Kenty, Phys. Rev. **32**, 624 (1928).

[3] Stueckelberg and Morse, Phys. Rev. **36**, 16 (1930).

[4] Francis G. Slack, Phys. Rev. **31**, 527 (1928).

[5] The low concentration of undissociated hydrogen apparently present in the arc region of the proton source of Lamar and Luhr (Phys. Rev. **44**, 941 (1933)); **46**, 87 (1934) would seem to provide a more satisfactory means of exciting such spectra and efforts on the initial problem are now being made in this direction by one of us.

[6] Kessel, Zeits. f. Physik **71**, 614 (1931).

Sinclair.[1] Mercury vapor from a reservoir diffused upward in a vertical tube and through the arc region between an oxide-coated filament and a cylindrical anode (placed upstream from the filament). Positive ions, electrons, and excited atoms were swept out of this arc region and into and along an approximately horizontal side tube of 4 cm diameter. The tube was mounted in a furnace and heat was applied in such a way that condensation was prevented at all points except at the end of the side tube outside the furnace, from which the condensed mercury was returned to the mercury reservoir. A grid of No. 20 P. and S. wire with 4 mm spacing was mounted in the horizontal tube at approximately 1 cm from the junction of vertical and horizontal tubes. The diameter of the circular grid was slightly less than the inside diameter of the tubing. Immediately behind this grid was a quartz observation window attached by means of a graded seal. A second window was attached 10 cm down the horizontal tube from the first window. Probes were placed in the center of the tube opposite the observation windows. Hydrogen was introduced at a point approximately midway between the two observation windows. The approximate pressure of the gas in the region opposite the second observation window was measured on a McLeod gauge. The pressure of mercury vapor at the same point was fixed as to its order of magnitude by a method similar to that used by Webb and Sinclair.

The electron temperatures and concentrations at the point of observation were measured in the usual manner[7] immediately after the corresponding exposure had been made. The use of probes in the measurement of low electron temperatures was found to be difficult due to changes in its contact difference in potential, probably brought about by changes in the gas layer on the probe. Webb and Sinclair reported the same difficulty. We found that fairly reproducible measurements could be made by flashing the probe to a dull red temperature before each series of measurements. A few photographs at the second window (downstream window) are reproduced in Fig. 1 under conditions given in their captions. The exposure time in each case was 15 minutes.

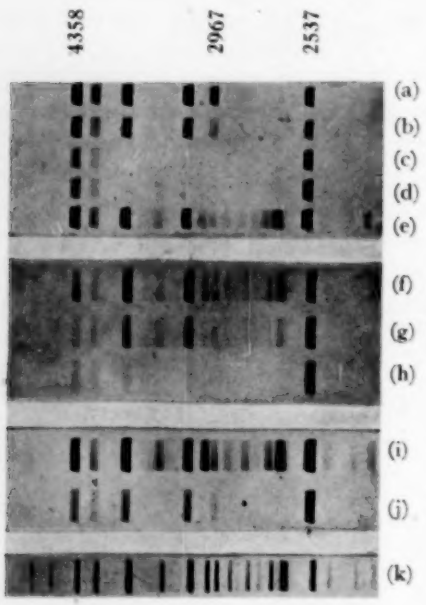

FIG. 1. Typical spectra of mercury afterglow. Arc voltage 5 volts, and arc current 0.5 ampere. Other conditions as indicated.

Exposures *a* to *e* inclusive showing effect of positive grid potential on afterglow with no foreign gas present.

Exposure	*a*	*b*	*c*	*d*	*e*
Grid voltage	0	1.1v	2.2v	3.3v	4.4v
Electron Temperature	756°K	760°K	1344°K	3452°K	4681°K

Exposures *f*, *g*, *h* showing effect of hydrogen with accelerating voltage of 3.6 volts on grid.

Exposure	*f*	*g*	*h*
Hydrogen pressure in mm Hg	0	4×10^{-4} mm	1.6×10^{-3}

Exposures *i*, *j* showing effect of hydrogen with accelerating voltage on grid of 4.0 volts.

Exposure	*i*	*j*
Hydrogen pressure in mm Hg	0	8×10^{-4}

Exposure *k*, Mercury Spectrum.

RESULTS

In Fig. 1 *a*, *b*, *c*, *d* and *e*, we have reproduced typical spectrograms obtained with no foreign gas present in the vapor stream. For this group of exposures the mercury vapor pressures was 0.09 mm of mercury. The electron concentration decreased from 1.6×10^{11} per cc in exposure *a* to 6.0×10^{9} per cc in exposure *d*. The variation in positive ion concentration was probably of a comparable magnitude. The electron concentration in exposure *e* was 6.5×10^{9} per cc. The densities of the sharp triplet and other lines of longer wave-length are probably not recorded correctly in this group of exposures because of

[7] Langmuir and Compton, Rev. Mod. Phys. **3**, 191 (1931).

scattered light from the arc region in the early experiments.

In Table I are given values of the densities as measured with a Moll microphotometer of a

TABLE I. *Results of microphotometric measurements of densities on typical spectrograms with grid floating.*

Wave-length	Densities at different hydrogen pressures $p=0$ mm	4×10^{-4}	1.6×10^{-3}	3.6×10^{-3}	6.4×10^{-3}
2537A	0.140	0.096	0.072	0.057	0.045
2967	.071	.053	.083	.097	.107
4358	.071	.056	.071	.096	.111

few of the lines of the afterglow spectrum on spectrograms taken at the second window with grid floating for various pressures of hydrogen. These results are given in this form because of the reproduction difficulties connected with small differences in density. The mercury vapor pressure was fixed at 0.09 mm of mercury. The electron temperature and electron concentration with no hydrogen present were approximately the same as for exposure *a* above. No attempt was made to measure electron temperatures and concentrations with the gas flowing. One would not expect the small pressures of hydrogen to be effective in directly preventing the diffusion of positive ions and electrons down the stream.

Exposures *f*, *g* and *h* show the effect of hydrogen on the afterglow with a higher potential applied to the grid. The electron temperature and concentration for exposure *f* were of the same order of magnitude as in *e* above. The mercury pressure for this group of exposures was 0.08 mm of mercury.

Exposures *i* and *j* were taken with a slightly higher positive grid voltage than in *f*, *g* and *h*. Unfortunately, measurements were not made on the probe volt-ampere characteristics. In this case the visible glow around the grid becomes more intense and the volt-ampere characteristics of the accelerating grid show an abrupt increase in electron current. The other conditions were the same as in *f*, *g* and *h*.

Photographs of the emitted radiation at the first window (upstream) indicated no perceptible change in intensity on the addition of hydrogen under the same conditions as obtained in Fig. 1 and Table I. Apparently the small gas pressures used were not sufficient to alter conditions in the arc region and the amount of hydrogen diffusing against the vapor stream was small.

DISCUSSION

One would expect on simple theories[8] of the recombination of positive ions and electrons that the intensity of the spectral lines radiated as a result of such processes would vary as the square of the electron concentration (assuming positive ion and electron concentrations to be equal) and to decrease with increase in electron temperature. The spectra *a*, *b*, *c* and *d* are then not inconsistent with what one might expect on the assumption that we are here only concerned with recombination. On the other hand the marked enhancement of all of the arc lines in exposure *e* for the highest grid voltage cannot be associated with recombination. In the latter case the electron concentration is practically equal to that in exposure *d*. The small difference in electron concentration in exposure *e* is offset by an increase in electron temperature. Apparently, as will be made more obvious later, excited atoms are produced in the vicinity of the grid. This additional excitation upon being carried down the stream either in the form of excited atoms or resonance radiation makes a contribution to the emitted radiation at the point of observation. Under such conditions the intensity of the λ3025 group which has its origin in the $7\,^3D_{123}$ and $7\,^1D_{23}$ states is noticeably greater than λ2967, the upper state of which is the $6\,^3D_1$ state. As will be discussed later in connection with the quenching by hydrogen, we are probably here concerned with a form of excitation in which the $^3P_{012}$ states plays an important part. If such is the case, the decrease in intensity of the radiation in *a*, *b*, *c* and *d* cannot definitely be assigned to a decrease in recombination alone. Changes in electron temperature may decrease the lifetime of atoms in the metastable $6\,^3P_0$ and in this way alter the importance of any process in which they are involved. It would probably be extremely difficult to examine experimentally in a quantitative way such changes in populations of excited states.

The data of Table I indicate that for small additions of hydrogen the line radiation of the

[8] F. L. Mohler, Rev. Mod. Phys. 1, 216 (1929).

afterglow under these conditions decreases in intensity. For the higher hydrogen pressures with the same grid conditions, the density of the lines with the exception of λ2537 increases until at the highest pressure used (approximately 10^{-2} mm Hg) their densities exceed their initial values. The small but definite decrease in the intensity for small additions of hydrogen may be associated with the destruction of excited atoms by collisions of the second kind. The recovery of the intensity of the afterglow with grid floating and with higher hydrogen pressures may possibly be due to an increase in the probability of recombination due either to a lowering of the electron temperature or possibly to the fact that such hydrogen molecules or atoms may provide third bodies which aid in recombination. Whether or not the addition of hydrogen causes an increase or decrease in the intensity of the afterglow should depend on the relative importance of the contribution associated with excited atoms and the radiation due to recombination.

As is shown in Fig. 1 *f*, *g* and *h*, the quenching effect of hydrogen is much more pronounced with higher grid voltages. The addition of hydrogen to a measured pressure as low as 4×10^{-4} mm of mercury shows a very noticeable decrease. With slightly less positive voltages on the grid (about 3.5 volts), at these mercury vapor pressures, it is possible practically to wipe out all lines except λ2537 which is still detectable but very much weaker. The decreased effectiveness of hydrogen in the quenching of some of the lines in the afterglow at the higher grid voltage (exposures *i* and *j*) may be due to the fact that the grid may become surrounded by a sheath and thus lose its ability to affect the diffusion of positive ions and electrons from the arc region to the point of observation.

The fact that the half value pressure for the quenching of resonance radiation by hydrogen[9] is of the order of 0.2 mm of mercury, a value considerably greater than those effective here, would seem to indicate that the quenching of the metastable $6\,^3P_0$ and $6\,^3P_2$ states may also be involved. In connection with the marked enhancement of the λ3025 group with no hydrogen present as in exposures *e* and *i* of Fig. 1 it is of interest to point out that the energies of these states is approximately the sum of the energies of the $6\,^3P_0$ and $6\,^3P_1$ states. It may therefore well be that these as well as other higher excited states are filled by collisions between two such excited atoms as might be suggested by the work of Rayleigh.[10] It is also possible that these levels may be excited by collision between such excited atoms and some of the high speed electrons present in the discharge under these conditions. Under both conditions one would expect the emitted radiation to be quenched by hydrogen. The introduction of a stream of hydrogen such as to build up a pressure of only 8×10^{-3} mm of mercury at the point of observation quenches the λ3025 group as well as other lines completely as shown in exposure *j*. The line λ2967 although weaker under such conditions is definitely present on the original spectrograms.

As indicated above, this quenching action of hydrogen on the afterglow is apparent under the conditions of this experiment not only at high electron speeds but under conditions where the electron temperature is quite low. It is, of course, much more apparent under the former conditions.

It would seem therefore that the intensity of the lines in the afterglow of mercury vapor, when excited under conditions such as in this experiment (arc voltage, Hg vapor pressure, electron temperature etc.) is in part dependent upon the concentration of atoms in the $6\,^3P_{012}$ states.

The results here presented are not necessarily inconsistent with the assumption of Webb and Sinclair that they were primarily concerned in their work with recombination of ions and electrons, and, that excited atoms played a minor rôle in their work. Their measured arc voltage was about 8 volts and their arc current was approximately 10 amperes. It is, however, the purpose of this note to present additional evidence that the intensity in the mercury afterglow of some of the lines which have their origin in the higher energy states may be perceptibly altered under certain conditions by changes in the concentration of atoms in the $^3P_{012}$ states.

[9] Ruark and Urey, *Atoms, Molecules and Quanta*, p. 497.

[10] Lord Rayleigh, Proc. Roy. Soc. **A132**, 650 (1931); **A135**, 617 (1932).

On the Theory of Fusion

K. F. HERZFELD AND MARIA GOEPPERT MAYER, *The Johns Hopkins University*

(Received June 18, 1934)

Although equilibrium between two phases is in general determined by both phases, fusion stands somewhat apart in that a crystal cannot be overheated. As a type of the simplest possible crystal, the exact equation of state of frozen argon has been developed here. It has been found that the pressure as function of the volume at a given temperature has a minimum, which means the breakdown of the crystal under these conditions. The temperature at which this minimum occurs at zero pressure is interpreted as the melting point. It has been found in accordance with experiment that a positive pressure is necessary for the existence of crystalline helium but the numerical agreement is bad.

INTRODUCTION

SOME time ago, we attempted[1] to get a better understanding of the liquid state through investigation of a simplified one-dimensional model but succeeded only in recognizing the conditions for the existence of definite phases. Here the same problem is attacked in a different manner. The equation of state of simple crystals (e.g., frozen rare gases) is calculated from the forces according to lattice theory. We find that the isotherms in which p is plotted against V have a minimum. Now a state in which the pressure increases with volume is unstable. Accordingly the crystal breaks down at the minimum pressure. Above the temperature at which this pressure minimum lies at zero pressure, the crystal cannot exist without external pressure. This temperature we interpret as the melting point.

In general, equilibrium between two phases is not defined by any particular happening in one of the two but by the equality of the free energies of the two at given pressure and temperature. For example, the equilibrium between liquid and vapor being given by the equality of their free energies, one can undercool the vapor or overheat the liquid without any discontinuous change in the properties of either. The same is even true for equilibria between allotropic crystals. It is possible to overheat grey tin or undercool white tin without any discontinuity appearing anywhere. The only known exception is the fact that no crystal can be heated above the melting point at the given pressure. It seems therefore reasonable to assume that fusion is conditioned by something happening in the crystal alone and to identify the point of instability of the crystal, which was described above, with the melting point. But then another question arises. At the melting point, the melt is in equilibrium with the crystal, i.e. the pressure, temperature and free energy of the melt must have values which are prescribed completely by the crystal (while in other equilibria, as stated above, the pressure is *selected* so as to give the equality of free energies). The only variables that seem to be left to the liquid to adjust its free energy are the values of the constants that appear in the potential energy and frequency and these are again determined by the arrangement of the molecules. Accordingly, the arrangement of the molecules in the liquid has to adjust itself so as to give the correct free energy.[1a] What this arrangement has to be is not investigated here but is reserved for later consideration.

If this view of fusion is correct, one would expect, for all normal substances, the volume of the liquid to be greater than that of the solid for the same temperature. It is then clear why, in the process of melting, the crystal does not melt in different small regions inside. A small molten region inside would have to contain the liquid in a highly compressed state, which would have a considerably higher free energy than the surrounding solid. It is, however, quite possible for the fusion to occur in channels communicating with the outside.

[1] K. F. Herzfeld and M. Goeppert Mayer, J. Chem. Phys. **2**, 38 (1934).

[1a] However it seems that this arrangement should be the one to give the smallest free energy of the liquid. How that is possible is not yet clear.

On the other hand, it seems not impossible for small crystals to persist in a liquid, a fact for which there appear to be experimental indications.[2] Up to now three other theories of fusion exist.

Lindemann[3] made the assumption that melting takes place if the amplitude of the vibrations is a certain fraction of the distance between nearest neighbors. Upon determining this fraction from the data for one crystal of each type and applying it to all crystals of the same type, one gets very good agreement.

Braunbeck[4] considers the mutual vibrations of two parts of the lattice, taken as rigid, assumes a suitable form of the mutual potential curve and finds positions of minimum energy. One of these he interprets as belonging to the solid, the other to the liquid state. The melting point is then determined as the temperature at which the free energies corresponding to these two states are equal.

Raschevsky[5] has come close to the ideas followed in this paper by pointing out that the heat of fusion is of the same order of magnitude as the elastic energy necessary to expand the lattice to the breaking point, i.e., the point where the tension has a maximum.

The Energy and the Elastic Constants for a Face-centered Lattice

Argon has a face centered lattice.[6] Call r the distance to the nearest neighbor, which is at the center of the face, so that the side of the cube is $r\sqrt{2}$. The volume per atom is

$$(r\sqrt{2})^3/4 = r^3/\sqrt{2}. \tag{1}$$

As potential energy φ_1 of attraction between two atoms we use a van der Waals expression (A, a constant)

$$-\varphi_1 = A/r^6, \tag{2}$$

which, summed up over the lattice, gives[7]

$$\Phi_1 = -14.4539A/r^6 \tag{3}$$

with $\Phi_1 = \Sigma\varphi_1$. The repulsive potential is written[8]

$$\varphi_2 = ABe^{-r/\rho}, \tag{2'}$$

(B, ρ constants) which gives for the whole crystal

$$\Phi_2 = 12ABe^{-r/\rho}\{1+\tfrac{1}{2}e^{-(\sqrt{2}-1)r/\rho} + 2e^{-(\sqrt{3}-1)r/\rho}+\cdots\}. \tag{3'}$$

This includes the atoms at the corners of the cube and in the centers of all the faces on all four cubes surrounding the atom considered here.

For ρ two values were used: $\rho = 0.345$A, which Born and Mayer found to fit best the behavior of alkali-halides, and $\rho = 0.2091$A which Bleick found theoretically for the interaction of two Ne atoms. Unfortunately, it is not possible to determine A and B directly from the normal value of r, $r_0 = 3.83$A and the normal heat of sublimation because the zero point energy plays a considerable part in the heat content and displaces the lattice distance by about 0.05A beyond the value given by the minimum of the potential energy alone.

A method of trial and error leads to[9] (N, Avogadro number)

$$NA = 6.706\times10^{-35}\ \text{erg cm}^6, \quad B = 1.270\times10^{49} \quad \text{for } \rho = 0.345.$$

$$NA = 4.729\times10^{-35}\ \text{erg cm}^6, \quad B = 0.9484\times10^{52} \quad \text{for } \rho = 0.2091.$$

These give as the heat of sublimation,[10] the value 1655 cal. The experimental values are rather uncertain.

There are three elastic constants, given by[11]

[2] P. Othmer, Zeits. f. Allgem. und anorg. Chemie **91**, 209 (1915). A. Goetz, R. C. Hergenrother and A. B. Focke, Phys. Rev. **34**, 546 (1929); A. Goetz, Phys. Rev. **35**, 193 (1930); A. Soroos, Phys. Rev. **41**, 516 (1932).

[3] F. A. Lindemann, Phys. Zeits. **11**, 609 (1910).

[4] W. Braunbeck, Zeits. f. Physik **38**, 549 (1926).

[5] N. Raschevsky, Zeits. f. Physik **40**, 214 (1927).

[6] F. Simon and Cl. v. Simson, Zeits. f. Physik **25**, 160 (1924).

[7] E. Jones (Lennard-Jones) and A. E. Ingham, Proc. Roy. Soc. **A107**, 636 (1925).

[8] M. Born and J. E. Mayer, Zeits. f. Physik **75**, 1 (1932); W. Bleick, Dissertation, The Johns Hopkins University (1933). W. E. Bleick and T. E. Mayer, J. Chem. Phys. **2**, 252 (1934).

[9] The value of $NAB = 8.517\times10^{14}$, which we find for $\rho = 0.345$, is to be compared with $N\times10^{-12}e^{-2.060/\rho} = 13.53\times10^{14}$ which would follow from J. E. Mayer and M. Huggins, J. Chem. Phys. **1**, 633 (1933), if one puts the radius of $2Av = K^+ + Cl^-$. Furthermore, the value of NA is to be compared with the theoretical values of 3.3 and 3.7×10^{-35} calculated by F. London, Zeits. f. physik. Chemie **B11**, 222 (1930).

[10] A. Eucken, Verh. D. Phys. Ges. **18**, 4 (1916); A. Eucken and F. Hauck, Zeits. f. physik. Chemie **134**, 161 (1928); F. Born, Ann. d. Physik **69**, 473 (1922).

[11] M. Born, *Dynamik der Krystallgitter*, p. 536, 548, 554, Leipzig, 1923; M. Born and M. Goeppert Mayer, *Handb. d. Phys.* **24**, 2nd half, 2nd Ed., p. 630, Berlin, 1933. c_{11}

$$c_{11}=\frac{1}{\sqrt{2}r^3}\left\{\Sigma\frac{r}{3}\frac{d\varphi}{dr}+\Sigma\frac{1}{r}\frac{d}{dr}\left(\frac{1}{r}\frac{d\varphi}{dr}\right)x^4\right\}$$

$$=\frac{d}{dV}\frac{N\Phi}{2}+\frac{1}{2V}N\Sigma\frac{1}{r}\frac{d}{dr}\left(\frac{1}{r}\frac{d\varphi}{dr}\right)x^4, \quad (4)$$

$$c_{12}=\frac{1}{2V}N\Sigma\frac{1}{r}\frac{d}{dr}\left(\frac{1}{r}\frac{d\varphi}{dr}\right)x^2y^2, \quad (4')$$

$$c_{44}=\frac{d}{dV}\frac{N\Phi}{2}+c_{12}, \quad (4'')$$

where V is the mol volume.

At the minimum of the potential energy $d\Phi/dV=0$ so that there are only two elastic constants, because $c_{12}=c_{44}$. This does not hold, however, for other distances, where the general form must be used.

By using (2) and (2′) one finds[12]

$$c_{11}=\frac{NA}{V}\left\{B\frac{r^2+r\rho}{\rho}e^{-r/\rho}\left[1+\frac{2r+\sqrt{2}\rho}{r+\rho}e^{-(\sqrt{2}-1)r/\rho}\right.\right.$$

$$\left.\left.+2\frac{3r+\sqrt{3}\rho}{r+\rho}e^{-(\sqrt{3}-1)r/\rho}+\cdots\right]-\frac{24\times2.544}{r^6}\right\}+\frac{d}{dV}\frac{N\Phi}{2}, \quad (5)$$

$$c_{12}=\frac{NA}{V}\left\{\frac{B}{2}\frac{r^2+r\rho}{\rho^2}e^{-r/\rho}\left[1+2\frac{3r+\sqrt{3}\rho}{r+\rho}\right.\right.$$

$$\left.\left.\times e^{-(\sqrt{3}-1)r/\rho}+\cdots\right]-\frac{24\times1.137}{r^6}\right\}. \quad (6)$$

measures the tension in one direction due to an expansion in the same direction with the cross dimensions kept constant, c_{12} measures the tension in the cross direction which tries to contract the specimen and determines largely the Poisson constant, c_{44} measures the shearing stress. The summation is to be extended over all the lattice points with the coordinates x, y, z.

[12] A calculation of the numerical factors of r^{-6} was effected by directly summing up over the nearest 168 atoms, i.e. up to and including a distance $3r$. Then an integration was performed over a continuum reaching from a sphere of radius $3r$ to infinity and from this half the contribution of the atoms at distance $3r$, which had already been taken into account in the summation, was subtracted. The values calculated in that way were 2.541 and 1.135. But in a cubic crystal one must have

$$(x^4+2x^2y^2)/r^4=(x^4+x^2y^2+x^2z^2)/r^4=x^2r^2/r^4=x^2/r^2=\tfrac{1}{3}.$$

As $2.541+2\times1.135=\frac{1}{3}$ of 14.433 instead of 14.454 (3), the constants were raised to the values above.

The Frequency

According to Debye the maximum frequency of a cubic crystal is

$$\nu=w(3N/4\pi V)^{\frac{1}{3}} \quad (7)$$

where w is the sound velocity. In dependence of the direction this is given by a determinant of the third order. The method used by Born and Kármán[13] which consists in a development into powers of $3c_{12}-c_{11}/c_{11}-c_{12}$, cannot be applied here because this quantity is by no means small.

But on the other hand there is no particular reason why one should average just in the way proposed by Debye, using in (7) the quantity found from

$$1/w^3=\overline{(1/w_1^3)}+\overline{(1/w_2^3)}+\overline{(1/w_3^3)},$$

where w_1, w_2, w_3 mean the three roots of the characteristic equation and the bars an averaging over the direction. It is much simpler to form one of the symmetric functions of the roots and average. We have used

$$D^3\overline{w^6}=D^3\overline{w_1^2w_2^2w_3^2}=c_{11}c_{44}^2$$

$$+c_{44}[(c_{11}-c_{44})^2-4c_{12}^2]\overline{[\cos^2(xr)\cos^2(yr)}$$

$$+\overline{\cos^2(yr)\cos^2(zr)}+\overline{\cos^2(zr)\cos^2xr}]$$

$$+[(c_{11}-c_{44})^3-12(c_{11}-c_{44})c_{12}^2+16c_{12}^3]$$

$$\times\overline{\cos^2xr\cos^2yr\cos^2zr} \quad (8)$$

in which D is the density. In terms of numerical values and the atomic weight M this becomes

$$\nu^6=V(9N^2/16\pi^2M^3)\{c_{11}c_{44}^2$$

$$+\tfrac{1}{3}c_{44}[(c_{11}-c_{44})^2-4c_{12}^2]+(1/105)$$

$$\times[(c_{11}-c_{44})^3-12(c_{11}-c_{44})c_{12}^2+16c_{12}^3]\}. \quad (9)$$

The Equation of State

The total energy at 0° abs. and any volume is given by the lattice energy plus the zero point energy $\frac{3}{2}Nh\bar{\nu}$ ($\frac{1}{2}h\nu$ for each degree of freedom).

$$U=\frac{N\Phi}{2}+\frac{3}{2}Nh\bar{\nu}. \quad (10)$$

The limiting ν calculated in (9) is for the Debye spectrum 4/3 of the average $\bar{\nu}$ meant above. At

[13] Born, ref. 11, p. 647, Born and Goeppert-Mayer, p. 672; M. Born and Th. von Kármán, Phys. Zeits. **14**, 15 (1913); L. Hopf and G. Lechner, Verh. d. D. phys. Ges. **16**, 643 (1914).

TABLE I. *Frequency, elastic constants and energy.* r in A, energy in kilojoule, $\rho=0.345A$, $\Theta=h\nu/k$ in degree kelvin.

r	3.73	3.78	3.83	3.88	3.93	3.98	4.03	4.08
Θ	94.31	81.90	72.80	66.58	60.31	54.47	48.98	43.68
$c_{11}\times10^{-10}$	3.901	2.742	2.015	1.573	1.207	0.9064	0.6606	0.4583
$c_{12}\times10^{-10}$	2.273	1.613	1.183	0.9198	0.7028	0.5249	0.3800	0.2609
$c_{44}\times10^{-10}$	2.115	1.592	1.262	1.048	0.8657	0.7122	0.5830	0.4737
$\frac{N\Phi}{2}$	−7.627	−7.647	−7.600	−7.501	−7.356	−7.129	−6.974	−6.756
$\frac{3}{2}Nh\frac{3}{4}\bar{\nu}$	0.882	0.766	0.681	0.623	0.564	0.510	0.458	0.409
$-U$	6.745	6.881	6.919	6.878	6.792	6.619	6.516	6.347

TABLE II. *Pressure.* (Fig. 1.) V in cc, pressure in 10^9 dynes/cm², $\rho=0.345A$.

r	3.73	3.78	3.83	3.88	3.93	3.98	4.03	4.08
V	22.26	23.17	24.10	25.06	26.04	27.05	28.08	29.14
$\frac{\partial \ln \nu}{\partial V}$	0.167	0.143	0.109	0.097	0.102	0.102	0.104	0.113
p_1	15.82	2.08	−7.93	−12.82	−16.29	−18.73	−20.30	−21.28
p_2	15	10.9	7.42	6.04	5.74	5.18	4.78	4.62
$0°\ p$	31	13.0	−0.51	−6.78	−10.55	−13.55	−15.52	−16.66
$70°\ p_3$	17	15.6	12.61	11.65	12.67	13.10	13.88	15.50
p	48	28.6	12.10	4.87	2.12	−0.45	−1.64	−1.16
$76°\ p_3$	19	17.6	14.16	13.04	14.13	14.57	15.41	17.17
p	50	30.7	13.65	6.26	3.58	1.02	−0.10	0.51
$100°\ p_3$	29	25.8	20.46	18.67	20.07	20.55	21.56	23.84
p	60	38.8	19.95	11.89	9.52	7.00	6.04	7.18

higher temperatures, the free energy pro mole at constant volume is

$$f=U+F, \tag{11}$$

where

$$F=\int_0^T CdT-\int_0^T \frac{C}{T}dT=-T\int_0^T \frac{dT}{T^2}E. \tag{11'}$$

Here C is the specific heat and $E=\int_0^T CdT$. The pressure is given by

$$p=-\partial f/\partial V \tag{12}$$

and is accordingly made up of three parts:

$$p=p_1+p_2+p_3. \tag{12'}$$

p_1 is the elastic tension

$$p_1=-(\partial/\partial V)(N\Phi/2). \tag{12''}$$

p_2 is the zero point pressure

$$p_2=-\frac{\partial}{\partial V}\frac{3}{2}Nh\bar{\nu}=-\frac{\partial}{\partial V}\frac{3}{4}\cdot\frac{3}{2}Nh\nu. \tag{12'''}$$

Both these values depend only on V, not on T. At higher temperature, one has to add the thermal pressure[14]

$$p_3=-(\partial F/\partial V)=E(\partial \ln \nu/\partial V). \tag{12''''}$$

Here it has been assumed that F/T is a function of ν/T only. F and E can be found tabulated.[15]

It is necessary for possible existence of a state that

$$(\partial p/\partial V)<0. \tag{13}$$

If a p, V curve for constant T shows a minimum, the crystal breaks down (cannot exist) beyond that minimum.

THE DISCUSSION OF THE RESULTS

All total pressures are underlined, the minimum pressure for each temperature is doubly underlined. The results are shown in the Tables I–IV.

If, according to this interpretation, the melting point is given by

$$p=0,\quad \partial p/\partial V=0,\quad \partial^2 p/\partial V^2>0, \tag{14}$$

it follows that the compressibility of the crystal at the melting point must be infinite. The same should be true for the coefficient of expansion.

In considering the tables, one sees that for the equilibrium distance $r=3.83$A $\Theta=73$ for $\rho=0.345$ and $\Theta=96$ for $\rho=0.2091$ while the experimental value is $\Theta=85$. For $\rho=0.2091$, Θ is

[14] $F/T=-\int_0^T(E/T^2)dT=-\int_0^T(E/T^2)\nu d(T/\nu)$. If we put $T/\nu=x$ and assume that C is a function of x only $E=\int CdT=\nu\int Cdx$. $F/T=-\int x^2dx\int Cdx$ is a function of x only, say $\psi(x)$, $(\partial\psi/\partial x)=-(E\nu/T^2)$. Then

$$(\partial F/\partial V)=T(\partial\psi/\partial x)(\partial x/\partial V)$$
$$=-(T^2/\nu^2)(\partial\psi/\partial x)(\partial\nu/\partial V)=(E/\nu)(\partial\nu/\partial V).$$

[15] F. Simon, Handb. d. Physik **10**, 368 (1926), Berlin.

TABLE III. *Frequency, elastic constants, energy.* r in A, energy in kilojoule, $\rho = 0.2091$ A.

r	3.73	3.78	3.83	3.88	3.93	3.98	4.03
Θ	128.5	111.2	96.46	82.81	70.56	59.06	48.44
$c_{11} \times 10^{-10}$	7.165	5.169	3.660	2.523	1.673	1.0383	0.5724
$c_{12} \times 10^{-10}$	3.908	2.796	1.957	1.328	0.8594	0.5118	0.2578
$c_{44} \times 10^{-10}$	3.761	2.821	2.099	1.547	1.1263	0.8057	0.5634
$\frac{N\Phi}{2}$	−7.891	−7.923	−7.841	−7.666	−7.425	−7.143	−6.830
$\frac{3}{2} Nh \frac{3}{4} \nu$	1.202	1.040	0.902	0.775	0.660	0.552	0.453
$-U$	6.689	6.883	6.939	6.891	6.765	6.591	6.377

TABLE IV. *Pressure* (in 10^8 dynes/cm^2), volume in cc, $\rho = 0.2091$ A. (Fig. 2.)

r	3.73	3.78	3.83	3.88	3.93	3.98	4.03
V	22.26	23.17	24.10	25.06	26.04	27.05	28.08
$\frac{\partial \ln \nu}{\partial V}$	0.168	0.156	0.156	0.160	0.169	0.185	0.198
p_1	14.72	−2.45	−14.17	−21.91	−26.69	−29.39	−30.56
p_2	20	16.3	14.09	12.39	11.17	10.20	8.98
0° p	35	13.8	−0.08	−9.52	−15.52	−19.19	−21.58
50° p_2	7	7.8	8.84	10.20	11.98	14.39	16.87
p	42	21.6	8.76	0.68	−3.54	−4.80	−4.71
61° p_2	11	11.3	12.56	14.13	16.26	19.19	22.10
p	46	25.1	12.48	4.61	0.74	0	0.52
65° p_2	12	12.7	13.94	15.59	17.84	20.96	24.02
p	47	26.5	13.86	6.07	2.32	1.77	2.44
100° p_2	25	25.1	26.64	28.85	32.05	36.64	41.00
p	60	38.9	26.56	19.33	16.53	17.45	19.42

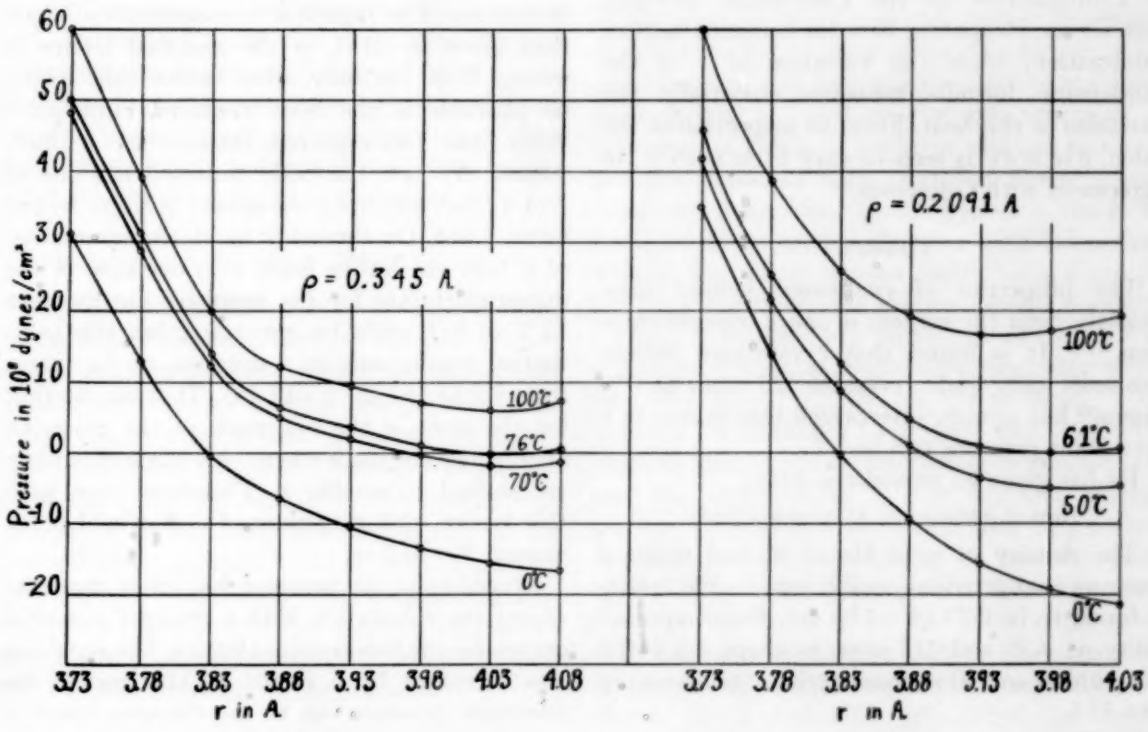

FIG. 1.

FIG. 2.

FIG. 1. pr isotherms for argon. $\rho = 0.345$A, the value Born and Mayer found for the alkali-halides.
FIG. 2. pr isotherms for argon. $\rho = 0.2091$A, the value found by Bleick and Mayer for He atoms.

83 for $r=3.88$, which corresponds to 50°. On theoretical grounds, one should expect to have ρ rather alike for argon and neon and therefore prefer $\rho=0.2091$.

The melting points are both too low, 76° and 61° compared with 84° observed. It is true that we have, following Born, used only a first approximation insofar as we considered the vibrations as purely harmonic around the given lattice distance with the frequency appropriate for that distance. A higher approximation would need rather lengthy calculations, but one should expect that the effect would be to lower the melting point still further.

The thermal pressure is determined essentially by $\partial \ln \nu/\partial V$. A higher melting point would result if $\partial \ln \nu/\partial V$ would be lower; then a higher temperature would be necessary for the same thermal pressure. A smaller $\partial \ln \nu/\partial V$ means a slower falling off of the repulsive forces.

In comparing the melting points and Θ's (or ν's) for the two ρ-values, one might be astonished to find the higher T with the lower $\nu(\rho=0.345)$ in contradiction to the Lindemann formula. But we are comparing here for constant heat of sublimation, while the variation of ν in the Lindemann formula measures essentially the variation of this heat. From an inspection of the table, $\partial \ln \nu/\partial V$ is seen to vary little with V, in agreement with Grüneisen.[16]

Helium

The properties of condensed helium have recently been the subject of much experimentation.[17, 18] It is found that crystallized helium can exist only under pressure (25 atm. at 0°). Simon[18] has already interpreted this as due to a zero point pressure $p_2 > |p_1|$.

He has given as provisional data:

Heat of sublimation: 11 cal. = 46.1 joule.

The density of solid He at 4° and under a pressure that provides equilibrium ($\sim$100 atm.?) is found to be 0.23 ($V=17.4$ cc), the compressibility at 3.7° and 115 atm. is about 1.5×10^{-9} abs. units and the characteristic temperature $\Theta=32.5$.

Now the potential energy of two helium atoms has been calculated from the model by Slater and Kirkwood[19] to

$$\varphi=\{7.7e^{-2.43-(r/a_0)}-0.68(a_0/r)^6\}10^{-10}\text{ erg} \qquad (15)$$

where a_0 is the Bohr radius.[20] With this, the same calculation as for argon was performed under the assumption that solid helium, like argon, has a face centered cubic lattice. The result is given in the Tables V and VI.

One sees that there is a pressure minimum at 0° at about 3.12A. The pressure there is positive, so that the crystalline helium cannot exist without pressure. However, the volume is much smaller than the experimental one (13 cc against 17.4; at $V=17.4$ and $r=3.45$ one is already far beyond the maximum of p_1, all the elastic constants are negative). The minimum pressure is too high, about 1250 atm. instead of 25 atm., finally Θ is too large (about 55° instead of 32°). On the other hand, the heat of sublimation seems about right.

There are two possible explanations for these deviations: The repulsion is considerably larger than given by (15), or the assumed lattice is wrong. Now the only other lattice that might be plausible is the body centered cubic one. While the face-centered lattice has a molvolume $Nr^3/\sqrt{2}$, the body centered has one of $N(4/3\sqrt{3})r^3$, which, for the same r is larger by the factor 1.088. On the other hand, the summation of φ over the lattice leads to a decrease of the numerical factor for the repulsive energy from 12/2 to 8/2 while for the attraction this summation results only in a decrease of the factor from $\frac{1}{2}\times14.454$ to[7] $\frac{1}{2}\times12.253$. That means that for the same φ the minimum of the potential energy and the place where $-p_1$ has a maximum are shifted to smaller r. Therefore, even with this lattice, this maximum of $-p_1$ would occur around $V=13.5$ cc.

Accordingly, an attempt has been made to repeat the calculation with a changed potential energy for the face centered lattice. The repulsion was increased by a factor 3. This moves the minimum pressure out to the distance where it

[16] E. Grüneisen, Ann. d. Physik **39**, 257 (1912).
[17] W. Keesom and co-workers, Leid. Comm. No. 184b, 190b, 216b, 219e, 221e. Suppl. 67b, 71e, 76b. Physica **1**, 128, 161 (1934).
[18] F. Simon, Nature **133**, March 24 and April 7, 1934.
[19] J. C. Slater and J. G. Kirkwood, Phys. Rev. **37**, 682 (1931).
[20] It might be remarked that this amounts to a $\rho=0.219$, very close to the Mayer-Bleick value for neon.

TABLE V. *Energy, elastic constants and frequency for He. Energy in joule, r in A.*

r	2.8	3.0	3.05	3.10	3.15	3.20	3.25
Θ	169.5	80.8	68.75	57.29	46.41	34.35	
$c_{11}\times10^{-9}$	164.6	26.47	16.99	9.856	4.648	0.901	−1.666
$c_{12}\times10^{-9}$	94.86	14.77	9.228	5.151	2.204	0.089	−1.344
$c_{44}\times10^{-9}$	80.36	18.29	13.35	9.577	6.715	4.540	2.940
$\frac{N\Phi}{2}$	−1586	−756.4	−645.5	−536.1	−434.3	−321.4	
$\frac{3}{2}Nh\frac{3}{4}\nu$	598.0	593.5	570.8	544.7	516.5	487.4	
$-U$	+988	+162.9	+74.7	−8.6	−82.2	−166.0	$-U$

TABLE VI. *Pressure.* Pressure in 10^9 dyne/cm², V in cc.

r	3.0	3.05	3.10	3.15	3.20
V	11.58	12.14	12.78	13.41	14.06
$\frac{\partial \ln \nu}{\partial V}$	0.379	0.322	0.310	0.333	0.677
p_1	−3.52	−4.12	−4.43	−4.51	−4.45
p_2	22.5	18.4	16.9	17.2	∽33
$0°\ p$	19.0	14.3	12.5	12.7	∽28.5
$4°\ p_3$			0.021	0.041	0.21

should be (actually a little further), namely to 3.50A ($V=18.4$ cc). That reduces Θ to 50, the minimum pressure is reduced to about 530 atm. but it gives a positive energy content, that is to say a negative heat of sublimation. The zero point energy is then about 450 joules, the lattice energy about 250, having been cut to about ½ of its former value by the increase of the distance and the repulsive term. The compressibility also comes out far too small. Without further calculations it cannot be said what has to be done to improve the agreement. We reserve this calculation and shall only indicate that a slower falling off of the repulsion might be necessary.

SUBSTANCES WITH HIGH MELTING POINTS

Approximations for substances with melting points sufficiently high that the classical specific heat is reached should simplify the calculations considerably because in that case the zero point energy can be neglected and E in equation (12'''') can be replaced by $3RT$. However, we do not know the potential energy in the metals well enough to perform the calculation and in the case of ionic crystals there is still a certain difficulty in calculating the frequencies correctly.[21] Attempts at an approximate calculation were made. The lattice energy U was developed into a power series up to the 3rd power

$$U=U_0+(U''/2)(V-V_0)^2+(U'''/6)(V-V_0)^3.$$

For $\partial \ln \nu/\partial V$ two alternate approximations were made, either $\partial \ln \nu/\partial V$ was assumed constant or ν^2 was put proportional to $\partial^2 U/\partial r^2$. For the first case the calculations were very simple. If the experimentally found coefficient of expansion is given by

$$\alpha=\alpha_0(1+\beta T).$$

then the melting point should be given by

$$T=1/2\beta.$$

For the second assumption the calculations are rather complicated but in both cases the calculated melting points are far too low.

The general results of this paper, however, should hold for all substances. The existence of an upper limit of temperature for the stability of a crystal is based on the appearance of a minimum in the p, V isotherm, shifting to more positive pressures with increased temperature. Now such a minimum should appear in the p, V curve of every crystal, because with increasing volume the elastic tension must finally go to 0. On the other hand, the thermal pressure should increase to infinity. It is namely given by (12''''). ν goes to 0 at a certain volume, probably with the first power of the deviation from that volume. Accordingly $\partial \ln \nu/\partial V$ must go to positive infinity when this volume is approached and the combination of the negative elastic tension, decreasing with volume, and the positive thermal pressure, increasing to infinity with increasing volume, must give a minimum. Because of the factor E in the thermal pressure this minimum will always shift to more positive pressures with increasing temperature. But, of course, for a numerical calculation the exact energy formula must be known.

[21] See, for example, Born and Goeppert-Mayer, Handb. d. Physik **24**, 2nd half, 733, 2nd edition.

On the Interaction of Electrons in Metals

E. WIGNER, *Princeton University*

(Received October 15, 1934)

The energy of interaction between free electrons in an electron gas is considered. The interaction energy of electrons with parallel spin is known to be that of the space charges plus the exchange integrals, and these terms modify the shape of the wave functions but slightly. The interaction of the electrons with antiparallel spin, contains, in addition to the interaction of uniformly distributed space charges, another term. This term is due to the fact that the electrons repell each other and try to keep as far apart as possible. The total energy of the system will be decreased through the corresponding modification of the wave function. In the present paper it is attempted to calculate this "correlation energy" by an approximation method which is, essentially, a development of the energy by means of the Rayleigh-Schrödinger perturbation theory in a power series of e^2.

1.

THE attempt has been made in previous work[1] to give a more general expression for the wave function of free electrons in metals than that provided by Hartree's method of the self-consistent field[2, 3] or Fock's equations. The form of the wave function assumed in Fock's equations for a system of $2n$ electrons, occupying n doubly-degenerate states is

$$\frac{1}{n!}\begin{vmatrix}\psi_1(x_1) & \cdots & \psi_1(x_n)\\ \cdot & & \cdot\\ \cdot & & \cdot\\ \cdot & & \cdot\\ \psi_n(x_1) & \cdots & \psi_n(x_n)\end{vmatrix}\cdot\begin{vmatrix}\psi_1(y_1) & \cdots & \psi_1(y_n)\\ \cdot & & \cdot\\ \cdot & & \cdot\\ \cdot & & \cdot\\ \psi_n(y_1) & \cdots & \psi_n(y_n)\end{vmatrix}, \quad (1)$$

where x stands for three Cartesian coordinates of electrons with upward spin, and y for those of electrons with downward spin. The ψ_ν are the solutions of a Schrödinger equation in which the potential of the charge distribution of the other electrons enters as well as the potential arising from the ions.

In a metal the charge distribution of all electrons is practically unaltered by removing one so that the second quantity may be replaced by the former and the potential for a given electron at the point u is given by adding to the Coulomb field of the ions the fields of all electrons with parallel and with antiparallel spin. The former distribution may be obtained by inserting u for x_n in (1) and integrating over all coordinates except x_1 and u, while the latter is obtained by a similar operation with the exception that the integration should be carried out over all coordinates except y_1 and u.

Actually, it had been shown in[1, 4] that the wave functions ψ_ν of the free electrons in a Na-lattice are very nearly plane waves $e^{2\pi i\nu\cdot x/L}$ where L is the cube edge of the crystal and ν stands for a set of three integers, $\nu\cdot x$ denotes the scalar product of ν and x. Hence the charge distribution of the electrons with opposite spin is practically uniform, that of the electrons with parallel spin uniform with a "hole" around u.[5]

In no wave function of the type (1) is there a statistical correlation between the positions of electrons with antiparallel spin. The purpose of the aforementioned generalization of (1) is to allow for such correlations. This will lead to an improvement of the wave function and, therefore, to a lowering of the energy value. This energy gain will be called "correlation energy."

2.

The new form of the wave function, assumed in[1] was

$$\frac{1}{n!}\begin{vmatrix}\psi_1(y_1\cdots y_n;x_1) & \cdots & \psi_1(y_1\cdots y_n;x_n)\\ \cdot & & \cdot\\ \cdot & & \cdot\\ \cdot & & \cdot\\ \psi_n(y_1\cdots y_n;x_1) & \cdots & \psi_n(y_1\cdots y_n;x_n)\end{vmatrix}\cdot\begin{vmatrix}\psi_1(y_1) & \cdots & \psi_1(y_n)\\ \cdot & & \cdot\\ \cdot & & \cdot\\ \cdot & & \cdot\\ \psi_n(y_1) & \cdots & \psi_n(y_n)\end{vmatrix}, \quad (2)$$

[1] E. Wigner and F. Seitz, Phys. Rev. **46**, 509 (1934).
[2] D. R. Hartree, Proc. Camb. Phil. Soc. **24**, 89 (1928).
[3] J. C. Slater, Phys. Rev. **35**, 210, 1930; V. Fock, Zeits. f. Physik **61**, 126 (1930).
[4] J. C. Slater, Phys. Rev. **45**, 794 (1934); A. Sommerfeld and H. Bethe, Geiger-Scheel's Handbuch der Physik, Vol. **24**, 2nd part, 2nd edition, p. 406.
[5] E. Wigner and F. Seitz, Phys. Rev. **43**, 804 (1933).

which contains the functions $\psi_\nu(y_1 \cdots y_n; x)$ which are different functions of x for different configurations $y_1, \cdots, y_n$ of the electrons with opposite spin, instead of the $\psi_\nu(x)$. It is proposed to find the best wave function, i.e., that with the lowest total energy of the form[6] (2). The $y_1, \cdots, y_n$ in $\psi_\nu(y_1 \cdots y_n; x)$ are to be viewed merely as parameters. (Cf. Eq. (23) ref. 1.) The total energy of the wave function (2) was previously calculated and relative to the solution of Fock's equations yielded the following energy

$$E_1=\frac{1}{n!}\int dy\,|y|^2\left\{\sum_\nu \epsilon_\nu-\frac{h^2}{2m}\sum_{\nu\nu'}\sum_\kappa\left|\int \psi_{\nu'}(y;x_1)^*\frac{\partial\psi_\nu(y;x_1)}{\partial y_\kappa}dx_1\right|^2\right\}, \tag{3}$$

where $|y|$ denotes the second determinant of (1), the summation κ runs over all $3n$ coordinates y and that over ν and ν' over all occupied states, i.e., over all indices occurring in the wave functions in (1) or (2); $\psi_\nu(y;x)$ stands for $\psi_\nu(y_1 \cdots y_n; x)$ and dy for $dy_1 \cdots dy_n$. The quantities ϵ_ν are the integrals

$$\epsilon_\nu(y_1 \cdots y_n)=\int \psi_\nu(y;x_1)^*\{V-(h^2/2m)(\Delta_{x_1}+\Delta_{y_1}+\cdots+\Delta_{y_n})\}\psi_\nu(y;x_1)dx_1$$
$$+\int \psi_\nu(x_1)^*(h^2/2m)\Delta_{x_1}\psi_\nu(x_1)dx_1, \tag{3a}$$

where again $V(y_1 \cdots y_n; x)$ is the difference between the potentials at the point x of a charge distribution corresponding to $\psi_1(y)$, $\psi_2(y)$, $\cdots$, $\psi_n(y)$, on the one hand, and point charges at $y_1, \cdots, y_n$, on the other.

It is necessary now to assume for $\psi_\nu(y_1, \cdots, y_n; x)$ the form

$$\psi_\nu(y;x)=\psi_\nu(x)\{1+f_\nu(y_1-x)+f_\nu(y_2-x)+\cdots+f_\nu(y_n-x)\} \tag{4}$$

and that if ν and ν' are both occupied states

$$\int \psi_{\nu'}(y;x_1)^*(\partial\psi_\nu(y;x_1)/\partial y_\kappa)dx_1=0 \tag{4a}$$

so that the second term in (3) vanishes. Both (4) and (4a) will turn out to be correct in the approximation to be used. By means of (4) it is possible to transform (3a) so as to get rid of all derivatives with respect to the y, after which one may minimize (3) by minimizing $\epsilon_\nu(y_1, \cdots, y_n)$ for every combination of the y. This would lead to a differential equation for the $\psi_\nu(y_1 \cdots y_n; x)$ in which the y would be merely parameters. (The solutions $\psi_\nu(x)$ of Fock's equations which also enter into this equation are supposed to be known.) The result of the transformation is especially simple if one uses for $\psi_\nu(x)=e^{2\pi i\nu\cdot x/L}$, namely,

$$\epsilon_\nu(y_1 \cdots y_n)=\int \psi_\nu(y;x)^*\{V-(h^2/m)(\Delta_x-(2\pi i\nu/L)\,\mathrm{grad}_x)\}\psi_\nu(y;x)dx. \tag{3b}$$

In addition to the energy contribution (3) which is negative and was calculated in[1] there is a further one which is generally positive. This arises from the fact that the probabilities of the relative distances of electrons with upward spin are changed by the transition from the $\psi_\nu(x)$ to the $\psi_\nu(y_1, \cdots, y_n; x)$. Since the latter will be large for x's, which lie in regions comparatively free from y's, the distribution of the x's will not be uniform throughout space and they will be nearer together than they were under the previous assumption.

[6] The form (2) of the wave function is certainly not the correct one. It does not belong even to one single multiplicity but is a linear combination of functions of different "multiplicities" (belonging to different representations of of the symmetric group). If, however, the functions $\psi_\nu(y_1 \cdots y_n; x)$ are not too different from the functions $\psi_\nu(x)$, they all belong to very low multiplicities. This is the only case, anyway, in which the present approximation is good and it can be expected that the real wave function is in this case near to (2).

In order to evaluate this energy change, one may first calculate the probability of two electrons with parallel spin being at the points x_1 and x_2, respectively, if the complete wave function is given by (1). Under the approximate assumption that $\psi_\nu(x)=\psi_0(x)e^{2\pi i\nu\cdot x/L}$ one obtains for this in the way given in reference 5,

$$|\psi_0(x_1)\psi_0(x_2)|^2 g(|x_1-x_2|), \tag{5}$$

where

$$g(r)=1-9\left(\frac{\sin(r/d)-(r/d)\cos(r/d)}{(r/d)^3}\right)^2 \tag{5a}$$

is the probability of the distance $|x_1-x_2|=r$ for free electrons with parallel spin,

$$d=(v_0/3\pi^2)^{\frac{1}{3}}=(4/9\pi)^{\frac{1}{3}}r_s=0.521r_s \tag{6}$$

is $1/(2\pi)$ times the wave-length of the fastest electron, v_0 is the atomic volume and r_s the radius of the sphere with this volume. If we make the assumption $\psi_\mu(y,x)=\psi_\nu(y,x)e^{2\pi i(\mu-\nu)\cdot x/L}$, an expression of the form (5) is valid for the wave function (2) as well as for (1) and the change of mutual potential energy of the electrons with upward spin arising from the transition from (1) to (2) is

$$E_2=\frac{1}{n!}\int dy|y|^2\sum_\nu \epsilon_\nu'(y_1\cdots y_n), \tag{7}$$

where

$$\epsilon_\nu'(y_1\cdots y_n)=\int dx_1dx_2(ne^2/2r)\{|\psi_\nu(y;x_1)\psi_\nu(y;x_2)|^2-|\psi_\nu(x_1)\psi_\nu(x_2)|^2\}g(r). \tag{7a}$$

The $\frac{1}{2}$ enters once again because the interaction of a pair of electrons should be counted once only. In order to be able to evaluate the integral (7a), $g(r)$ has been replaced by

$$1-e^{-1.6r/d}(1+1.6r/d+1.2(r/d)^2), \tag{8}$$

which, as is shown in Fig. 1, runs rather near to $g(r)$.

3.

The task of Section 4 will be to calculate the wave functions $\psi_\nu(y_1\cdots y_n;\ x)$ which minimize the sum of expressions (3b) and (7a) and to calculate E_1+E_2 corresponding to these wave functions. Before doing this, however, an estimate of the order of magnitude of the effect to be expected should be given. This can be taken from calculations of atomic spectra by the method of Fock's equation or Hartree's field, and their comparison with experimental results. The best result in this connection seems to be that on the normal state of He, where Fock's equation is identical with Hartree's. The discrepancy here is[7] $0.077Ry$ (Rydberg units) for both electrons, or 12 Cal. per electron. This must be the amount of correlation energy in He.

The situation is somewhat more complicated in the calculation of the terms of O^{++}, O^+, and O by Hartree and Black,[8] since Hartree's method has been used instead of Fock's, and also because in the latter cases more than two electrons play important rôles. For O^{++} the differences between observed values (in brackets) and theory are

$^3P(4.050)0.074$; $^1D(3.868)0.090$; $^1S(3.658)0.176$.

If we denote the radial wave function for the electrons by $P(r)$, these terms correspond to the linear combinations $P(r)P(r')$ multiplied by

$$xy'-yx';\quad (x+iy)(x'+iy');\quad xx'+yy'+zz'.$$

In the first case the correlation energy is very small, since the electrons are probably far away

[7] Cf. D. R. Hartree and A. L. Ingman, Mem. of the Manchester Lit. and Phil. Soc. **77**, 69, 87 (1933).

[8] D. R. Hartree and M. M. Black, Proc. Roy. Soc. **A139**, 311 (1933).

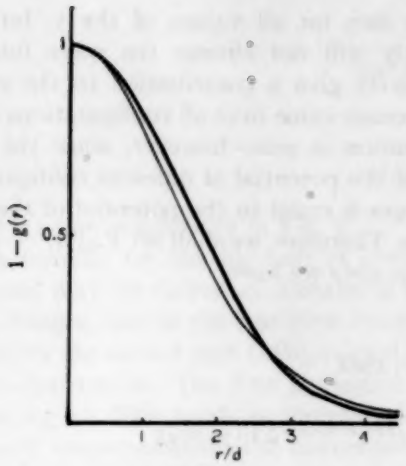

FIG. 1.

from each other anyway, because their spins are parallel. In such cases in the theory of metals we do not take into account any correlation energy at all. The discrepancy in this case may, to a considerable extent, be due to the use of Hartree's instead of Fock's method, and certainly would be further diminished by the use of the latter. On the other hand, in the case of singlet's, Hartree's equations correspond much more closely to Fock's equation and the increased discrepancy of about $0{\cdot}050Ry$ is probably due to the neglect of the correlation energy. It is not quite clear, however, why it is so much greater in the ^1S than in the ^1D term.

A comparison of experimental and theoretical values in O^+ and O points in a similar direction, the correlation energy is smaller though in these cases by a factor of the order 2. It is evident that it must diminish eventually if one goes over to more and more loosely bound electrons, since because of the lower electron densities the total interaction energy diminishes and the correlation energy is only the non-appearance of part of this.

If one goes over to a metal like Na, on first sight the effect could be expected (because of the low electron density) to be much smaller than in He, about as great as in O. This will not be quite so, however, because the fluctuations in the potential of the electrons with downward spin will be greatly increased by their great number. The effect to be calculated in the next section will be about equal, therefore, to the effect per electron in He.

4.

Although the actual wave functions $\psi_\nu(x)$ in the Na lattice are actually different from plane waves $e^{2\pi i\nu\cdot x/L}$ in the Hartree-Fock approximation, we shall use plane waves for $\psi_\nu(x)$ in the subsequent calculation. Since only integrals over the unperturbed functions occur in the perturbation calculation, this will not introduce a great error, because the $\psi_\nu(x)$ are extremely near to plane waves in much the greatest part of the volume.

The whole following calculation will be performed in the approximation which corresponds to the second approximation in the Rayleigh-Schrödinger perturbation theory. The wave functions will be developed into a Fourier series

$$\psi_\nu(y;x)=L^{-\frac{1}{2}}(e^{2\pi i\nu\cdot x/L}+\sum_\mu \alpha_{\nu\mu}e^{2\pi i\mu\cdot x/L}), \quad (9)$$

$e^{2\pi i\nu\cdot x/L}$ being taken as unperturbed function and $V(y_1, \cdots, y_n; x)$ the perturbation. The $\alpha_{\nu\mu}$, which are functions of the y, are supposed to be small, so that third order terms of α and V will be neglected for the energy, and second order terms for the wave function.

For the actual calculation it can be seen, first of all, that one can replace a set of $\psi_\nu(y;x)$ by any orthogonal linear combination of them without affecting the final result. The orthogonality condition between $\psi_\nu(y;x)$ and $\psi_{\nu'}(y;x)$ gives

$$\alpha_{\nu\nu'}+\alpha_{\nu'\nu}^*+\sum_\mu \alpha_{\nu\mu}\alpha_{\nu'\mu}^*=0. \quad (10)$$

By Schmidt's method one can build a set of orthogonal $\psi_\nu(y;x)$ such that $\alpha_{\nu\nu'}=0$ for $\nu<\nu'$

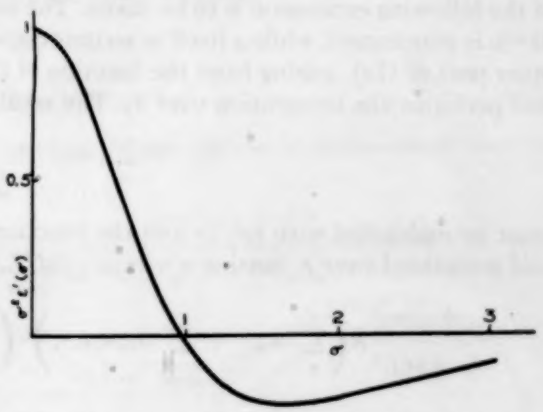

FIG. 2.

if ν' is occupied. It then follows under omission of the last term in (10) that $\alpha_{\nu\nu'}=0$ if ν and ν' are both occupied states, whence the summation over μ in (9) must be extended only over the unoccupied states. It is then seen at once that (4a) is satisfied in our approximation.

In order to calculate $\epsilon_\nu(y_1\cdots y_n)$ one must first calculate the matrix elements of $V(y_1, \cdots, y_n; x)$. The matrix elements $V_{\nu\nu}(y_1, \cdots, y_n; x)=V_{00}$ will not be zero for all values of the y, but they evidently will not change the wave functions and merely give a contribution to the energy. The average value over all configurations of this contribution is zero, however, since the mean value of the potential of different configurations of charges is equal to the potential of the mean charges. Therefore, we shall set $V_{\nu\nu}(y_1, \cdots, y_n; x)=0$. For $\mu\neq\nu$ we have

$$\begin{aligned} V_{\nu\mu}(y_1\cdots y_n; x) &= L^{-3}\int e^{2\pi i(\mu-\nu)\cdot x/L}V(y; x)dx \\ &= -(1/4\pi^2(\mu-\nu)^2L)\int e^{2\pi i(\mu-\nu)\cdot x/L}\Delta V(y; x)dx \\ &= (e^2/\pi(\mu-\nu)^2L)\sum_{\kappa=1}^{n}e^{2\pi i(\mu-\nu)\cdot y_\kappa/L} \end{aligned} \tag{11}$$

because of Poisson's equation.

For ϵ_ν, (3b) yields

$$\epsilon_\nu(y_1\cdots y_n)=\sum_\mu(\alpha_{\nu\mu}V_{\nu\mu}+\alpha_{\nu\mu}^*V_{\nu\mu}^*)+\sum_{\mu\mu'}\alpha_{\nu\mu}^*\alpha_{\nu\mu'}V_{\mu\mu'}+\sum_\mu\frac{4\pi^2h^2}{mL^2}(\mu^2-\mu\cdot\nu)|\alpha_{\nu\mu}|^2, \tag{12}$$

In order to calculate the $\epsilon_\nu'(y_1\cdots y_n)$ by means of (7a), the charge distribution for $\psi_\nu(y; x)$ will first be found:

$$|\psi_\nu(y; x)|^2=L^{-3}+L^{-3}\sum_\mu(\alpha_{\nu\mu}e^{2\pi i(\mu-\nu)\cdot x/L}+\alpha_{\nu\mu}^*e^{2\pi i(\nu-\mu)\cdot x/L})+L^{-3}\sum_{\mu\mu'}\alpha_{\nu\mu}^*\alpha_{\nu\mu'}e^{2\pi i(\mu-\mu')\cdot x/L}. \tag{13}$$

Now $g(r)$ is 1 minus the function of the "hole," which decreases rapidly with increasing r. The 1, inserted into (7a), simply gives the energy difference of a uniform charge distribution and that corresponding to $\psi_\nu(y; x)$, namely,

$$4\pi ne^2L^{-3}\left\{\sum_\mu\frac{|\alpha_{\nu\mu}|^2}{4\pi^2(\mu-\nu)^2/L^2}+R\sum_{\substack{2\nu-\mu\\ \text{unocc.}}}\frac{\alpha_{\nu\mu}\alpha_{\nu 2\nu-\mu}}{4\pi^2(\mu-\nu)^2/L^2}\right\}, \tag{14a}$$

in which the terms higher than the second order in α are omitted, and R means that the real part of the following expression is to be taken. The second sum must be taken only over those μ's for which $2\nu-\mu$ is unoccupied, while μ itself is an unoccupied state in *all* summations. For the calculation of the other part of (7a), arising from the function of the hole, one sets x_1+r for x_2 in (7a), introduces (13), and performs the integration over x_1. The result

$$2L^{-3}R\{\sum_\mu|\alpha_{\nu\mu}|^2+\sum_{\substack{2\nu-\mu\\ \text{unocc.}}}\alpha_{\nu\mu}\alpha_{\nu 2\nu-\mu}\}e^{2\pi i(\nu-\mu)\cdot r/L}$$

must be multiplied with $ne^2/2r$ and the function of the hole $g(r)-1$, which must be taken from (8), and integrated over r. Setting $\sigma=2\pi(\mu-\nu)d/L$, this yields

$$-\frac{4\pi d^2ne^2}{2.56L^3}R\left(\sum_\mu|\alpha_{\nu\mu}|^2+\sum_{\substack{2\nu-\mu\\ \text{unocc.}}}\alpha_{\nu\mu}\alpha_{\nu 2\nu-\mu}\right)\cdot\left(\frac{1}{1+\sigma^2/2.56}+\frac{1.063}{(1+\sigma^2/2.56)^2}+\frac{3.75}{(1+\sigma^2/2.56)^3}\right). \tag{14b}$$

Added to (14a) this gives with help of the relation $4\pi r_s^3/3=v_0$

$$\epsilon_\nu'(y_1\cdots y_n)=\frac{2^{\frac{1}{2}}}{3^{\frac{1}{2}}\pi^{\frac{1}{2}}}\frac{e^2}{r_s}R\left(\sum_\mu|\alpha_{\nu\mu}|^2+\sum_{\substack{2\nu-\mu\\ \text{unocc.}}}\alpha_{\nu\mu}\alpha_{\nu 2\nu-\mu}\right)\epsilon'(\sigma),$$

$$\epsilon'(\sigma)=\frac{1}{\sigma^2(1+\sigma^2/2.56)}-\frac{0.415}{(1+\sigma^2/2.56)^2}-\frac{1.465}{(1+\sigma^2/2.56)^3}. \tag{14}$$

$\sigma^2\epsilon'(\sigma)$ is given graphically in Fig. 2.

This formula for the increase of potential energy between electrons with upward spin is not exact and may be viewed as containing two parts: First (14a), the increase of the potential of the space charges, due to the less even charge distribution for $\psi_\nu(y;x)$ than for $\psi_\nu(x)$. This increase is lowered by the second part (14b), caused by the greater efficiency of the Fermi hole in a non-uniform charge distribution. The first neglection was made in setting $\psi_\mu(y;x)=e^{2\pi i(\mu-\nu)\cdot x/L}\psi_\nu(y;x)$ when calculating ϵ_ν'. This tends to increase the ϵ_ν' especially for those ν, for which it is large anyway, because it overemphasizes the unevenness in the charge distribution. The second neglection was to keep no terms higher than the second order terms in α. This certainly decreases ϵ_ν', because part of the uneveness in the charge density is due to the higher terms, especially to those of the fourth order. Finally, the normalization constant, which is smaller than 1, enters in the second power in (14) and only in the first in (12). Its omission again increases (14). In the whole these errors will about compensate.

The final quantity to be minimized is, after omission of the higher order terms,

$$\epsilon_\nu+\epsilon_\nu'=R\sum_\mu\{2\alpha_{\nu\mu}V_{\nu\mu}+(t_{\nu\mu}+t_{\nu\mu}')|\alpha_{\nu\mu}|^2+t_{\nu\mu}'\alpha_{\nu\mu}\alpha_{\nu 2\nu-\mu}\}, \tag{15}$$

where

$$t_{\nu\mu}=\frac{4\pi^2\hbar^2}{mL^2}(\mu^2-\mu\cdot\nu),\qquad t_{\nu\mu}'=\frac{2^{\frac{1}{2}}}{3^{\frac{1}{2}}\pi^{\frac{1}{2}}}\frac{e^2}{r_s}\epsilon'\left(\frac{2\pi(\mu-\nu)d}{L}\right). \tag{15a}$$

$V_{\nu\mu}$ is given in (11), $\epsilon'(\sigma)$ in (14), ν is an occupied state, the last term in (15) should be taken only if $2\nu-\mu$ is an unoccupied state. By setting the derivative of (15) with respect to $\alpha_{\nu\mu}^*$ equal to zero, one obtains

$$V_{\nu\mu}^*+(t_{\nu\mu}+t_{\nu\mu}')\alpha_{\nu\mu}=0 \tag{16a}$$

if $2\nu-\mu$ is occupied. If it is unoccupied

$$V_{\nu\mu}^*+(t_{\nu\mu}+t_{\nu\mu}')\alpha_{\nu\mu}+t_{\nu\mu}'\alpha_{\nu 2\nu-\mu}=0,\qquad V_{\nu\mu}^*+(t_{\nu 2\nu-\mu}+t_{\nu\mu}')\alpha_{\nu 2\nu-\mu}^*+t_{\nu\mu}'\alpha_{\nu\mu}=0. \tag{16b}$$

The last equation is obtained by differentiating (15) with respect to $\alpha_{\nu 2\nu-\mu}$ and considering that $V_{\nu 2\nu-\mu}=V_{\nu\mu}^*$ and $t_{\nu 2\nu-\mu}'=t_{\nu\mu}'$. Solving (16), one finds if $2\nu-\mu$ is occupied

$$\alpha_{\nu\mu}=-V_{\nu\mu}^*/(t_{\nu\mu}+t_{\nu\mu}') \tag{17a}$$

and

$$\alpha_{\nu\mu}=-V_{\nu\mu}^*t_{\nu 2\nu-\mu}/[(t_{\nu\mu}+t_{\nu\mu}')t_{\nu 2\nu-\mu}+t_{\nu\mu}t_{\nu\mu}'] \tag{17b}$$

if $2\nu-\mu$ is unoccupied, while μ is, of course, always unoccupied. These formulas show that the $\psi_\nu(y_1,\cdots,y_n;x)$ do have the form (4) with

$$f_\nu(y-x)=-\frac{e^2}{\pi L}\left(\sum_{\substack{2\nu-\mu\\ \text{occ.}}}\frac{e^{2\pi i(\nu-\mu)\cdot(y-x)/L}}{(\mu-\nu)^2(t_{\nu\mu}+t_{\nu\mu}')}+\sum_{\substack{2\nu-\mu\\ \text{unocc.}}}\frac{e^{2\pi i(\nu-\mu)\cdot(y-x)/L}}{(\mu-\nu)^2(t_{\nu\mu}+t_{\nu\mu}'+t_{\nu\mu}t_{\nu\mu}'/t_{\nu 2\nu-\mu})}\right). \tag{18}$$

Inserting (17) into (15) one obtains for the total energy

$$\epsilon_\nu+\epsilon_\nu'=-\sum_{\substack{2\nu-\mu\\ \text{occ.}}}\frac{|V_{\nu\mu}|^2}{t_{\nu\mu}+t_{\nu\mu}'}-\sum_{\substack{2\nu-\mu\\ \text{unocc.}}}\frac{|V_{\nu\mu}|^2t_{\nu 2\nu-\mu}}{(t_{\nu\mu}+t_{\nu\mu}')t_{\nu 2\nu-\mu}+t_{\nu\mu}t_{\nu\mu}'}. \tag{19}$$

Instead of the second term one could write half of the sum of the terms for μ and $2\nu-\mu$, which makes it somewhat more symmetric.

5.

It would be rather difficult to perform the summation over μ in (19) for an arbitrary set of $y_1, \cdots, y_n$. Fortunately only the mean value of (19) with the weight $|y|^2/n!$ is needed and this can be computed quite easily. Since the t do not depend on the y, one finds

$$\frac{1}{n!}\int |V_{\nu\mu}|^2|y|^2dy=\frac{e^4}{\pi^2(\mu-\nu)^4L^2}\sum_{\kappa,\lambda=1}^{n}\int e^{2\pi i(\mu-\nu)\cdot(y_\kappa-y_\lambda)/L}|y|\,e^{2\pi i(\nu_1y_1+\cdots+\nu_ny_n)/L}dy$$
$$=\frac{e^4}{\pi^2(\mu-\nu)^4L^2}\left(\sum_{\kappa=1}^{n}1-\sum_{\kappa\neq\lambda}\delta(\nu-\mu+\nu_\kappa-\nu_\lambda)\right). \tag{20}$$

The first term comes from $\kappa=\lambda$, the second from $\kappa\neq\lambda$. In the second, the summation over λ can be carried out, and it yields 1 if $\nu-\mu+\nu_\kappa$ is an occupied state, zero otherwise. The whole bracket is, therefore, equal to the number of occupied states ν', for which $\nu+\nu'-\mu$ is not occupied. Fig. 3 shows a cross section of the ν'-space through the origin and the point $\nu-\mu$. The radius of the circles is $(3n/4\pi)^{\frac{1}{3}}=L/2\pi d$. The sphere through the weak circle contains the points $\nu-\mu+\nu'$ and the hatched part is unoccupied. As a consequence, it is

$$\frac{1}{n!}\int |V_{\nu\mu}|^2|y|^2dy=\frac{e^4n}{\pi^2(\mu-\nu)L^2}\eta(2\pi(\mu-\nu)d/L),\qquad \eta(\sigma)=\begin{cases}1 & \text{for } |\sigma|>2\\ \dfrac{3|\sigma|}{4}-\dfrac{|\sigma|^3}{16} & \text{for } |\sigma|<2\end{cases} \tag{21}$$

and hence

$$F_\nu=\frac{1}{n!}\int(\epsilon_\nu+\epsilon_\nu')|y|^2dy=-\frac{2Ry}{3\pi^3}\int_{\substack{|\sigma+\rho|>1\\|\sigma-\rho|<1}}\frac{\eta(\sigma)d\sigma}{\sigma^4[\sigma^2+\sigma\cdot\rho+c\epsilon'(\sigma)]}-\frac{2Ry}{3\pi^3}\int_{\substack{|\sigma+\rho|>1\\|\sigma-\rho|>1}}\frac{\eta(\sigma)d\sigma}{\sigma^2[\sigma^4-(\sigma\cdot\rho)^2+2c\sigma^2\epsilon'(\sigma)]}. \tag{22}$$

Here $\rho=2\pi\nu d/L$, $\sigma=2\pi(\mu-\nu)d/L$ and the summation over μ has been replaced by an integration over σ. The total energy is expressed in Rydberg units. The constant c is

$$c=(2^{\frac{1}{3}}/3^{\frac{1}{3}}\pi^{\frac{1}{3}})(e^2md^2/h^2r_s)=0.1106r_s/a_0 \tag{22a}$$

when expressed as function of the radius of the "s-sphere" in Bohr units a_0.

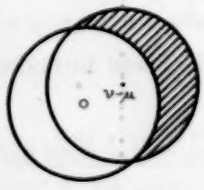

FIG. 3. Cross section of ν' space.

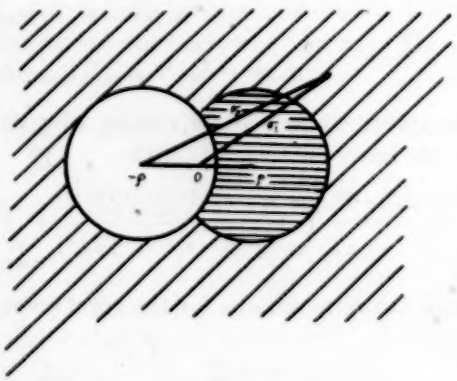

FIG. 4. Section of σ space.

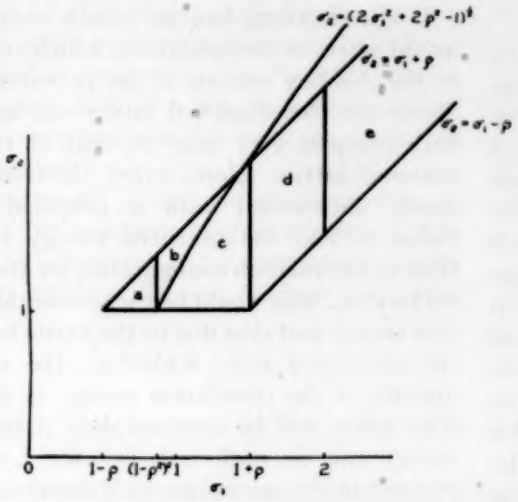

FIG. 5. *Note:* $(1-\rho^2)^2$ should read $(1-\rho^2)^{\frac{1}{2}}$.

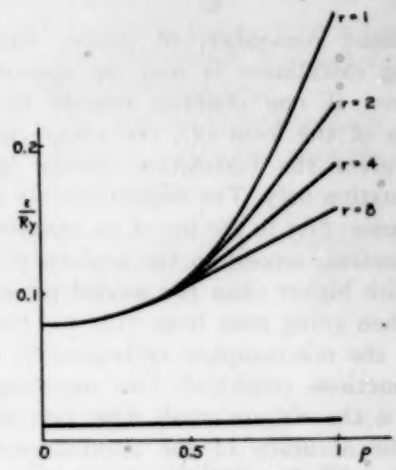

FIG. 6.

In order to perform the integration of (22), one may first introduce elliptic coordinates $\sigma_1=|\sigma|$, $\sigma_2=|\sigma+\rho|=|2\pi\mu d/L|$ in the σ-space, using as centers the origin and the point $-\rho$ (cf. Fig. 4). The first integral is to be extended over the horizontally, the second over the obliquely hatched region. The first will be a sum of two integrals (a) and (b) in Fig. 5, in both of which $\eta(\sigma)=3\sigma_1/4-\sigma_1^3/16$. The second integral is a sum of three integrals (c), (d) and (e), and in the first two of them the same expression is valid for $\eta(\sigma)$ while $\eta(\sigma)=1$ in the last. For $d\sigma$ one writes $2\pi\sigma_1 d\sigma_1\sigma_2 d\sigma_2/\rho$, σ_1^2 for σ^2, and $\sigma\cdot\rho=\frac{1}{2}(\sigma_2^2-\sigma_1^2-\rho^2)$. The integration over σ_2 can be carried out simply and gives the five integrals

$$-F_\rho=\frac{4Ry}{3\pi^2\rho}\int_{1-\rho}^{(1-\rho^2)^{\frac{1}{2}}}\ln\frac{2c\epsilon'(\sigma_1)+2\sigma_1^2+2\sigma_1\rho}{2c\epsilon'(\sigma_1)+\sigma_1^2+1-\rho^2}\left(\frac{3\sigma_1}{4}-\frac{\sigma_1^3}{16}\right)\frac{d\sigma_1}{\sigma_1^3}$$

$$+\frac{4Ry}{3\pi^2\rho}\int_{(1-\rho^2)^{\frac{1}{2}}}^{1+\rho}\ln\frac{2c\epsilon'(\sigma_1)+2\sigma_1^2+2\sigma_1\rho}{2c\epsilon'(\sigma_1)+3\sigma_1^2+\rho^2-1}\left(\frac{3\sigma_1}{4}-\frac{\sigma_1^3}{16}\right)\frac{d\sigma_1}{\sigma_1^3}$$

$$+\frac{4Ry}{3\pi^2\rho}\int_{(1-\rho^2)^{\frac{1}{2}}}^{1+\rho}\ln\frac{2\sigma_1 v+\sigma_1^2+\rho^2-1}{2\sigma_1 v-\sigma_1^2-\rho^2+1}\left(\frac{3\sigma_1}{4}-\frac{\sigma_1^3}{16}\right)\frac{d\sigma_1}{\sigma_1^2 v}$$

$$+\frac{4Ry}{3\pi^2\rho}\int_{1+\rho}^{2}\ln\frac{v+\rho}{v-\rho}\left(\frac{3\sigma_1}{4}-\frac{\sigma_1^3}{16}\right)\frac{d\sigma_1}{\sigma_1^2 v}+\frac{4Ry}{3\pi^2\rho}\int_2^\infty\ln\frac{v+\rho}{v-\rho}\frac{d\sigma_1}{\sigma_1^2 v},$$

where v stands for $(2c\epsilon'(\sigma_1)+\sigma_1^2)^{\frac{1}{2}}$. A calculation of this quantity for $r_s=4$ shows that it is practically equal σ_1 if $\sigma_1>2$ and the last integral can be evaluated accordingly. It yields

$$\frac{4Ry}{3\pi^2\rho}\left\{\left(\frac{1}{8}-\frac{1}{2\rho^2}\right)\ln\frac{2+\rho}{2-\rho}+\frac{1}{2\rho}\right\}\approx\frac{Ry}{9\pi^2}\left(1+\frac{\rho^2}{20}\right).$$

The other integrals were evaluated numerically and the results are plotted against ρ. Fig. 6 shows the plots for $r_s=1, 2, 4, 8$. From this, the mean value of the correlation energy which is the mean value of $-\frac{1}{2}F_\rho$ with the weight ρ^2, was calculated, and plotted against r_s. The $\frac{1}{2}$ enters, because the whole energy correction is present only for half of the electrons, that is, those with upward spin. In Fig. 7 the upper curve represents the values calculated in this way. The energy is given in multiples of ϵ^2/r_s.

6.

One must remember, of course, that the preceding calculation is only an approximate one. Even if one confines oneself to wave functions of the form (2), the upper curve of Fig. 7 gives the correlation energy in first approximation only. The neglections are due to three causes: first to the use of an unnormalized wave function, second to the neglection of the terms with higher than the second power of α in ϵ_ν, when going over from (12) to (14a) and third to the non-complete orthogonality of the wave functions employed. Our approximation is good if the α's are small. One gets an idea about the accuracy of the approximation by calculating $\sum_\mu \int |\alpha_{\nu\mu}|^2 |y|^2 dy/n!$ (which is the reciprocal square of the normalization constant minus one), though an idea only, since $\sum_\mu |\alpha_{\nu\mu}|^2$ should really be small for all configurations of the y, not only its mean value. A calculation of the former quantity shows[9] that it stays well below one, except for large r_s and for ρ which are very near to 1. It is in these cases that our approximation must be expected to break down.

The real value of the correlation energy will be smaller in these cases than the calculated one. The correction with the normalization constant could easily be taken into account, as has been shown at another place.[10] It always decreases the correlation energy, not very much, however, as the magnitude of the normalization constant or the formulas in[10] show. The second neglection is probably more dangerous and also more laborious to correct. It has been done for one point ($r_s=4$) only and for this one very roughly. The second neglection also increased the calculated value of the correlation energy, since it amounts to taking $1-2f$ instead of $(1-f)^2$ for the probability of the electron being at a certain point, and the minima of $1-2f$ are much deeper than those of $(1-2f)^2$ (the maxima are lower but less important).

If the electrons had no kinetic energy, they would settle in configurations which correspond to the absolute minima of the potential energy. These are closed-packed lattice configurations, with energies very near to that of the body-centered lattice. Here, every electron is very nearly surrounded with a spherical hole of radius r_s and the potential energy is smaller than in the random configuration by the amount $0.75=e^2/r_s$. This would be the sum of the correlation energy and that due to the Fermi hole. Since the latter one is,[11, 1] $0.458e^2/r_s$, the maximum amount of the correlation energy is $0.292e^2/r_s$. This value will be attained only if the kinetic energy can be neglected, i.e., for $r_s=\infty$, and represents the asymptote to the real correlation energy curve, which is attempted to be drawn into Fig. 7. It appears to run much higher than one would have thought without calculation. I believe it to be in error everywhere by less than 20 percent.

The dotted line at $0.142e^2/r_s$ corresponds to a correlation energy as great as assumed in the first calculation[5] giving $0.6e^2/r_s$ together with the energy of the Fermi hole.

The calculated constants of the Na lattice with the correlation energy of Fig. 7 and the other quantities as in reference 1 are as follows: lattice constant 4.62A as compared with the observed value of 4.23A. The binding energy associated with this is 26.1 Calories, to be compared with the observed value of 26.9. The calculated value of the binding energy for the observed lattice

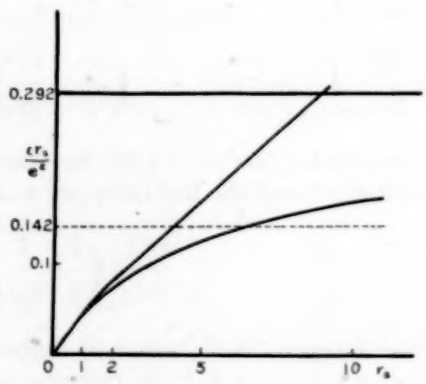

FIG. 7.

[9] The greatest part of the numerical work has been done by Dr. M. Vermes of Budapest. A table of the calculated values is given here:

ρ	$r=1$	4	8
0	0·006	0·10	0·45
0·4	0·009	0·14	0·54
1	0·04	0·30	0·94

[10] To appear shortly in the Bull. of the Hung. Acad.

[11] F. Bloch, Zeits. f. Physik **57**, 545 (1929).

constant is 22.3 Cal. As far as the lattice constant goes, one must remember, however, that both the correlation energy and that due to the Fermi hole are calculated for a flat wave function and the wave functions are flat only for $r_s=4$ and its neighborhood.

The magnitude of the correlation energy is important for questions of paramagnetism and ferromagnetism as well as for questions of lattice energy. It modifies Bloch's original theory on the ferromagnetism of free electrons[11] in such a way that it yields ferromagnetism in fewer cases than in its original form.[12] I hope to return to this question at another time.

I wish to express my gratitude to Dr. F. Seitz for his kind help in connection with the preparation of this manuscript.

[12] A paper of S. Schubin and S. Wonsowsky, Proc. Roy. Soc. **A145**, 159 (1934) which appeared recently, points in the same direction.

DECEMBER 1, 1934 PHYSICAL REVIEW VOLUME 46

Thermal Expansion and the Ferromagnetic Change in Volume of Nickel

CLARKE WILLIAMS, *Columbia University*

(Received October 11, 1934)

The coefficient of thermal expansion is measured at intervals of 2.5°C between 200°C and 500°C for single and polycrystalline specimens of nickel of varying known degrees of purity. The data yield the value $3.24\pm0.15\times10^{-4}$ for the ferromagnetic change in volume per unit volume of pure nickel.

INTRODUCTION

WHEN the coefficient of thermal expansion of nickel is plotted as a function of temperature the resulting graph has a hump which starts at about 200°C and terminates in the neighborhood of the Curie point. The area under the graph represents a change of length (and hence of volume), and the area under the hump may properly be taken as a measure of the change in volume associated with those interatomic forces (or energies) in terms of which the ferromagnetism of the material finds its explanation. Fowler and Kapitza[1] were the first to point out that Heisenberg's theory of ferromagnetism is competent to offer a quantitative description of this phenomenon. Their calculation has been extended by Powell,[2] who obtained an expression relating the change in volume per unit volume to the exchange energy between pairs of electrons belonging to neighboring atoms. The observations upon which Powell based his numerical estimate of the former quantity were obtained by Colby,[3] who worked with polycrystalline nickel of unspecified purity. It seemed worth while to repeat Colby's measurements upon single and polycrystalline nickel of varying known degrees of purity, and to extend them over a greater range of temperature in order to increase the precision of the base line from which the hump is reckoned. The present paper is a report based upon these experiments.

APPARATUS AND METHOD

The dilatometer (Fig. 1) is constructed entirely of fused quartz. A knife edge, A, and a table, B, rest upon a flat plate, C. The top of the table is ground flat and polished, and carries a ground roller about 1 mm in diameter. The specimen, S, is a circular cylinder about 5 mm in diameter and 6 cm to 7 cm long. A tiny lateral scratch is made near one end and the other end is polished. The scratch engages the knife edge and the polished end rests on the roller. Mirrors M_2 and M_4, of gold sputtered on quartz, are fused to the ends of the roller. These mirrors are rotated slightly with

[1] Fowler and Kapitza, Proc. Roy. Soc. **A124**, 1 (1929).
[2] Powell, Proc. Phys. Soc. **42**, 390 (1930).
[3] Colby, Phys. Rev. **30**, 506 (1910).

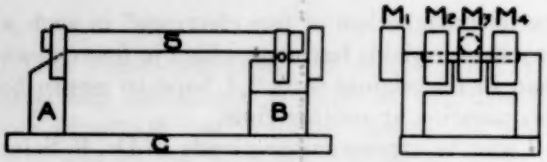

FIG. 1. The quartz dilatometer.

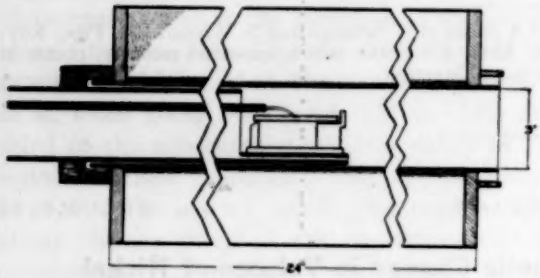

FIG. 2. The dilatometer and furnace assembly.

respect to each other about the roller axis to increase the range of the instrument. A mirror, M_1, is fused to the knife edge, and another, M_3, to the table.

Fig. 2 is a diagram of the dilatometer and furnace assembly. The dilatometer rests in the center of the furnace on a quartz plate fused to one end of a quartz tube 2.5 inches in diameter and 2 feet long. The other end of this tube is held in a mounting insulated against building vibration. The heating element of the furnace is a bifilar winding of No. 18 Constantan wire on a quartz tube 3 inches in diameter and 26 inches long, together with an auxiliary winding over a length of 6 inches at each end. The open end of the furnace is closed with a microscope cover glass.

The junction of a platinum *vs.* platinum—10 percent rhodium thermocouple nearly touches the specimen at its center. The thermal e.m.f. is measured with a Leeds and Northrup Type K potentiometer.

The mirrors are so aligned that they reflect into a theodolite light from four vertical scales, one for each mirror. The scales are four meters from the dilatometer, and can be independently illuminated. Readings on the scales associated with mirrors M_1 and M_3 reveal any rotation of the dilatometer as a whole.

Prior to each set of observations the specimen is demagnetized in an alternating magnetic field, mounted in the dilatometer, and carried through several cycles of heating and cooling over the temperature range 300°C to 400°C. Thermal equilibrium is then established and observations are made at 5° intervals over a complete cycle of heating and cooling. The initial temperature is then altered 2.5 degrees and the procedure repeated. The data thus yield mean values of the coefficient of thermal expansion over 5° intervals corresponding to mean temperatures which differ by 2.5°.

RESULTS

Observations are here reported upon five different specimens of nickel, namely:

I. A single crystal of Mond nickel grown in an atmosphere of hydrogen at a pressure of about 1 mm;[4]

II. A single crystal grown of nickel purified in the manner described by Fink and Rohrman,[5] but contaminated with carbon, and with molybdenum from the winding of the furnace in which the crystal is grown;

III. A polycrystalline specimen of the same material as II, but containing more molybdenum;

IV. A specimen of hard drawn commercial nickel;

V. Specimen IV, annealed 1 hr. in hydrogen at 1100°C and cooled slowly.

Table I shows the purity of the several specimens. The analysis of specimen IV was supplied by the International Nickel Co. The carbon content of specimen III was determined chemically by Dr. L. A. Wooten, of the Bell Telephone Laboratories. The remainder of the data represent quantitative spectroscopic analyses made by Lucius Pitkin, Inc. of New York.

Laue photographs taken through thin sections sawn from the ends of specimens I and II indicate that the orientations of the respective

TABLE I. *Percent impurity in specimens.*

	I	II	III	IV
Mo	0.075	0.5–0.6	0.75–0.9	0.11
C	0.02–0.06	0.06–0.1	0.05–0.09	0.3–0.4
Co	*	*	*	0.13
Cu	0.01–0.02	0.005–0.01	0.001–0.005	0.41
Fe	0.001–0.005	0.005–0.01	0.01–0.02	
Mg	trace	trace	trace	
Mn	*	*	*	0.02
Al	*	*	*	
Si	trace	trace	trace	0.09
Sn	*	trace	trace	

* Not found.

[4] Dingwall, Zacharias and Siegel, Trans. Electrochem. Soc. **63**, 395 (1933).

[5] Fink and Rohrman, Trans. Electrochem. Soc. **57**, 325 (1930); **58**, 403 (1930); **59**, 359 (1931).

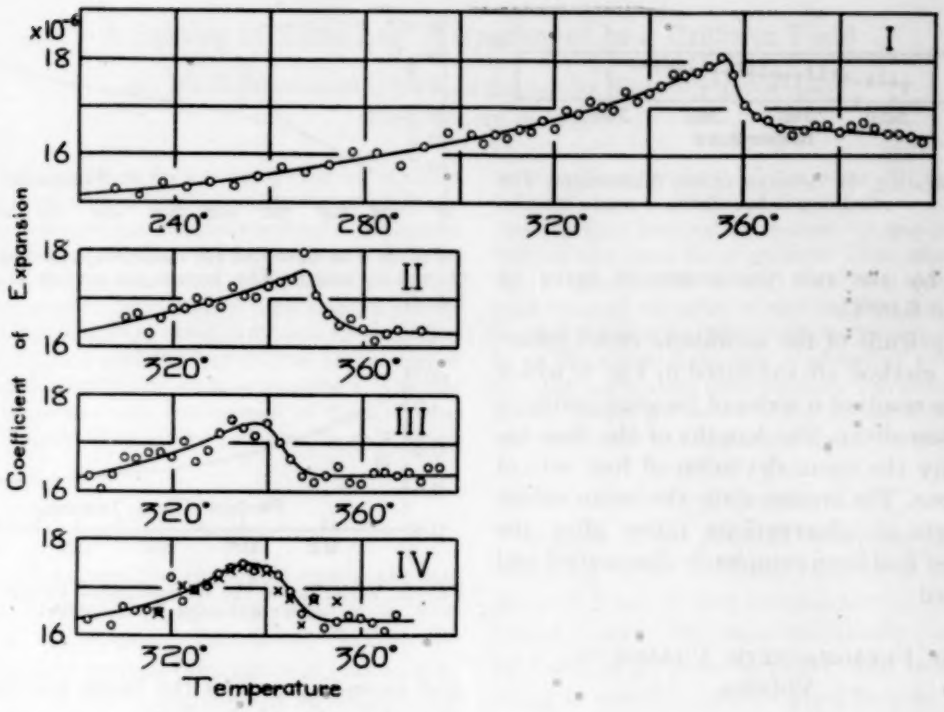

FIG. 3. Variation of coefficient of thermal expansion with temperature for various specimens of nickel.

cylinder axes relative to the crystal axes are quite dissimilar.

The data obtained with the several specimens are shown graphically in Fig. 3. The crosses on curve IV represent observations made on specimen V. Each point in the range 320°–380° represents the mean of four to six observations. All the observations are corrected for the expansion of the quartz dilatometer.

It is to be noted that there is no evidence of hysteresis in this phenomenon; the heating and cooling curves are indistinguishable. Again, the annealing process to which specimen IV was subjected leaves the phenomenon unaltered. Rough measurements of the magnetization as a function of temperature in specimen I indicate that the Curie point of this material is in the neighborhood of 370°C.

PRECISION

The sources of systematic error in these measurements are (1), errors in measurement of the specimen length and of the quantities which determine the dilatometer magnification; (2), a longitudinal temperature gradient in the furnace; (3), the thermocouple calibration; and (4), a difference in temperature between the thermocouple junction and the specimen.

The distance between the roller and knife edge is measured with a travelling microscope to 0.1 percent, and the dilatometer magnification to 0.2 percent. The maximum allowed temperature gradient near the center of the furnace, measured with the specimen removed, is 0.13°C per cm. Accordingly, the actual temperature of the specimen must be uniform to better than 0.5°C. The thermocouple calibration used is that given by the Bureau of Standards.[6] This is checked and the remaining sources of error estimated by replacing the specimen with a glass encased Leeds and Northrup platinum resistance thermometer calibrated by the Bureau of Standards. Under these circumstances the maximum discrepancy between the two thermometers over a period of eighteen months was 0.8°C in the range 300°–400°. Furthermore, the 5° intervals as

[6] Bur. Standards J. Research **10**, 280 (1933).

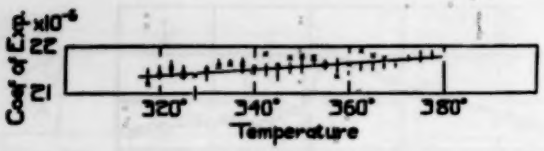

FIG. 4. Illustrating the behavior of the dilatometer. The substance is fine silver.

measured by the two thermometers agree to better than 0.09°C.

The magnitude of the accidental errors inherent in the method are exhibited in Fig. 4, which depicts the result of a series of measurements on a bar of fine silver. The lengths of the lines indicate twice the mean deviation of four sets of observations. The crosses show the mean values of two sets of observations taken after the dilatometer had been completely dismantled and reassembled.

THE FERROMAGNETIC CHANGE OF VOLUME

An evaluation of the ferromagnetic change in length requires an authentic base line from which to calculate the area under the hump. This is secured by combining the data obtained in these experiments with those reported by Hidnert.[7] Hidnert worked with a specimen of electrolytic nickel which contained 0.03 percent iron and 0.03 percent of other metallic impurity, and reported mean values of the thermal expansion coefficient over temperature intervals of 100°C between 100°C and 900°C.

Fig. 5 is a graph of the composite data. The crosses indicate Hidnert's values and the circles in the temperature range 400°–500° indicate values obtained in these experiments. The humps are reproductions, on the altered scale, of curves I and II of Fig. 3. With the exception of the single observation of Hidnert over the range 400°–500°, the data are in excellent accord, and yield a fairly satisfactory base line shown by the dotted portion of the curve. It appears that 0.6 percent or less of impurity leaves the base line

[7] Hidnert, Bur. Standards J. Research **5**, 1305 (1930).

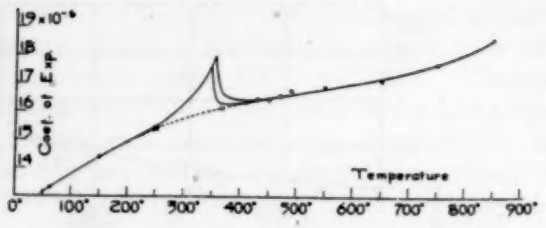

FIG. 5. The base line for measuring the ferromagnetic change in length. The humps are curves I and II of Fig. 3.

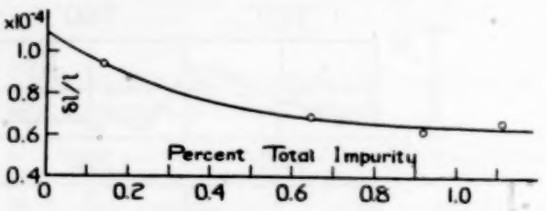

FIG. 6. Variation of the ferromagnetic change in length with total impurity for nickel.

and ascending part of the hump unaltered, and that the value of the change in length per unit length diminishes with increasing amount of impurity. Accordingly it is suggested that the value of the ferromagnetic change in length for pure nickel be obtained by extrapolation.

Fig. 6 is a curve for which the ordinates of the plotted points are the areas under the four curves of Fig. 3 with respect to the base line shown in Fig. 5, while the abscissae are the percentages of total impurity as given in Table I. The extrapolated value of the ferromagnetic change in length per unit length for pure nickel is

$$1.08 \pm 0.05 \times 10^{-4}.$$

The precision measure is obtained from the uncertainty in the total impurity as given in Table I.

In conclusion the author desires to express his thanks to the Physics Department of Columbia University for the facilities placed at his disposal to Dr. L. A. Wooten for the determination of the carbon content of specimen III, and to Dr. S. L. Quimby, who suggested the problem and followed the progress of its solution with helpful counsel and encouragement.

A Survey of Time Lag of Sparkover in a Uniform Field

ABE TILLES, *Department of Electrical Engineering, University of California*

(Received July 14, 1934)

An original instrument for measuring time lag of sparkover has been developed. This is capable of measuring lags over a range from one one-hundred-thousandth of a second up to *any* longer values. This entire time range is available for any individual measurement without readjustments and independently of the method or wave shape of voltage application. Spark lags are found to fall into three distinct domains. First, long *initiatory* lags (10^{+2} to 10^{-3} second or less) of random distribution spent in awaiting a favorable fortuitous space and time arrangement of the somewhat insufficient supply of initiatory electrons. Second, intermediate *formative* lags (of the order 10^{-4} second) distributed about a definite peak value of the order of time required for a positive ion to cross the gap and assist in building up a space charge gradient. Third, short formative lags (of the order 10^{-7} second) distributed about a definite peak value of the order of time required for an electron to cross the gap. A picture of the mechanism of sparkover in an initially uniform field is presented accounting for the existence of these three domains. The available experimental reports are correlated and shown to be consistent with each other and with the proposed explanation.

INTRODUCTION

As is well known the theory of sparkover has long been based on the original formulations of Townsend. Increasing knowledge brought to light serious difficulties in this formulation. First, at the field strengths envisaged, the positive ion could not possibly attain an energy requisite to produce ionization. Second, because of the difference in electron and positive ion mobilities, a space charge is produced which must render the field at the time of sparkover decidedly non-uniform. From theoretical consideration of these factors, Rogowski[1] and Loeb[2] independently concluded that the Townsend mechanism did occur but at field strengths greatly multiplied locally by distortion caused by the space charge. They pointed out that this modified Townsend mechanism demanded a definite formative time for the sparkover of the order of time required for a positive ion to cross the gap, e.g., 10^{-4} second, and that a measurement of the time lag of sparkover under conditions which eliminated the random variations found by Zuber[3] would therefore provide a crucial verification of the conclusions reached. Shortly thereafter much shorter time lags, e.g., 10^{-8} second were observed for impulse sparkover at substantial overvoltages by Beams,[4] Tamm,[5] et al. This apparent direct contradiction left the subject in confusion.

Because of the possible variety of phenomena occurring under different conditions this divergence did not in fact invalidate the above mentioned theory. This was specifically pointed out by Loeb in an ensuing paper[6] and in a seminar which it was the author's good fortune to attend in 1931. Loeb pointed out that it still remained necessary to check the theory by means of a time lag measurement under those conditions of static sparkover *for which the theory had been formulated*, namely, small overvoltage and initial ionization adequate to eliminate random variations.

It was, accordingly, the object of this present work first to ascertain under which conditions the spark lag distribution was random and under which the distribution curve was peaked about some definite value. Secondly, it was desired to measure the time lag for the important case, hitherto unexplored, of adequate initial ionization and small overvoltage. Third, by means of these results it was desired, if possible, to correlate the available data on spark lag and on the nature of its dependence on initial ionization and on overvoltage and thereby, perhaps, to clarify the mechanism of sparkover in a uniform field.

APPARATUS AND PROCEDURE

The timing instrument evolved used common three electrode vacuum tubes in a resistance-coupled amplifier so biased that a small increment of gap voltage at minimum sparking

[1] Rogowski, Archiv f. Elektrotechnik **16**, 761 (1926).
[2] Loeb, J. Frank. Inst. **205**, 305 (1928).
[3] Zuber, Ann. d. Physik **76**, 231 (1925).
[4] Beams, J. Frank. Inst. **206**, 809 (1928).
[5] Tamm, Archiv f. Elektrotechnik **19**, 235 (1928).
[6] Loeb, Phys. Rev. **38**, 1891 (1931).

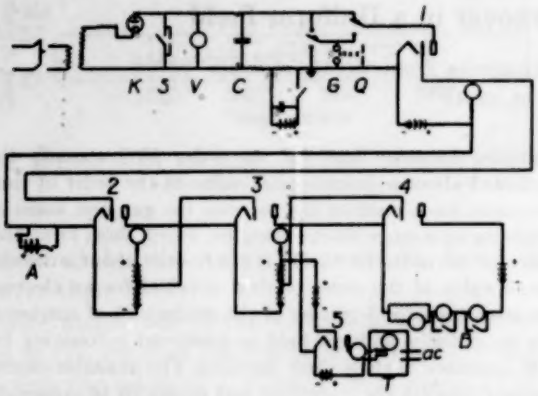

FIG. 1. An instrument to measure time lag of sparkover. *K*, kenetron rectifier tube; *S*, safety gap and discharge switch; *V*, electrostatic voltmeter; *C*, storage condenser 7.2×10^{-10} f; *G*, test gap; *Q*, quartz mercury arc; *A*, bias adjustment; *T*, synchronous timer; *B*, ballistic galvanometers.

Tube	Plate battery voltage	Plate circuit resistor
1 OM 5	156	1.92 MΩ
2 CX 340	180	0.5 MΩ
3 CX 345	180	0.1 MΩ
4 CX 340	90	0.25 MΩ
5 CX 345	180	500 Ω

voltage was steeply amplified and applied to a tube whose output current was thereby swept from zero to a constant maximum value. This constant current flowed until the sparkover occurred. The current was passed through a ballistic galvanometer whose throw was directly calibrated in seconds, thus measuring the spark lag.

The wiring of the instrument is fully shown in Fig. 1. Tube 1 is directly across the spark gap, acting as an inverted vacuum tube voltmeter and reducing the voltage to a conveniently small value. This reduced voltage in series with an adjustable bias is applied to the input of tube 2. Tubes 2 and 3 act as a two-stage, resistance-coupled, linear amplifier. The output of tube 3 applied to the grid of tube 4 swings this grid from a substantial negative voltage to a substantial positive voltage causing the output current of tube 4 to sweep from zero to the maximum obtainable (i.e., plate supply voltage divided by external plate resistance) for a small rise in voltage at the gap. The adjustable bias determines at which gap voltage increment this sharp response takes place and is set so that the minimum sparking voltage of the gap gives half maximum output current. It is evident that for the approximately trapezoidal wave shape of current the total charge measured by the galvanometer divided by the known maximum value of current gives the time that the current has remained above *half* maximum value, hence the bias setting mentioned. The galvanometer throw is calibrated to give directly in seconds the time that the voltage at the gap has remained higher than the value for which the bias was set, i.e., higher than the minimum sparking voltage of the gap. Thus the galvanometer reads directly the time lag of sparkover of the gap. The output current is passed through two ballistic galvanometers of different sensitivities in series. It is feasible manually to short circuit one or both of these after the beginning of its swing when necessary to prevent its being damaged by an excessive swing. Tube 3 also supplies the input of tube 5 which operates a synchronous timer from which any time intervals greater than 0.05 second are easily read. Theoretically computed transients in simple series circuits were applied to the instrument and these gave a calibration check to better than 4 percent. The instrument reads times from 10^{-5} second up.

The timing circuit itself serves also for measurement of voltage. It is to be noted that the curves of output current of tubes 2, 3 and 4 may be calibrated and used to read the relative voltage at the gap, i.e., the difference between the voltage at the gap and the minimum sparking voltage for which the bias has been adjusted. Tube 2 allows readings over a wider range before saturation is reached but with a lesser precision than tube 3; similarly in comparing tube 3 to tube 4. In most of the tests the plate current of tube 2 was used to read directly with a precision of about 1/4 percent overvoltages less than 7 percent of the sparking potential (which was near 4000 volts).

When the resistances of the instrument were adjusted for maximum amplification a shift of *six* volts at the gap, i.e., 0.15 percent of 4000 volts, produced a change in the output current from zero to the maximum. Thus even if the voltage were raised slowly, e.g., at the rate of 100 percent of sparking potential per 0.01 second, the time required for the output current to rise from zero to maximum would still be only 1.5×10^{-5} second. Thus the instrument can be readily used to measure lags of this or any larger

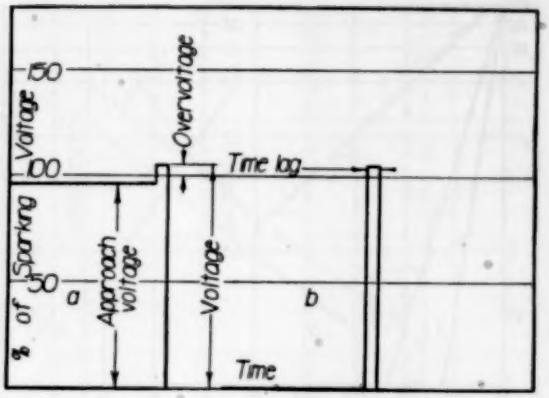

FIG. 2. Voltage wave shapes. *a*, "static" sparkover; *b*, "impulse" sparkover. (The time for the voltage changes drawn vertically is about 1/1000 of the smallest spark lags measured.)

order even for such slow rates of voltage application and, of course, for any more rapid rates. (In the present test series the tube 4 plate resistance was readjusted to give a larger current than at the above mentioned setting, necessitating the use of larger voltage increments at the gap than mentioned above. There was no difficulty on this score, however, as in this test series increments of more than 100 volts were used throughout.)

In order that the effect on the spark lag of the magnitude of the overvoltage might be clearly evident, it was decided to use a rectangular voltage wave shape. That is, the circuit was arranged so that the time duration of the voltage rise from minimum sparking potential to the constant maximum voltage applied to the gap throughout the time lag interval, and also the time duration of the drop of voltage from its full value to the minimum sparking potential, were each very much less than the time lag being measured. The voltage was swept past the sparking voltage very rapidly by applying all or an increment of the voltage suddenly, i.e., within some 10^{-8} second. In most cases this was accomplished by applying the voltage to the gap by closing a switch having higher insulation resistance than the gap. An auxiliary spark was thus obtained at the closing switch which served, therefore, to apply the voltage to the gap very quickly. Two wave shapes were utilized (Fig. 2). For the first, which conveniently approximated "static" sparkover, the main d.c. voltage on the gap was set at 96 percent of sparking potential and a bank of "B" batteries was then thrown across a resistance in the circuit to suddenly raise the gap voltage to some percent above sparking potential. The second wave shape, constant d.c. voltage suddenly applied, approximated "impulse" sparkover but at small overvoltages. The d.c. voltage was obtained from a synchronously driven self-excited motor-generator set, transformer, kenetron tube and condenser. Time lags of sparkover were obtained for both these voltage shapes, for various voltages, mostly in the neighborhood of 105 percent of static sparking potential, and for ultraviolet illumination of measured intensity varied over a very large range.

Ultraviolet light from a quartz mercury arc illuminated the test gap and also a plate of clean nickel in vacuum—both of these being illuminated through identical quartz windows. The intensity of illumination was measured by measuring the saturation current liberated from the nickel photo-cell. This was allowed to flow through a specially constructed resistor consisting of a micarta strip buried in paraffin; the voltage drop across the resistor was measured by a Dolazelek electrometer, the resistance being measured after each voltage measurement by means of the voltage time decay curve when the illumination was intercepted. The spark gap used consisted of copper spheres at small spacing in dehydrated air at atmospheric pressure.

The coherence of the distribution curves increases decidedly as the number of sparkovers per run is increased, but so too, does the work involved. Accordingly, as a compromise, a run of 50 points for the random distribution and of 25 for the peaked was selected as a standard procedure. It may be noted that the adherence of the points to the curve is always best at the top where the points are most numerous and poorest at the bottom where the scale is stretched and a small number of points is used to locate a statistical distribution. For this reason the curve is placed so that the number of points above it equals the number below, no weight being allowed to the added "moment" of the straggling points at the lower end of the curve.

Data and Results

Fig. 3*a* shows three curves of spark lag distribution at "static" sparkover at three different voltages and at one intensity of initial ionization. As labelled this intensity is measured by the current I, in micro-micro-amperes per square centimeter, ejected from a plate of clean nickel in vacuum by the ultraviolet illumination utilized. The lower left hand corners of the light curves give the actual data points which are plotted by listing all the spark lags of the set in order of magnitude and listing also the percent order of magnitude. Thus the fourth largest of a set of 50 is 8 percent etc. This percentage is plotted against the time duration of the particular lag. The equation of the resultant curve is $n_t = 100e^{-pt}$ wherein n_t is the percentage of the total number of lags which are greater than the time t and p is the probability of a lag terminating within unit time. It is evident since the curves are linear on semi-logarithmic paper that p is constant and the distribution truly random. As is well known,[7] the average time lag $T = 1/p$ and can be taken from the curve at $n_t = 36.8$.

The average time of these distributions is plotted against percent overvoltage in Fig. 3*b*. From this curve the average time at 5 percent overvoltage is readily interpolated, thus giving a point on the master curve 1 of Fig. 5. Each of the curves similar to 3*b*, i.e., average time *vs.* overvoltage, was roughly exponential for overvoltages from 1 to 6 percent and the several exponents were approximately the same.

As the illumination was further increased, however, a different transitional distribution appeared wherein some 70 percent of the lags formed a true random distribution and one, moreover, fitting the same master curve 1 of Fig. 5, as shown by its dotted portion. The other 30 percent of the lags were grouped into an entirely different type of distribution. As the illumination was further increased larger percentages of the total were in the second group, and for somewhat greater illuminations yet all the lags fell on the second type of distribution curve. This was a highly peaked distribution containing a few large and many small deviations from a definite peak value. In fact, some 40 percent of the total lags fell within a single time increment only 10 percent as large as the maximum time intervals represented in the distribution. For the peaked distributions no appreciable shift in the time lag was produced by slight changes of overvoltage nor by extensive further increase in illumination. This also is shown on the curves of Fig. 5. Fig. 4 illustrates the two distributions and the transitional distribution by curves at different illuminations and near 5 percent overvoltage.

A series of tests similar to the above was repeated for the "impulse" wave shape with very similar results which are also plotted on Fig. 5 as

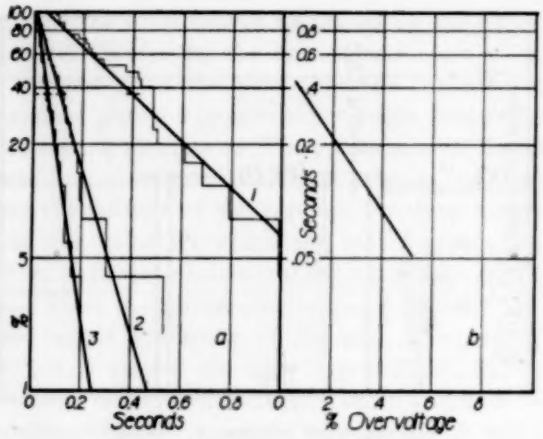

Fig. 3. Domain one spark lags. *a*, spark lag distributions, percent of lags greater than given by abscissa; *b*, average lag *versus* percent overvoltage. Approach voltage = 96 percent; overvoltage, curve 1 = 0.7 percent; overvoltage curve 2 = 3.5 percent; overvoltage, curve 3 = 4.9 percent; $I = 0.00183$.

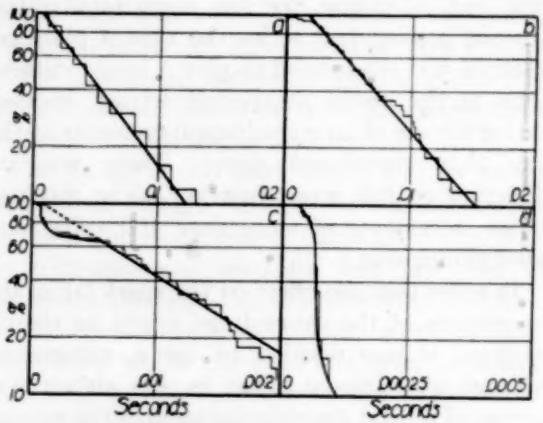

Fig. 4. Spark lag distributions for different illuminations; *a*, random at $I = 0.00183$; *b*, random at $I = 0.0258$; *c*, transitional at $I = 0.365$; *d*, peaked at $I = 5.75$.

[7] von Laue, Ann. d. Physik **76**, 261 (1925).

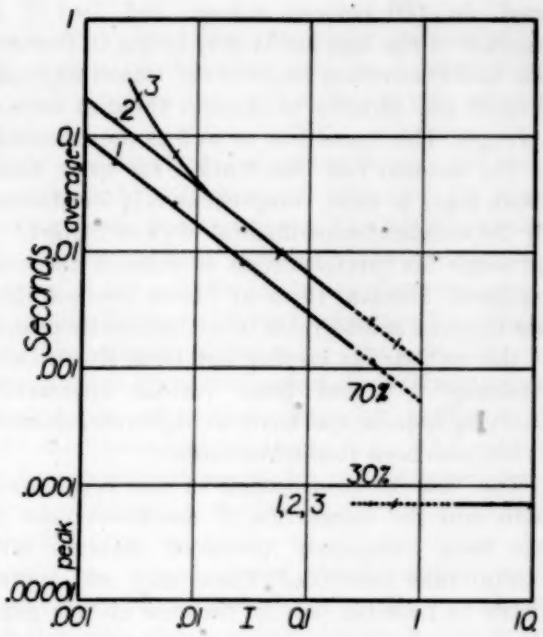

FIG. 5. Master curve of average or peak values. Time lag of sparkover *versus* illumination

Curve	Approach voltage	Voltage
1	96%	105%
2	96%	103%
3	0%	105%

curve 3. Throughout the random distributions the lags at impulse sparkover are longer by a factor of two or more than those at static sparkover. Apparently the only difference is that the 96 percent approach voltage, due to cumulative ionization, causes a greater concentration of initial ions to exist in the gap than exists with the 0 approach voltage. At the smallest ionizations studied, i.e., at the upper end of the impulse sparkover curve 3 of Fig. 5, the curve takes on a greater slope. This is perhaps to be expected as at the lower ionization density one would expect a unit slope. That is, a tenfold increase in ionization should effect a tenfold shortening of the time lag. For higher initial ion densities the lesser slope observed indicates that the increasing ultraviolet illumination becomes in some way progressively less efficient in precipitating sparkover.

It is apparent that if this 96 percent approach voltage is lowered, the random spark lags will be lengthened and that at some low approach voltage, for which the cleansing action entirely outweighs the ionization caused, the random lags must reach a maximum duration greater than that at zero approach voltage. This was checked by a brief test series at 50 percent approach voltage which gave nearly three times as great an average lag as that for zero approach voltage. A few brief tests were taken, also, with overvoltages as high as 50 percent. As was expected increasing the voltage, thus, substantially decreased the observed spark lag. At 50 percent overvoltage, again, a peaked distribution was obtained at a high illumination $I=9$, but a somewhat lower illumination, $I=1.75$, which had been adequate to give a peaked distribution at 5 percent overvoltage was inadequate to give a peaked distribution at the higher overvoltage. That is for $I=1.75$, at 5 percent overvoltage the initiatory lags were negligible compared to the formative lags, but at 50 percent overvoltage the greatly shortened formative lags were negligible compared to the initiatory lags.

The results of these tests may be summarized as follows: Spark lags are found to fall into three distinct domains. First, long *initiatory* lags (10^{+1} to 10^{-3} second or less) of random distribution spent in awaiting a favorable fortuitous space and time arrangement of the somewhat insufficient supply of initiatory electrons. Second, intermediate *formative* lags (of the order 10^{-4} second) distributed about a definite peak value of the order of time required for a positive ion to cross the gap and assist in building up a space charge gradient. Third, short formative lags (of the order 10^{-7} second) distributed about a definite peak value of the order of time required for an electron to cross the gap.

In the first domain with small overvoltages for the gap studied (copper spheres of 0.952 cm radius at 0.0683 cm separation, and 3820 volts static sparking potential) the average time lag is given by:

$$t=f(v)I^{-0.78}, \qquad (1)$$

where t = *average* time lag in seconds of a group of sparkovers taken under identical conditions.

I = intensity of photoelecric illumination as measured by the current, in micro-micro-amperes per square centimeter, exepelled from a clean nickel plate in vacuum.

$f(v)$ = a function of the applied voltage wave shape and magnitude.

Although $f(v)$ varies somewhat with the illumination, it

may be inclusively stated for the "static" sparkover (i.e., voltage suddenly shifted from 96 percent of static sparking potential to a constant value more than 100 percent) as:

$$f(v)=0.0037e^{-(0.30\pm 0.08)v} \tag{2}$$

and for the "impulse" sparkover (i.e., a constant maximum voltage suddenly applied) as:

$$f(v)=0.0078e^{-(0.30\pm 0.13)v} \tag{3}$$

where v = the *percent overvoltage*

$$=\frac{\text{max. applied voltage}-\text{static sparking voltage}}{\text{static sparking voltage}}\times 100.$$

Eqs. (2) and (3) hold for from 1 to 6 percent overvoltage; outside of this range the function is not exponential. The central value of exponent indicated is correct at 5 percent overvoltage in every case. For static sparkover Eq. (1) holds for illumination from $I=0.002$, the lowest studied, to $I=0.5$ where transition to the second domain occurs. For impulse sparkover the curve deviates slightly, the exponent becoming greater as I decreases; Eq. (1) is adequate, however, from $I=0.02$ to $I=0.5$.

At the transition to domain two, i.e., at $I=0.5$, 70 percent of the sparkovers occur in a distribution whose average exactly fits equation (1) of domain one and 30 percent fit into the domain two distribution. For successively larger illuminations a successively smaller percentage of sparkovers come into domain one and a larger percentage into domain two.

The existence of the *second domain*, which had been anticipated by Rogowski,[1] and specifically predicted by Loeb,[2, 6] is now *experimentally verified for the first time*. From $I=0.5$ to $I=10$, the highest studied, for this gap and either of the voltage wave shapes mentioned and for overvoltages of from 2 to 6 percent, the lags have a highly peaked distribution, some 40 percent of them falling within one 10 percent increment of the maximum time intervals encountered. Throughout this region the formative time lag, as given by the peak of the distribution curve, remains at $(0.70\pm 0.15)\times 10^{-4}$ second. The above mentioned prediction[2] applied to the present gap length calls for a formative time lag of 0.5×10^{-4} second, an excellent agreement.

When the voltage is raised to 150 percent of static sparking potential at $I=9$, the lags become less than 1.5×10^{-5} second, this being about the smallest interval that could be measured. At 150 percent voltage and $I=1.75$ a fraction of the lags are larger, falling in domain one and illustrating roughly the transition from domain one directly to domain three at higher voltages. This transition, as well as the existence of the domain one distribution for quite brief spark lags, is more comprehensively illustrated by the excellent experimental work of Strigel,[8, 9] although his interpretation of domain three is confused. Domain three at higher overvoltages has received considerable investigation by means of the cathode ray oscillograph from Rogowski's students[10, 5, 11] and from various engineers[12] studying impulse sparkover at high overvoltages. It has also been studied optically.[4]

The time of propagation of the breakdown path and the completion of sparkover once it has been adequately produced involves still shorter time intervals.[13] These may add appreciably to time lag only in the case of long gaps (i.e., initially non-uniform field) and do not concern us here.

Sparkover Mechanism

The mechanism of sparkover in an initially uniform field is envisaged as follows.

Domain one

With somewhat *inadequate initial ionization* the *initiatory lag* in awaiting the fortuitous occurrence of electrons so located as to be capable of commencing sparkover is very much greater than the formative lag. In general, since this fortuitous occurrence is as likely within one time interval as within any other, distribution of these initiatory lags is truly *random*. The order of magnitude of the initiatory lag depends on the external ionizing forces and may be extremely large if these are small. In general, with a probable exception at voltages barely large enough to produce breakdown upon the appearance of a single electron at the cathode, it is the *density of ionization* in the gap that controls the initiatory lag rather than the *rate* of production of *new* electrons. As the initial ion density is

[8] Strigel, Wissenschaftliche Veroffentlichungen a.d. Siemens-Konzern **11**, 52 (1932).
[9] Strigel, Archiv f. Elektrotechnik **27**, 137 (1933).
[10] Buss and Masch, Archiv f. Elektrotechnik **25**, 787 (1931).
[11] Viehmann, Archiv f. Elektrotechnik **25**, 253 (1931).
[12] Torok, A. I. E. E. Trans. **47**, 349 (1928).
[13] Dunnington, Phys. Rev. **38**, 1535 (1931).

sufficiently increased the entire initiatory lag becomes negligibly small and the formative lag of either domain two or three as the case may be, prevails.

At one level of ionization density we may visualize the variation of initiatory lag with voltage variation as follows. The initiatory time lag is the random time spent *in awaiting the arrival* of the suitable initiatory electrons within a specific *effective* volume in the gap. The extent of this volume effective for the initiation of adequate electron avalanches obviously increases with increased voltage. Thus for sparkover at the very lowest overvoltages, e.g., 0.1 percent, it is certainly necessary for the initiatory electrons to appear at the *very surface of the cathode* and it is also necessary—in all probability—for several to appear almost simultaneously, each one taking advantage of the gradient produced by the space charge of its predecessor. For somewhat higher voltages it is certainly sufficient for sparking that the initiatory electrons appear anywhere within an "effective" shell of appropriate depth extending from the cathode; also, a smaller number of electrons probably suffices. As the voltage increases the thickness of this effective shell increases. For *very high* voltages certainly it is sufficient that a *single* initiatory electron exist *anywhere* within an effective volume including all the gap except a thin shell at the anode. Further voltage increases will then have little effect in shortening this initiatory lag.

Domain two

For a *sufficient initial ionization* the formative lag prevails. Each initial electron avalanche leaves behind it an increasing phalanx of positive ions pointed toward the cathode and hence a space potential which increases about exponentially as one leaves the cathode and starts towards the anode. The slope of this curve gives the field strength at each point. Using *low overvoltages*, e.g., 3 percent and a small gap length, this field strength is at no point great enough at the first instance to cause positive ion ionization. As the whole phalanx of positive ions, however, proceeds relatively slowly toward and into the cathode, the resultant field between the cathode and the next row of positive ions becomes successively steeper. As the last row of positive ions approaches the cathode, the field there becomes great enough to cause positive ion ionization giving a tremendous self-accelerating increase in the number of new electrons formed. As soon as this burst of electrons reaches the anode, the voltage begins its complete drop and sparkover is very rapidly completed. *The total elapsed time is about that required for a positive ion to cross the gap.*

With slightly higher overvoltages (e.g., 15 percent) since, as Sanders[14] has shown, the Townsend coefficient for the initial electron ionization is greatly increased as the voltage increases, the exponential potential curve mentioned above is much steeper. Hence a sufficient gradient for positive ion ionization is created as soon as a *portion* of the positive ion phalanx is swept into the cathode. Thus sparkover ensues after a lag corresponding to time for a positive ion to cross a fraction of the gap length. As the overvoltage is increased this fraction becomes smaller.

Domain three

For an *adequate initial ionization* and a *higher overvoltage* on the same gap (or the same *percent* overvoltage in a longer gap[13]) another effect intervenes. Owing to the intense electron ionization at increased voltage[14] the exponential curve mentioned is itself steep enough near the anode so that positive ion ionization commences there at once. (If this secondary ionization is extremely close to the anode it might not be sufficiently cumulative until this active rear portion of the positive ion phalanx has moved an adequate distance *away from* the anode.) For still *higher overvoltages* (e.g., 60 percent), however, the potential curve caused by the passage of the initial electron avalanche is steep enough to give positive ion ionization at some point in the middle of the gap *at once* before the positive ions have moved any appreciable distance. The mammoth flood of electrons released by this positive ion ionization starts for the anode before the original avalanche has reached there and arrives, starting the voltage drop, one step behind the initial avalanche, as it were. *Thus the time lag is of the order of time for an electron to cross the gap.* The above explanations for domains two and three are worded, for simplicity, as if a single electron avalanche sufficed for spark-

[14] Sanders, Phys. Rev. **41**, 667 (1932).

over. It may well be that the space and time coincidence of several is essential under most conditions; this does not, however, alter the general argument. (Because of such coincidence a marked increase in initial ionization may tend slightly to shift the sparkover from the second domain to the third but not to the same degree as an increase in voltage.)

Correlation of the Literature

It is particularly gratifying that in the light of the above explanation the various available experimental reports are seen to be consistent with each other and with the spark mechanism envisaged, whereas hitherto they had appeared isolated and even contradictory. The more important of these are briefly presented.

Zuber[3] and von Laue,[7] working at *low initial ionization* showed that the spark lags were very long (running into seconds) and of *random distribution* and that they decreased as the ionizing illumination was increased. They established the nature of, but not the determining conditions for, the *first domain*. Strigel,[8, 9] using fairly high ionization and fairly high overvoltages, also found a random distribution of spark lags at much smaller times, illustrating that for test conditions giving a short formative time domain one extended into quite short intervals. Strigel established that the magnitude of the random time lags varied greatly with the composition and condition of the illuminated *cathode*. Strigel also observed, but was at a loss to interpret, the transition from the random distribution to a specific, formative time lag.

Because no instrument existed combining the necessary swiftness with sufficient precision as to voltage to allow measurements of the formative lags of sparkover at low overvoltages, adequate measurements in the *second domain* have not hitherto been obtained. Perhaps the only previous experimental work bearing on this matter is Reukema's[15] study of the shift of a.c. sparking *voltage* at high frequency, which gives strong indirect verification of the necessity of positive ion motion for completion of sparkover at small overvoltages.

Among others, Buss and Masch[10] using the cathode-ray oscillograph and Beams[4] using the Kerr cell, working at *high overvoltages*, found that the spark lag was very *brief*, e.g., 3×10^{-8} second, and had the *definite value* of the third domain. Viehmann[11] used the oscillograph in conjunction with a saw tooth wave shape of voltage whose slope was changed from test to test. This, together with the small number of sparkovers per series, entirely obscured the difference *in kind* between the various lags he observed. He did, however, observe lags in all three domains and demonstrated roughly the tremendous range of spark lags existing and their very great shortening as the ionizing illumination or overvoltage is increased.

Observations of the initiation of the visible spark directly establish that spark initiation may occur by one of two distinct mechanisms. This was first observed, in a qualitative way by Torok.[12] Dunnington's[13] precise Kerr cell observations at various pressures and gap lengths and at small overvoltages, supplemented by the similar work of von Hámos[16] at high overvoltages, establish two types of sparkover. First, one in which the visible spark initiates exclusively at the cathode. Second, one in which the spark commences somewhere in mid gap. It is further established that this second sparkover type is caused to replace the first, either by increasing the gas pressure or the gap length while using the same percent overvoltage, or by increasing the percent overvoltage. It is to be noted that any one of these three increases corresponds merely to an increased magnitude of electron ionization. Thus for the test conditions of *domain two*, whose time lag indicates a travel of positive ions to the cathode, the spark is *seen*, literally, to initiate *at the cathode*. For the conditions of *domain three* at which more intensive electron ionization must occur, the time lag does not allow for positive ion migration but calls for positive ion ionization at once and the spark is *seen* to commence at once *in mid-gap*.

In closing, the author wishes to express his indebtedness to Professors L. F. Fuller, L. E. Reukema and L. B. Loeb for their kind and unfailing guidance throughout the course of this investigation; to Professor D. D. Davis and Mr. L. E. Evans for their invaluable cooperation in furnishing equipment; and to his brother, Mr. I. H. Tilles, for assistance in the laboratory.

[15] Reukema, A. I. E. E. Trans. **47**, 38 (1927).

[16] von Hámos, Ann. d. Physik **7**, 857 (1930).

The Arc Spectrum of Europium

HENRY NORRIS RUSSELL AND ARTHUR S. KING, *Carnegie Institution of Washington, Mount Wilson Observatory*

(Received November 1, 1934)

AN extension of the temperature classification[1] for longer wave-lengths (now in progress) confirms the structure of the spectrum predicted by Albertson.[2] This resembles that of Mn I except that the multiplicities are greater by two. The lowest level is $4f^7 6s^2(^8S^\circ)$. Combinations with $4f^7 6s6p(^{10}P\ ^8P$ and $^8P)$ give the great blue triplet and strong furnace lines in the red. Higher $^{10}S^\circ$ and $^{10}D^\circ$ terms form series going to $^9S^\circ$ of Eu II as limit.

The terms so far identified are given in Table I.

TABLE I. *Terms in Eu I.*

Configuration	Designation	Level	Configuration	Designation	Level
$4f^7 6s^2$	$a^8S^\circ_{3½}$	0.00	$4f^7 6s6d$	$f^{10}D^\circ_{2½}$	34422.97
$4f^7 6s6p$	$z^{10}P^\circ_{3½}$	14067.80		$^{10}D^\circ_{3½}$	34440.43
	$^{10}P^\circ_{4½}$	14563.49		$^{10}D^\circ_{4½}$	34466.75
	$^{10}P^\circ_{3½}$	15581.58		$^{10}D^\circ_{5½}$	34505.26
				$^{10}D^\circ_{6½}$	34544.70
	$z^8P^\circ_{2½}$	15890.48		$f^8D^\circ_{1½}$	36045.20
	$^8P^\circ_{3½}$	15952.22		$^8D^\circ_{2½}$	36072.54
	$^8P^\circ_{4½}$	16611.65		$^8D^\circ_{3½}$	36097.52
	$y^8P^\circ_{2½}$	21444.64		$^8D^\circ_{4½}$	36218.82
	$^8P^\circ_{3½}$	21605.12		$^8D^\circ_{5½}$	36242.18
	$^8P^\circ_{2½}$	21761.14	$4f^7 6s7d$	$g^{10}D^\circ_{2½}$	39284.68
$4f^7 6s7s$	$e^{10}S^\circ_{4½}$	28763.68		$^{10}D^\circ_{3½}$	39290.09
	$e^8S^\circ_{3½}$	29517.62		$^{10}D^\circ_{4½}$	39305.89
	$f^8S^\circ_{3½}$	31217.08		$^{10}D^\circ_{5½}$	39332.91
$4f^7 6s8s$	$f^{10}S^\circ_{4½}$	37195.72		$^{10}D^\circ_{6½}$	39369.41

The two ^8P and $^8S^\circ$ terms of the same configuration belong to the ^9S and ^7S limits of Eu II. Their mutual repulsion separates them by more than the difference of the limits (1669.3). The terms of multiplicity 10 are the first to be detected.

The classified lines are listed in Table II. To save space they are given by multiplets.[3] The wave-lengths and intensities are from Eder[4] supplemented to the red of λ7400, and in a few other cases, by measures on Mount Wilson plates—the temperature class from determinations by King from these plates. The column headed $\Delta\nu$ gives the residual (O–C) of the observed wave number from the values resulting from Table I. The average value of $\Delta\nu$, regardless

TABLE II. *Lines in Arc Spectrum of Eu.*

	J	λ I.A.	Int.	Temp. Cl.	Δν
$a^8S^\circ - z^{10}P$	3½ – 3½	7106.48	6	I	−0.01
	3½ – 4½	6864.57	10	I	+ .05
$a^8S^\circ - z^8P$	3½ – 4½	6018.18	8	I	+ .08
	3½ – 3½	6266.97	3	IA	+ .06
	3½ – 2½	6291.34	6	IA	.00
$a^8S^\circ - y^8P$	3½ – 2½	4661.89	30	I	− .10
	3½ – 3½	4627.26	40	I	− .09
	3½ – 4½	4594.06	30	I	+ .02
$z^{10}P - e^{10}S^\circ$	3½ – 4½	6802.79	10	II	− .08
	4½ – 4½	7040.20	6	II	+ .04
	5½ – 4½	7583.91	5	II	+ .08
$z^8P - e^{10}S^\circ$	3½ – 4½	7803.33	1	IV	+ .06
	4½ – 4½	8226.81	3	IV	+ .01
$z^{10}P - e^8S^\circ$	3½ – 3½	6470.75	4	III	+ .08
	4½ – 3½	6685.27	5	II	+ .01
$z^8P - e^8S^\circ$	2½ – 3½	7336.28	2	III	.00
	3½ – 3½	7369.69	2	III	− .04
	4½ – 3½	7746.10	5	II	+ .20
$z^{10}P - f^8S^\circ$	3½ – 3½	5829.49	1	III	+ .14
	4½ – 3½	6003.08	2	III	− .08
$z^8P - f^8S^\circ$	2½ – 3½	6522.75	3	III	+ .13
	3½ – 3½	6549.14	3	III	+ .11
	4½ – 3½	6844.98	3	III	− .20
$z^{10}P - f^{10}D^\circ$	3½ – 2½	4911.39	8	III	.00
	3½ – 3½	4907.18	6	III	.00
	3½ – 4½	4900.86	5	III	− .05
	4½ – 3½	5029.54	5	III	+ .07
	4½ – 4½	5022.91	6	III	− .02
	4½ – 5½	5013.19	6	III	+ .06
	5½ – 4½	5293.68	2	III	+ .04
	5½ – 5½	5282.84*	3	III	+ .28
	5½ – 6½	5271.93	8	III	.00
$y^8P - f^8D^\circ$	2½ – 1½	6847.21	3	IV	−0.09
	2½ – 2½	6834.41	3	IV	− .09
	2½ – 3½	6822.65	1	IV	+ .13
	3½ – 2½	6910.19	3	IV	− .02
	3½ – 3½	6898.27	4	IV	.00
	3½ – 4½	6841.05	4	IV	− .08
	4½ – 4½	6914.83	3	IV	+ .01
	4½ – 5½	6903.71	5	IV	− .06

	J	λ I.A.	Int.	Temp. Cl.	Δν
$z^8P - f^8D^\circ$	2½ – 1½	4960.22	5	III	+0.07
	2½ – 2½	4953.52	4	IV	− .01
	2½ – 3½	4947.39	3	IV	+ .01
	3½ – 2½	4968.73	3	IV	− .05
	3½ – 3½	4962.55	5	III	+ .02
	3½ – 4½	4932.83	4	IV	+ .10
	4½ – 4½	5098.73	4	IV	+ .11
	4½ – 5½	5092.70	4	IV	− .04
$z^{10}P - f^8D^\circ$	3½ – 2½	4543.17	1	V	+ .16
	3½ – 3½	4538.06	1	V	− .02
	3½ – 4½	4513.20	1	V	+ .02
	4½ – 4½	4616.52	2	IV	− .04
	4½ – 5½	4611.52	1	V	+ .08
	5½ – 4½	4844.30	2	V	− .17
$z^{10}P - f^{10}S^\circ$	3½ – 4½	4322.56	2	III	+ .04
	4½ – 4½	4417.25	3	III	− .04
	5½ – 4½	4625.32	3	III	− .05
$z^{10}P - g^{10}D^\circ$	3½ – 2½	3964.48	1	IV	0.00
	3½ – 3½	3963.63	1	IV	.00
	3½ – 4½	3961.15	1	IV	− .03
	4½ – 4½	4040.48	2	III	+ .10
	4½ – 5½	4036.11	1	IV	− .02
	5½ – 5½	4209.09	2	III	+ .10
	5½ – 6½	4202.65	1	III	.00

* Close double.

[1] A. S. King, Astrophys. J. **72**, 221 (1930).
[2] W. Albertson, Phys. Rev. **45**, 499 (1934).
[3] Compare Miss Moore's Multiplet Table (Princeton 1933).
[4] Eder, Wien. Ber. **126**, IIa, 473 (1917).

of sign, is ±0.06 corresponding to about ±0.02A —a testimony to Eder's measures.

Rydberg formulae applied to the $^{10}S°$ and $^{10}D°$ terms give 46,058 and 45,803 for the limit $^{9}S°$ of Eu II. As the denominator n^* usually increases by slightly more than unity in similar series, the value 45,750 has been adopted. This gives for the components of highest J the values of n^*

$e^{10}S$	2.542	a^8S	1.549	$f^{10}D$	3.129	$z^{10}P$	1.908
$f^{10}S$	3.582	e^8S	2.600	$g^{10}D$	4.147		

which run nearly parallel with the corresponding values for Mn I. The terms f^8S and f^8D appear to belong to the ^7S limit. The principal ionization potential is 5.64 volts. The observed ^{10}D terms come from $6d$ and $7d$ electrons. The $5d$ term should be at about 20,000 (referred to $a^8S°$) and its combinations with the P terms are far in the infrared. Many strong lines, including some of Class I, are still unclassified, and may arise from other electron configurations.

DECEMBER 1, 1934 PHYSICAL REVIEW VOLUME 46

Proceedings of the Metropolitan Section of the American Physical Society

MEETING OF OCTOBER 26, 1934

THE first meeting of the Metropolitan Section of the American Physical Society for the season 1934–1935 was held on Friday, October 26, 1934, in Room 301 of the Physical Laboratory of Columbia University in New York City. An afternoon and an evening session were held. The presiding officer was Professor H. C. Urey.

The afternoon session was devoted for the most part to a symposium on the physics of the solid state; the papers were as follows:

Free Electrons as the Source of Metallic Binding Energy, F. SEITZ AND E. WIGNER, *Princeton University.*

The Internal Dissipation of Solids, R. L. WEGEL, *Bell Telephone Laboratories.*

Measurement of the Elastic Constants of Crystals at Low Temperatures, S. L. QUIMBY, *Columbia University.*

Some New Magnetic Properties of Alloys, R. M. BOZORTH, *Bell Telephone Laboratories.*

In the latter part of this session Professor Ladenburg of Princeton University gave a brief account of the sessions devoted to nuclear physics at the conference of the International Union of Pure and Applied Physics recently held at London.

The evening session was devoted to a lecture by Dr. J. A. Becker of the Bell Telephone Laboratories. His subject was "The Life History of Adsorbed Atoms and Ions."

W. S. GORTON
Secretary-Treasurer

LETTERS TO THE EDITOR

Prompt publication of brief reports of important discoveries in physics may be secured by addressing them to this department. Closing dates for this department are, for the first issue of the month, the twentieth of the preceding month; for the second issue, the fifth of the month. The Board of Editors does not hold itself responsible for the opinions expressed by the correspondents.

On the Velocity of Light

The determination of the velocity of light with the aid of mirrors furnishes some average between the velocities to and from the most remote mirror. This average may, of course, be a complicated function depending on various factors, although it seems universally assumed that the velocity either to or from the remote mirror is exactly equal to the average velocity. The recent anomalies observed by Pease and Pearson[1] in their experiments in California emphasize the need of a closer examination into these factors, among which is the structure of the light employed for such measurements.

All previous experiments have made use of light in which the incident ray and the reflected ray were essentially of the same kind, the difference consisting in the change in phase introduced on reflection. Because of this close relationship between the rays, I shall call them "related." Here, I wish to urge an experiment in which the rays are as unrelated in nature as possible and thus it is probable that the velocity obtained can be set equal to that of an unidirectional beam. The aim is to compare in a single measurement the average velocity furnished by such "unrelated" rays with the velocity of "related" rays. Should these velocities be found unequal, a greater discrimination in the definition of the velocity of light will be necessary. The possible repercussion on the theory of relativity which identifies the velocity of light with the fundamental[2] velocity of the Lorentz transformations would make the following experiment especially worth while.

A beam of light in the shape of a slit will pass through the apparatus (such as that of Foucault-Michelson) in the usual way but instead of being reflected at the distant mirror throughout its entire length, the image of the slit is to be reflected in one-half of its length at the mirror and the other half is to excite fluorescence of another color in an adjoining vessel. The comparison of the velocities consists in observing in what measure the fluorescent color is shifted with respect to the incident color in the return image.

Comments on the experiment: The time-lag in the fluorescence of numerous substances is so short that the image radiated back by the fluorescing medium will be practically as sharp as the one reflected by the mirror. The single bi-convex lens employed by Michelson in his early work may, for example, be replaced by two plane-convex lens so that one plane-convex lens can be situated close to the fluorescing material. A resonance lamp with its high efficiency may serve as the vessel adjoining the remote mirror. However, the incident and reflected rays under these conditions may not be as completely "independent" of each other as when the rays are of different wave-lengths. The time-lag of the fluorescence and the depth of penetration into the vessel, if the fluorescing medium be a transparent substance rather than a fluorescing surface, must of course be taken into account. Only such fluorescence need be used whose time-lag has been found (with the aid of the Abraham-Lemoine shutter for example) to be comparable with the time required by the mirror to rotate through the smallest detectable angular displacement and also it is to be very short as compared with the duration of the journey of the light. However, the latter errors may be minimized by carrying out the experiment with the fluorescing material at various distances from the rotating mirror.

The methods now available for constructing efficient fluorescing lamps would seem to make this experiment feasible without much further technical improvement. On the other hand, should the experiment confirm the general belief in the equality of the velocities, an experiment of this kind could determine the time-lag of various radiation processes.

SIMON FREED

Department of Chemistry,
University of Chicago,
October 19, 1934.

[1] To be published soon in the Astrophysical Journal.
[2] A. S. Eddington, *The Mathematical Theory of Relativity*, p. 19, 1923.

Remarks on the Band Spectrum of Sulfur and the Statistics of the Sulfur Nucleus

A few years ago Naudé and Christy[1] examined the fine structure of five of the bands of diatomic sulfur in the near ultraviolet and made an analysis of them from which they calculated that in the normal state of the sulfur molecule the internuclear distance is 1.603A. If this result were correct it would appear that the sulfur molecule were very abnormal since a distance somewhat greater than 1.8A is predicted by several rules, including the covalent bond radii and an empirical rule of the author[2] by which internuclear distances can be calculated from vibrational frequencies.

Since no other deviation from these rules of this magnitude is known, it occurred to the writer to examine the data to determine whether the analysis of Naudé and Christy were unique. He soon came to the conclusion that it is not and, for several reasons, is probably incorrect. He noticed, for example, that their Δ_2F' values show certain peculiarities. They appear to be identical within experimental error for the bands 8–1 and 9–1, and also for 10–1[3] up to the point where this band runs into the head of 8–0. Now when the Naudé-Christy Δ_2F' values for 10–1 and 10–2 are plotted against $\bar{K}$ they fall on straight

lines up to the point where these bands run into the heads of 8–0 and 8–1, respectively. The succeeding points deviate from these lines and follow lines with a considerably greater slope. This might be the result of a perturbation as these authors believed, but since it might also indicate that they failed to follow the branches of 10–1 and 10–2 through the regions where there is a great overlapping of lines, the data on these regions were carefully examined. It was found that the measured lines can be reassigned to the various branches in a very plausible way so that the deviation just mentioned vanishes and we obtain a set of combinations which agree for the bands 8–1, 9–1 and 10–1, and are slightly different for 8–0 and 10–2. This, together with the fact that the rotational constants obtained from these combinations are what we should expect for the ground level, is rather conclusive evidence that these combinations are Δ_2F'' rather than Δ_2F' as Naudé and Christy believed.

A new set of combinations was then made to find the true Δ_2F' values. From these one finds that the rotational constants vary in the vibrational states of the upper electronic level in such a fashion that it is difficult to make an extrapolation to the vibrationless state which has great significance. Furthermore some perturbations are found in the level $v'=8$. These duplicate in the bands 8–0 and 8–1 and are additional confirmation of the correctness of the new combinations. Large perturbations are to be expected in the upper state since it has been observed[4] that many of the band heads are considerably displaced from their expected positions.

The results of the new analysis are given in Table I. An important feature is that it shows that the *even* rotational

TABLE I. *Constants of the sulfur molecule.*

	B(cm^{-1})	D_e(calc), α_e, B_e(cm^{-1})	r_e
$v''=0$	0.309	$D_e''=-2.2\times10^{-7}$	$r_e''=1.840$A
$v''=1$	0.307	$\alpha_e''=0.0016$	
$v''=2$	0.306	$B_e''=0.309_6$	
$v'=8$	0.230	$D_e'=-2.4\times10^{-7}$	
	(0.211 for $K>21$)		
$v'=9$	0.229		
$v'=10$	0.239		

levels are present in the ground state of the sulfur molecule instead of the odd levels as found in oxygen. Since the electronic states of these two molecules are presumably of similar character, this shows that if the oxygen molecule is symmetric in the nuclei, as has been generally accepted, the sulfur molecule is antisymmetric. However, in case the character of the electronic states has been incorrectly assigned, it is possible that the symmetry character should be reversed in both cases.

RICHARD M. BADGER

Gates Chemical Laboratory,
California Institute of Technology,
Pasadena, California,
October 29, 1934.

[1] S. M. Naudé and A. Christy, Phys. Rev. **37**, 490 (1931).
[2] R. M. Badger, J. Chem. Phys. **2**, 128 (1934).
[3] The v' numbering of Naudé and Christy should be increased by one according to the results of Fowler and Vaidya, Proc. Roy. Soc. **A132**, 310 (1931).
[4] A. Christy and S. M. Naudé, Phys. Rev. **37**, 903 (1931).

Concerning the Recovery Time of Geiger-Mueller Counters

We have equipped a Braun tube with a timing "sweep" which is initiated by the phenomenon to be studied. Thus, pulses recurring at random will give retracing curves on the fluorescent screen and so may be photographed. Figs. 1–3 show three oscillograms with a schematic diagram at the right of each.

The ordinates of the curves represent the negative potential v of the wire of a Geiger-Mueller counter connected in the usual way, namely, with the outer cylinder at constant (negative) potential V, and the wire grounded through a high resistance R. Figs. 1 and 2 show that when a discharge occurs, v rises suddenly and then falls following an exponential curve. As one would expect its time constant is equal to RC where C is the total capacity between the wire and ground. Curves 1 and 2 in Fig. 1 show discharges for two values V_1 and V_2 of the applied voltage. The horizontal lines V_1-V_0 and V_2-V_0 show the excess of V over the starting potential V_0. In other words $V-V_0$ represents that value of v for which the voltage across the counter equals the starting voltage.

By suddenly applying x-radiation we have seen that a counter will discharge after v has fallen below $V-V_0$ but not before. Therefore, the recovery times for the respective systems are defined by the associated time intervals denoted by the τ's in the oscillograms.

In Fig. 1 V_2 is greater than V_1, so one sees that the excess of the initial value of v over $V-V_0$ increases with increasing V. Therefore the time τ is larger for higher operating voltages.

The two curves in Fig. 2 were taken with the same applied voltage V. In curve b the value of C was about

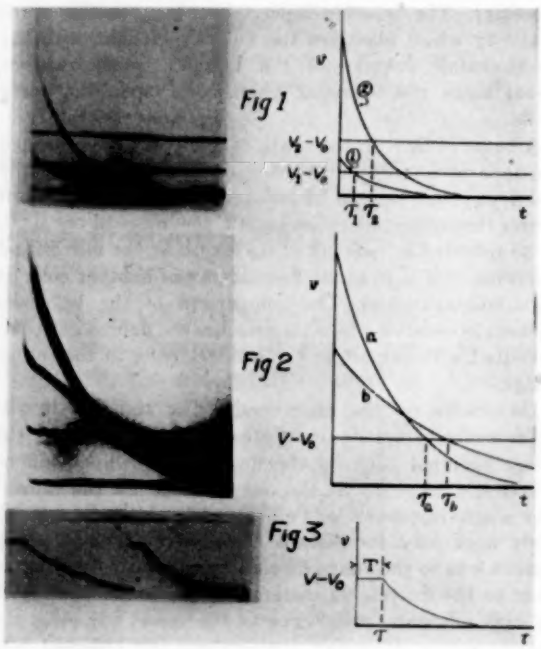

FIGS. 1–3.

twice that in curve *a*. This increase of C has increased the time constant of the curve but decreased the initial ordinate. The former change tends to increase τ while the latter tends to diminish it. In this particular case, doubling C has increased τ by about 27 percent. It seems quite possible that in some cases increasing C may actually decrease τ.

If a pulse occurs before the v of a preceding one has fallen to zero, it will be smaller than the preceding pulse and have a smaller τ. So for very rapid counting rates one has a statistical distribution of τ's.

For higher values of V or C, the discharges may take the form shown in Fig. 3. This is a photograph of a single sweep during which two discharges occurred. (Some 60 cycle induction is present.) Here v rises to $V-V_0$ and remains there for a time T before decaying exponentially. The time τ is of course given by T and may vary widely in successive pulses. The average T is an increasing function of C and decreases as R increases.

The observations described here are quite uniform throughout a set of counters made in the same "batch." The wire in all counters was 3 mil tungsten and the cylinders were oxidized copper. The pressure in all cases was 7 or 8 cm. The qualitative phenomena are independent of counter size, of whether the gas is air or argon and oxygen, and of change in R between 5×10^8 and 5×10^9 ohms.

We hope to submit a report of quantitative nature in the near future.

It is a pleasure to acknowledge the helpful support of Dr. W. F. G. Swann.

W. E. Danforth

The Bartol Research Foundation
of the Franklin Institute,
Swarthmore, Pennsylvania,
November 6, 1934.

On the Statistical Theory of Errors

Professor R. A. Fisher has most kindly responded to our request for criticisms of the article that appeared under the above title.[1] The material in his letter is much too valuable to be filed away, so with his consent we here present the substance of his comments, together with some additions here and there of our own.

It is doubtful if on page 135 it was made sufficiently clear that in the absence of a reliable estimate of σ, the u test cannot be used, and that the z test (which is equivalent to Fisher and Student's t test) is the only recourse. (By a *reliable estimate of* σ we mean an estimate that is considerably more reliable than can be obtained from the single sample under test.) The z test is not inherently misleading; it tests objectively a proposed value of z, and for this purpose it is of course perfectly valid (as we say). Like any statistical test, the z test lays down and accepts a perfectly definite hazard. Misinterpretations of the z test may be common, but the blame should be placed, not on the test itself, but on misunderstandings of the nature that we point out on page 135. What is more to be feared than over-confidence in the z test is the use of the normal probability integral (the u test) with an estimate of σ based *on the single sample* under test.

The separation of the parameters of the parent population from *estimates* of these parameters has been a gradual process. Many writers have been extremely careless in confusing that which is estimated with an estimate of it. Thinking to avoid any such looseness, we systematically used Greek and Latin letters to distinguish the two classes of quantity. It is perhaps well to go even further and use distinguishing names for the two classes. For this purpose there are in use today the terms "parameter" of the parent population and "statistic" of the sample, the work "statistic" having been introduced by Fisher (footnote 4 of our article) in 1921 to fill the need of a term antithetical to "parameter." A parent population is completely specified by its one or two or more parameters, but a sample of n would require n different statistics for its specification. To each of these statistics there corresponds a particular parameter or parametric function toward which the value of the statistic tends as the sample is indefinitely increased; but to each parameter there "corresponds," in this sense, as many statistics as there can be of samples from a given parent population, to which number there is no limit. For these reasons it would doubtless have been better to have written "corresponding statistic of a sample" on page 142, 7 lines below section (3*e*), to avoid giving the impression that there is a one to one correspondence between the two quantities s and σ.

In further connection with fiducial probability it should be mentioned that fiducial values can be taken only from distributions of statistics that contain the whole of the information that can be obtained from the sample. The distribution of s fulfills this requirement, and our discussion of fiducially related values of σ and s is therefore valid, but it is worth while to note that the distribution of, for example, the arithmetic mean deviation, from which Peters' formula (see any text on least squares) is derived, could not be so used. There is not room here, and neither was there in the original article, to discuss the criteria of "efficiency" and "sufficiency," but they might at least be mentioned with a reference. The reader will find them discussed in the papers cited in footnotes 4 and 31.

W. Edwards Deming,
Bureau of Chemistry and Soils,
Washington, D. C.
Raymond T. Birge,
University of California
Berkeley.

November 9, 1934.

[1] Deming and Birge, Rev. Mod. Phys. 6, 119–161 (1934).

A Low-Power Positive-Ion Source of High Intensity

Numerous tests have been made in this laboratory of various low voltage and high voltage ion-sources, all of which presented serious limitations in use. Dr. F. L. Mohler of the National Bureau of Standards kindly described to us last summer some experiments having a similar objective, in which with low power he had obtained

very large current-densities to a negative probe inserted from one side into a hot cathode, low voltage arc *confined in a quartz capillary*. We duplicated this result, but rapid deterioration of the quartz and the difficulty of its replacement with the necessary probe-canal accurately in alignment led us to consider other materials for the arc-capillary. Since every positive ion diffusing to the quartz wall is neutralized on contact it appeared that a *metal capillary*, allowed to "float" in potential, should serve equally well. This was promptly confirmed, and a series of subsequent experiments, concerned chiefly with the empirical space-charge problem of focussing such high ion-densities into a beam, led to the ion-source shown in Fig. 1. Difficulty has been encountered in brief efforts to focus these intense ion-beams on the target of the high voltage tube, but description of the ion-source may be of immediate value to other workers.

The important features of the ion-source are shown to scale in Fig. 1. The steel arc-body A is bored out, forming the arc-capillary B joining the arc-spaces which contain the oxide-coated filament C and anode D (110 volts with resistance). A side volume E for ions diffusing to the probe F is provided with the important "focussing-diaphragm" G which gives very high current-density to the small canal H in the center of the probe. Conical insert J provides flat gas-seal faces. The probe is supported on the Lavite insulator K, and is held at 500 to 7000 volts filtered direct current by a Variac-controlled '66 rectifier-set. Focussing electrode L is held at 2 to 15 kilovolts direct current by a *ZP*-85 kenotron set with condensers. Protective resistors of high value (50,000) are essential to prevent probe- and focus-voltages from "blowing out" the arc (possibly by oscillations). A self-striking "auxiliary arc" (0.1 ampere) to the steel arc-body is usually used to strike the main arc through the capillary (0.2 to 2 amperes); otherwise the application of a small spark-coil to the (floating) arc-body starts the capillary-arc. Pressures are roughly 2×10^{-2} in the arc and 2×10^{-4} in the tube; speed of Apiezon pumping system is about 30 liters/sec. (air); hydrogen flow is perhaps 10 cc per hour at N P T, allowing the use of deuterium gas without recovery at nominal cost. The ratio of atomic to molecular ions is high and is unimportant since magnetic analysis is used at the target.

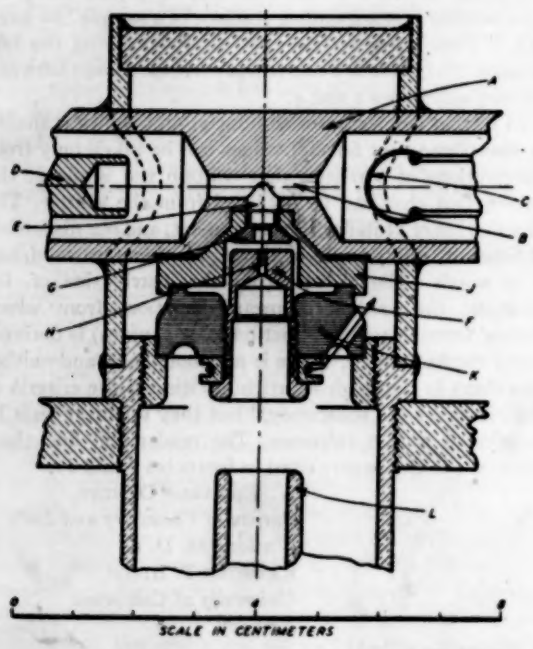

FIG. 1. Ion-source detail. (Department of Terrestrial Magnetism, Carnegie Institution of Washington, No. 3274.)

With a total power-consumption at maximum under 250 watts, and this gas flow which can be handled by modest pumping arrangements, true ion-currents (no secondary electrons) up to 1.5 *milliamperes* are readily obtained through the probe-canal 1 mm in diameter and 4 mm long shown in Fig. 1 (probe-voltage 7 kilovolts; probe-current 3 milliamperes; arc 2 amperes). Higher ion-currents undoubtedly can be obtained by using a larger probe-canal and higher current-density in the capillary. Application of 6 kilovolts to the focussing electrodes shown (we have made tests on various electrode-arrangements) will completely focus the probe-canal output-current of 25 microamperes through a 5-mm diameter hole at a distance of 11 cm (position of next electrode-gap) when the probe is held at 700 volts; 9 kilovolts are required with the probe at 1000 volts (80 microamperes), and 15 kilovolts are required to focus the probe-output of 250 microamperes at 1500 volts. The simple "lens" *FL* does not bring the whole ion-beam into good focus at large distances without proper intermediate focussing-gaps.

M. A. TUVE
O. DAHL
C. M. VAN ATTA[1]

Department of Terrestrial Magnetism,
Carnegie Institution of Washington,
Washington, D. C.,
November 14, 1934.

[1] National Research Fellow, Massachusetts Institute of Technology guest investigator at the Department of Terrestrial Magnetism.